Renewable and Sustainable Energy Reviews 166 (2022) 112640

Contents lists available at ScienceDirect

Renewable and Sustainable Energy Reviews

journal homepage: www.elsevier.com/locate/rser

Alternative architectures and materials for PEMFC gas diffusion layers: A review and outlook

F.C. Lee [a,*], M.S. Ismail [a,b,**], D.B. Ingham [a], K.J. Hughes [a], L Ma [a], S.M. Lyth [a,c,d], M. Pourkashanian [a,b]

[a] Energy 2050, Department of Mechanical Engineering, Faculty of Engineering, University of Sheffield, Sheffield, S3 7RD, United Kingdom
[b] Translational Energy Research Centre, University of Sheffield, Sheffield, S9 1ZA, United Kingdom
[c] International Institute for Carbon-Neutral Energy Research (WPI-I2CNER), Kyushu University, 744 Motooka, Nishi-ku, Fukuoka, 819-0395, Japan
[d] Platform of Inter/Transdisciplinary Energy Research (Q-PIT), Kyushu University, 744 Motooka, Nishi-ku, Fukuoka, 819-0395, Japan

ARTICLE INFO

Keywords:
Polymer Electrolyte Fuel Cells
Porous Media
Gas diffusion layer
Microporous layer
New materials and designs
Water Management

ABSTRACT

This paper reviews some of these new innovations in both the macroporous substrate and the microporous layer (MPL). A diverse range of macroporous substrates and designs is shown, encompassing various carbon-based and metal-based materials and innovative fabrication methodologies. A critical assessment of innovative MPL materials and designs for performance improvements is presented, taking into account pore size distribution and microstructure. An analysis of the effect of wettability and hydrophobic agents in the substrate and MPL is performed. One of the notable findings is that, among other key findings, significant performance enhancement is realised through employing graduated porosity and/or wettability GDLs. Finally, recommendations for future work into GDL materials and designs are made, with the aim of ultimately improving the overall cell efficiency.

1. Introduction

Recently, polymer electrolyte membrane fuel cells (PEMFCs) have received a significant amount of attention due to their high-power density, fast start-up time and zero/low emissions; as such they are regarded as a sustainable solution for a wide range of stationary, portable and vehicular applications. PEMFCs are electrochemical energy conversion devices, whereby hydrogen fuel is indirectly reacted with oxygen to produce water, electricity and heat. Hydrogen is oxidised in the hydrogen oxidation reaction (HOR) at the anodic side of the fuel to protons (or hydrogen ions) and oxygen is reduced in the oxygen reduction reaction (ORR) with protons (migrating from the anode side) at the cathodic side of the cell. The ORR kinetics are much slower than the hydrogen oxidation reaction; therefore, more platinum catalyst is normally used at the cathodic side to increase its rate of the reaction.

The gas diffusion layer (GDL) of PEMFC is placed between the catalyst and current collector on each side of the fuel cell, thus it is an essential performance-limiting component of the PEMFC. The GDL has multiple important roles within the PEMFC. First, it provides electrical connection between the electrocatalyst layers and the bipolar plates (and thereby the external circuit). Therefore, it should have high electronic conductivity. The GDL also conducts exothermically generated heat away from the electrocatalyst layer and should therefore have high thermal conductivity. It provides mechanical support to the fragile electrocatalyst layer during PEMFC assembly and operation, and therefore should demonstrate high mechanical stability. Most importantly, the GDL provides transport pathways for the supply of reactant gases (e.g. hydrogen at the anode and air (or oxygen) at the cathode) from the flow channels to the electrocatalyst layers. As such, the GDL should have suitable mass transport properties. Finally, the GDL facilitates the removal of excess liquid water produced at the cathode to the exhaust stream, and thus it should have suitable wettability [1]. Single-layer GDLs consist solely of a macroporous substrate (MPS). However, typical GDLs used in PEMFCs are dual layer, in which the MPS is coated with a microporous layer (MPL).

By supplying the reactants and removing the products, the GDL can significantly affect catalyst utilisation. Inefficiencies in the GDL structure which lead to lower voltages in the PEMFC current-voltage plots (or polarisation curves) can be classed as either ohmic losses, or mass transport losses. Ohmic losses are essentially related to the resistance of

* Corresponding author.
** Corresponding author. Energy 2050, Department of Mechanical Engineering, Faculty of Engineering, University of Sheffield, Sheffield, S3 7RD, United Kingdom.
E-mail addresses: fclee1@sheffield.ac.uk, florenceclee91@gmail.com (F.C. Lee), m.s.ismail@sheffield.ac.uk (M.S. Ismail).

https://doi.org/10.1016/j.rser.2022.112640
Received 14 May 2020; Received in revised form 12 May 2022; Accepted 23 May 2022
Available online 9 June 2022

the GDL and its interfaces with the electrocatalyst layer and the bipolar plate. Meanwhile, mass transport losses (also known as concentration losses) can be separated into two main contributions. First is the rate at which reactants can be supplied to the electrocatalyst layer. This must occur at a faster rate than that at which they are consumed, or a voltage drop will be observed, especially at high current density. Secondly, liquid water produced in the cathode electrocatalyst layer must be removed efficiently in order to prevent "flooding". This normally occurs at high current densities (e.g. ≥ 1 A cm^{-2}) [2], where liquid water is generated faster than it can be removed, causing it to accumulate. This water then blocks oxygen transport to the electrocatalyst layer, causing a voltage drop in the polarisation curves. Ohmic losses and mass transport losses must be minimised in order to enhance PEMFC performance.

In order to minimise ohmic losses, the electronic conductivity of materials must be high. This is usually dictated by the material properties. To minimise mass transport losses, the pore size distribution must be suitable. This is usually dictated by the microstructure. As such, carbon is generally selected as a material for the GDL due to its high electronic conductivity and the wide range of possible microstructures. In addition carbon-based materials can have high thermal conductivity, high strength, good thermal stability, and reasonable oxidative stability [3].

Over the last decade, a large body of work has focussed on the characterisation of commercially developed GDLs and the factors that affect the transport properties. Increasingly, structural modifications, innovative designs, and alternative materials are being developed. With the potential to improve the PEMFC activity, durability or lower cost. Previous review papers have summarised the existing problems with gas diffusion layers and the progress made with their design improvements [3–9]. Cindrella et al. [4] present a detailed background to the characteristics of the GDL with particular attention to the influence of these on water management in the PEMFC. Park et al. [3], presented a thorough review of the materials and designs of the GDL where analysis of the hydrophobic treatment of the GDL was examined as well as the materials used for the carbon framework of the substrate and the MPL. Like [4] although well researched this review omits more recent developments made in the field. Arvray [5] and Ozden [7] give a comprehensive review of the experimental methods used to characterise the GDL; these papers are a solid starting point to understand GDL; in terms of physical structure and the transport mechanisms underpinning gas diffusion layer diffusion layer designs. More recently Yang et al. [8] and Zhang [9] have presented detailed reviews are centred on the improvements to the MPL and do not tackle design innovations made to the macroporous substrate.

This review article provides an update to the current state of research in the field of gas diffusion layer materials and designs, assessing progress to both the macroporous substrate and the microporous layer. By collating and critiquing recent attempts to improve GDL functionality and PEMFC performance, this review paper presents the key developments and recommendations for future work. It is separated into five main sections dealing with: i) the macroporous substrate (MPS); ii) the hydrophobic agent in the MPS; iii) the microporous layer (MPL); iv) the hydrophobic agent in the MPL, and v) recommendations for future work.

2. Macroporous substrate (MPS)

2.1. Conventional carbon fibre-based MPS

The macroporous substrate is usually the primarily component of a GDL. Carbon fibres sheets are generally used for the MPS, due to their high gas permeability, impressive strength and elasticity under compression, corrosion resistance in acidic environment, and excellent electrical conductivity [3]. They are typically formed from extruded polymer fibres such as polyaniline, which are graphitized at high temperature (i.e. $<$ 2000 °C). The individual carbon fibres formed through this process generally have diameters of 5–10 μm, and the orientation of these depends on the manufacturing process [7].

The most common types of carbon fibre sheets used in GDLs are carbon cloth, carbon paper, or carbon felt. Carbon cloth typically comprises interlocking bundles of carbon fibre woven together with a regular structure (Fig. 1a). In carbon paper, the fibres are rigid, straight and randomly oriented (Fig. 1b). As such, they are generally less porous compared to carbon cloth [10] and because the fibres are preferentially orientated in-plane, the microstructure is highly anisotropic. This impacts the gas transport properties, the thermal conductivity, and the electrical conductivity [11]. Meanwhile, carbon felt is made-up of spaghetti-like fibres oriented randomly (Fig. 1c).

Carbon fibre sheet porosity is normally in the range of 70–90%, and the density can vary from between 0.2 and 0.75 g/cm^3, whilst the substrate thickness can vary between e.g. 100 and 500 μm [12]. The thickness, porous structure and structural anisotropy of the carbon fibres all influence the two-phase transport properties of the resulting GDL (i.e. how the reactant gases and liquid water pass through the layer) [13,14]. However, there is a trade-off between the gas transport properties and the electronic conductivity in GDLs, since electrons are conducted through the solid, non-porous phase of the carbon fibre sheet. As such, the structure of the substrates should be optimised to ensure adequate mass transport and sufficient electrical conductivity.

The porosity is a key factor in determining the fuel cell performance of a particular GDL. Macropores are defined as pores being over 5 μm in diameter, mesopores are defined as being between 0.07 μm and 5 μm in diameter, and micropores are defined as being less than 0.07 μm (70 nm) in diameter. In electrochemical systems, macropores are generally considered to be hydrophobic, functioning as gas transport pathways. Mesopores are considered to be both hydrophobic and hydrophilic, aiding both gas diffusion and liquid water transport. Finally, micropores are considered to be hydrophobic, helping to condense water vapour to liquid, which can subsequently be transported out of the cell [15]. The MPS is largely a macroporous component of the GDL, with larger pores designed to aid mass transport. Fig. 2 shows the representative pore size distribution of three different GDLs, as obtained by mercury intrusion porosimetry (MIP) which highlights the distribution of macropores [16]. A wide range of macropore diamters is observed, with prominent peaks at ~80 nm, ~1 μm, and ~40–70 μm. Each GDL has markedly different pore size distribution depending on the structure, as highlighted in Fig. 2b.

Our understanding of the ability of the substrate to transport mass, conduct electrons and transfer heat in conventional GDLs has been improved by extensive characterisation in a large number of studies. This has helped to inform the choice of substrate materials, and how their fabrication and design impacts the final properties of the GDL in a polymer electrolyte fuel cell. Key areas of improvement in GDL design are based around optimising the porosity, changing the surface properties, and improving the electrical conductivity. Recently in-situ imaging is emerging as a promising field to understand the performance of GDLs. For example, Fig. 3 shows in-operando images of liquid water at the cathode, obtained via x-ray computed tomography. This type of technique has provided significant insights into the state of liquid water and reactant gases, during operation [17–19], and this will enable further development of optimised pore structures for GDLs.

2.2. Alternative MPS materials

Here, we focus on summarising research into alternative materials for the macroporous substrate (MPS) in GDLs. Various groups have aimed to improve on conventional GDLs by changing the materials used. As well as improving cell performance and durability, other motivations for using alternative materials include reducing the cost of manufacture and improving sustainability.

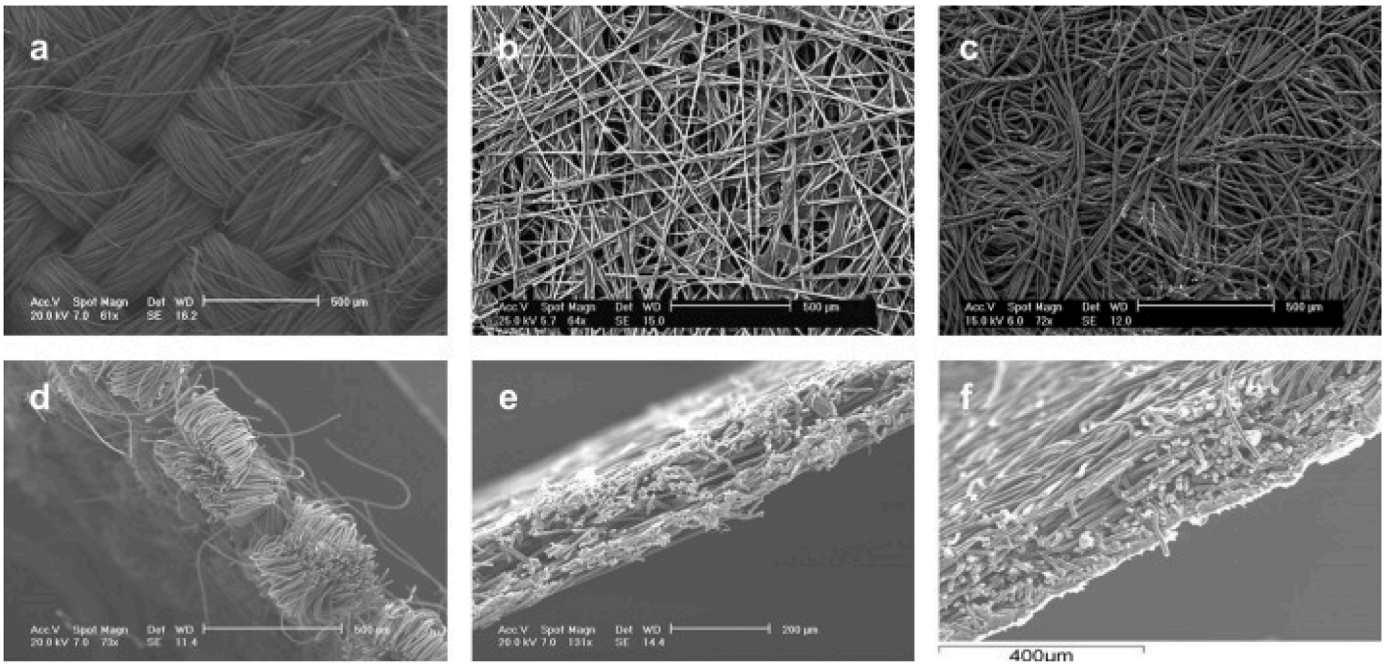

Fig. 1. SEM images the surfaces (top row) and cross-sections (bottom row) of: (a, d) carbon cloth (Ballard 1071HCB); (b, e) carbon paper (Toray H-060); and (c,f) carbon felt (Freudenberg C2). Reproduced with permission from Elsevier [12].

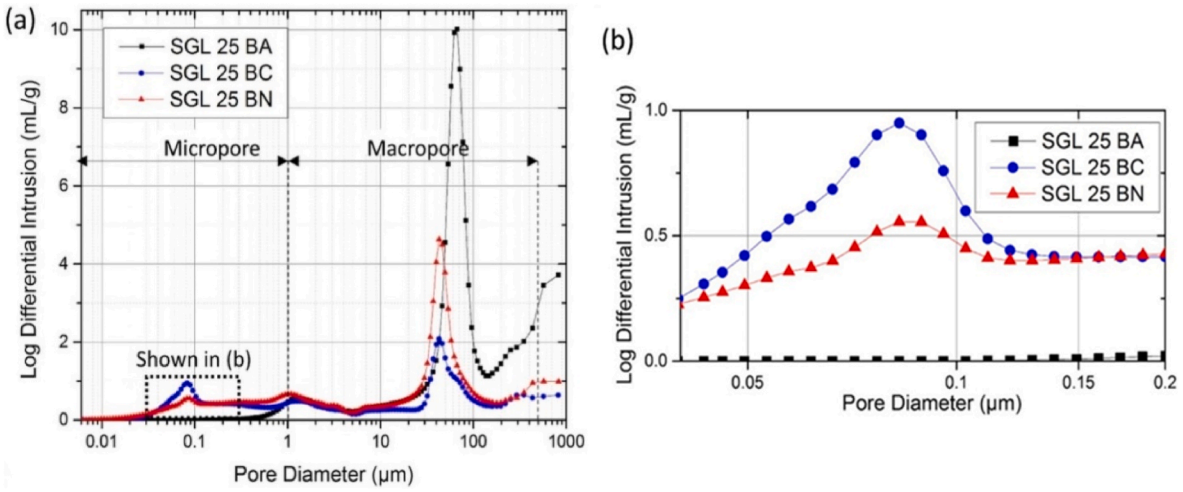

Fig. 2. (a) Pore size distribution of SGL 25 BA (uncoated carbon paper); SGL 25 BC (MPL-coated carbon paper); and SGL 25 BN (carbon paper coated with an in-house MPL), measured by mercury intrusion porosimetry (MIP). (b) Magnified region highlighted by the dashed area in (a). Reproduced with permission from ECS [16].

2.2.1. Electrospun MPS

Electrospinning is a recent manufacturing technique (from 2012) used for the production of continuous fibres of sub-micron to nanometer scale [20]. From adjustment of the parameters during the spinning process, it is possible to control the fibre diameter, pore size, fibre alignment and surface properties of a material. In essence, it is possible to fabricate a macroporous substrate, or e-GDL with an optimised microstructure for mass transport and for the management of liquid water. To this end, electrospinning has been used by several researchers to optimise GDL design in terms of: pore size [21–25], and hydrophobicity [23].

Chevalier et al. [25] conducted a comprehensive study into the optimisation of electrospun MPS, where various parameters were altered including fibre length, fibre diameter, wettability and fibre orientation. The eGDLs were then characterised in-situ and ex-situ; they reported that the e-GDL with the smallest fibre diameter (0.20 μm compared to 1.13 μm) had a smallest inter-fibre space and therefore smallest pore size, which promoted thus improved liquid water removal and decreased mass transport resistance. This resulted in an increased power density than the thicker fibre e-GDL (501 versus 275 mW cm^2). The wettability and the fibre alignment also had a significant effect on the MEA performance, increasing the maximum power density by 12%.

Ren et al. [23] attempted optimisation of the electrospun GDL for use in self-humidifying PEMFCs by modification of the production parameters, including concentration of the polymer solution and the fibre diameter. They reported that their e-GDL had greater water retention capabilities and therefore was suitable for low humidity conditions by alleviating membrane dehydration. However, electrochemical and polarisation curves were not performed and as such the full conclusion of the capability of the e-GDL in a PEMFC has yet to be confirmed.

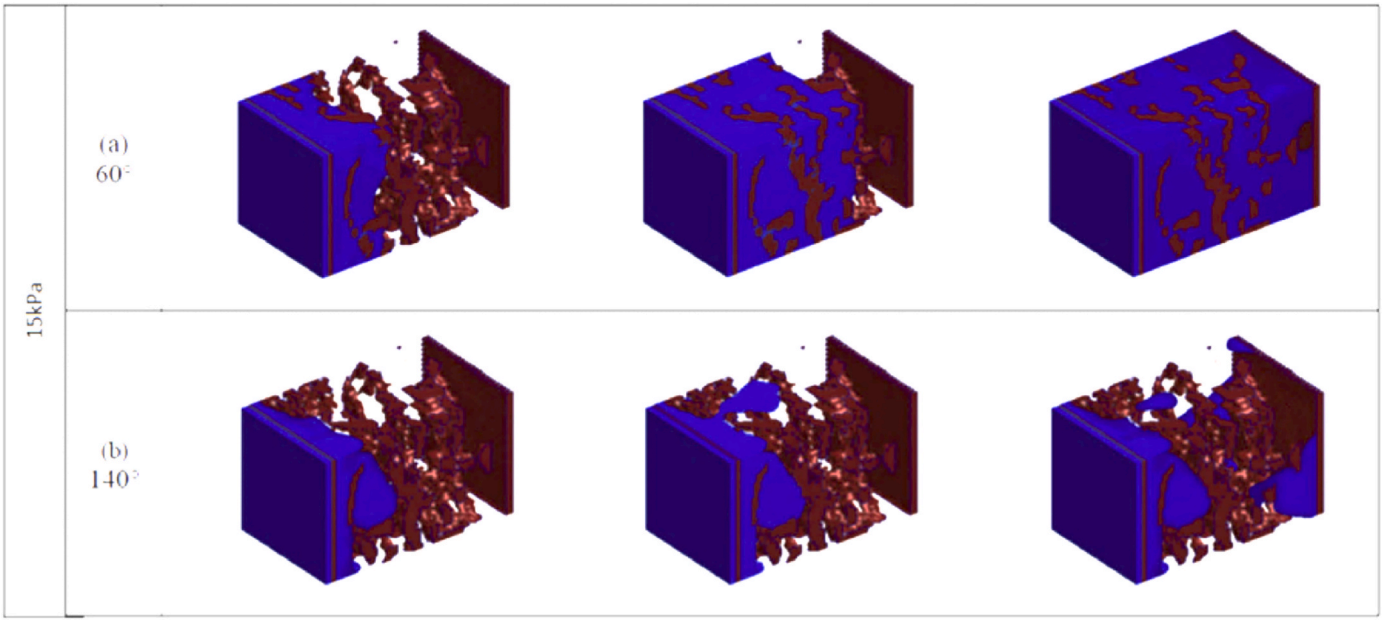

Fig. 3. Intrusion of liquid water into SGL 24AA, based on 3D reconstructions from X-ray computed tomography, for different water contact angles. Reproduced with permission from Elsevier [195].

Certain challenges need to be overcome to improve e-GDL durability as Balakrishnan et al. [26] reported a notable drop in contact angle (from 136° to 44°) after accelerated stress tests in hydrogen peroxide due to a degradation of the fluorinated monolayers. Polarisation curves indicated that the degraded electrospun GDL suffered higher levels of liquid water accumulation and mass transport losses than the pristine with a significant potential drop voltage following the 0.5 A cm^{-2}. The importance of durability tests, which are often neglected, should not be underestimated as they are as important as the performance tests (e.g. the peak power density or the limiting current density).

2.2.2. *Perforated MPS*

Attempts to improve the water management capabilities of the GDL have resulted in various modifications to the design of the macroporous substrate, one of which is the perforation of the cathode MPS [27–35]. Different methods have been used to create large holes (relative to the pore size of the substrate) in the cathode MPS substrate with the aim of creating pathways to divert liquid water from the pores of the cathode diffusion media and the catalyst layer to the gas flow channel, thus relieving the porous media of the cathode side from liquid water saturation and enabling mass transport.

Various techniques have been employed to create a pathway for excess water including manual micro-drilling [32], electric discharge machining [32], and laser perforation [27–30,33–35]. Laser perforation has been used the most extensively though researchers noted that it (and also electric discharge machining) resulted in the formation hydrophilic holes due to the removal of PTFE material from the surrounding area [30,32,34,35]. When using laser perforation to enhance water management it is essential that perforation diameter is optimised as other it may result in power loss.

Gersteisen et al. [28,29] extensively researched the effect of MPS perforations on liquid water transport and on MEA performance. In their initial study they produced 80 μm holes by laser perforation in a Toray TGP-H-090 MPS; this was reported to have enhanced PEMFC performance where limiting current density was increased by 22% [28]. Polarisation curves performed identified less mass transport losses with the perforated macroporous substrate indicating reduced accumulation of liquid water with this MPS. Scale-up from a single cell to a PEMFC stack showed the viability of their design for real world applications [29]. This is a crucial but often neglected step by researchers as the GDL designs and modifications are not extended beyond the single cell stage.

The imaging of the MEA through E-SEM [34], in-operando synchrotron X-ray radiography [30,35], and synchrotron tomography [30] has helped with the validation of this research and provided clarity on the effect of these modifications on the liquid water front. Haussman et al. [30] used synchrotron X-ray radiography and tomography to reveal the preferred water transport pathways in the perforated GDL; the optimal dimeter of the holes (60 μm) was attributed to the different filling behaviour of the pores. Numerical studies performed by Fang et al. [27] and Niu [31] supported the experimental work on the topic and aided in design optimisation. Niu et al. [31] modelled two phase fluid flow using the two-phase volume of fluid (VOF) model in a reconstruction of the perforated GDL where the diameter, depth and the location of the perforations were assessed. Their oxygen diffusion models supported the experimental data in that MPS perforation increases oxygen concentration and reduces oxygen transport resistance in the GDL. Their model, compared to the case with no perforations, predicted an increase of more than 100% in oxygen concentration with 100 μm perforations. However holes of a smaller diameter (e.g. 25 μm) was found to have negligible effects on the water saturation. This in agreement with the optimisation experimental data from Manahan et al. [36] who reported a 25% increase in power density with an MPS with 100 μm perforations and almost negligible improvements with much smaller perforations [28,30]. They [36] also reported that the perforation location far from the GDL centre and at the liquid water break-through point was more effective at reducing liquid water saturation. Experimental work on MPS perforation has fallen out of trend recently; however, the recreation of this study experimentally with water visualisation, i.e. by employing synchrotron X-ray radiography or X-ray computer tomography, would prove beneficial in terms of optimisation of the GDL design.

2.3. *Alternative MPS materials*

2.3.1. *Graphite*

Natural graphite has been explored as an additive to the MPS in order to enhance its electrical conductivity, density and mechanical strength. For example, Kaushal et al. [37] added natural graphite to

polyacrylonitrile fibres before carbonisation at 1800 °C, forming carbon fibres with increased bulk density, and lower in-plane electrical resistivity (from 6.7 vs 5.3 mΩ cm). Additions of graphite were 0.25, 0.5, 0.75, 1.0 and 1.5%, where fuel cell power density increased with graphite concentration, up to 563 mW cm^{-2} at 1.0 wt%. Graphite loading higher than this decreased the power density. Greater improvements could be seen if e.g. the graphitisation temperature were further increased to improve the conductivity, but this would increase the cost of manufacture.

Another innovation by Gurau et al. [38] used flexible graphite sheets produced from expanded graphite flakes. These were perforated to produce a flexible, macroporous graphite-based MPS, with high electrical and thermal conductivity, and low contact resistance compared to a conventional carbon fibre GDL. The perforation densities of up to 10, 000 holes per 6.5 cm^{2} and porosities of between 0.05% and 35% could be varied simply by altering the tooling geometry, thus optimising the porosity and pore size distribution for PEMFC operation. Larger porosity and lower density of perforations were reported to result in the highest power densities. Whilst this is an interesting concept, providing an easy way to introduce macropores into arbitrary substrates, the results were not compared with conventional GDLs, making it difficult to assess the usefulness of this innovation.

2.3.2. *Carbon nanotubes (CNT)/single wall carbon nanotubes (SWCNT)/ multi wall carbon nanotubes (MWCNT)*

Carbon nanotubes are useful materials for use in GDLs due to their large aspect ratio, excellent electrical conductivity (10^{6}–10^{7} S cm^{-2}), high thermal conductivity, and high strength/stiffness (>100 GPa and 1.2 TPa, respectively) [39–43]. The large aspect ratio of carbon nanotubes means that they can form free-standing membranes (known as buckypaper), without the need for a binder. Many research groups have explored carbon nanotubes as electrode materials in PEMFCs, but this has been largely limited to the electrocatalyst layer and the microporous layers [44–46]. A smaller amount of research has been conducted into the fabrication of carbon nanotube based MPSs.

For example, Tang et al. [44] produced a porous buckypaper via vacuum filtration of single wall carbon nanotubes (SWCNTs), and applied this as a gas diffusion electrode in PEMFCs, in comparison with conventional carbon cloth (ELAT®). Although innovative in design, the buckypaper resulted in much lower membrane electrode assembly (MEA) performance (despite being much thinner), and the polarisation curve exhibited significant fluctuation. This may be partly due to the much smaller pore size in SWCNTs (i.e. nanometer scale), compared the macroporous structure of conventional gas diffusion electrodes. However, the polarisation curve suggests that the activation region and the ohmic region are responsible for most of the voltage drops. This suggests that the SWCNT layer negatively affects catalyst utilisation, and that the contact resistance may be much higher (e.g. due to the lack of interpenetration between the electrocatalyst layer and the gas diffusion electrode).

Maheshwari et al. [46] also fabricated freestanding gas diffusion electrodes for PEMFCs, in this case from multiwall carbon nanotubes (MWCNTs) with different aspect ratios. As shown in Fig. 4, the buckypapers made from longer MWCNTs (referred to as B in Fig. 4) with larger diameter had the better PEFC performance (~60 mW cm^{-2}). This poor performance of smaller MWCNTs (~35 mW cm^{-2}) was attributed to the broader and uneven pore size distribution, and to the higher electrical resistance compared to the larger MWCNTs. Interestingly, a composite gas diffusion electrode comprising a layer of smaller MWCNTs on top of a layer of larger MWCNTs (referred to as D in Fig. 4) produced the highest power density (110 mW cm^{-2}). This more closely approximated the pore size distribution of conventional GDLs, with the smaller MWCNTs acting as the MPL, and the larger MWCNTs acting as the MPS.

Meanwhile, Gao et al. [47] produced a sintered carbon paper composite, fabricated from carbon nanotubes, polyacrylonitrile based carbon fibre, and PTFE. In a direct methanol fuel cell (DMFC) the

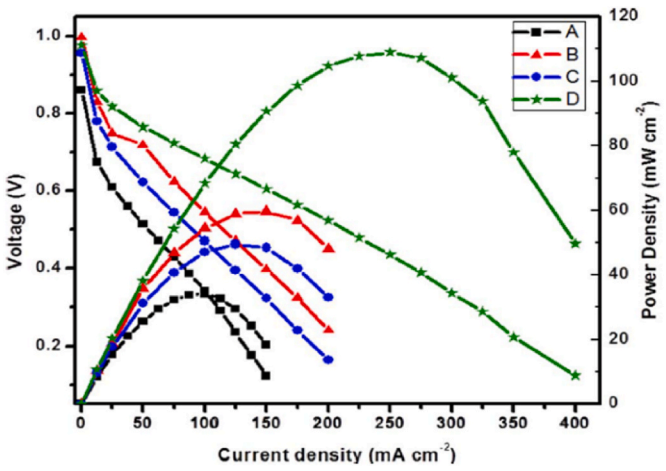

Fig. 4. Polarisation curves of gas diffusion electrodes fabricated from MWCNTs with: (A) 20–30 nm diameter and ~1.5 μm length, (B) 80–120 nm diameter and >500 μm length, (C) MWCNT (A) layered on top of MWCNT (B), and (D) MWCNT (A) layered on top of MWCNT (B). © The Electrochemical Society. Reproduced by permission of IOP Publishing. All rights reserved [46].

CNT-based MPS exhibited a higher maximum power density (76 mW cm^{-2}) than an MPL coated conventional Toray 060 GDL (60 mW cm^{-2}) at lower current densities (<400 mA cm^{-2}) which was attributed to the wider pore size distribution and higher porosity of the composite. Several other groups have performed similar studies. For example, Deng et al. [48] fabricated a MWCNT -based MPS, which demonstrated a 45% higher maximum power density (23.2 mW cm^{-2}) than an MPL coated commercial TGP-H-090 (16.2 mW cm^{-2}).

2.3.3. *Biomass-based carbon fibres*

Other research groups have attempted to reduce the cost of the MPS by fabricating them from more sustainable materials, such as cellulose [49,50], bamboo [51,52], coconut fibres [53,54], and other biomass-derived carbons. For example, Destyorini et al. [53] fabricated an MPS using activated carbon powder and carbon fibre derived from coconut coir, mixed with an ethylene vinyl acetate (EVA) as a binder, polyethylene glycol (PEG) as a dispersant, and PTFE as the hydrophobic agent. SEM micrographs of the cross-sections of the GDL substrates are shown in Fig. 5 (where (a),(b) and (c) are the carbon powder, carbon fibre and Toray TGP H-120 respectively). The electrical conductivity was much lower (1.53 S cm^{-1}) compared to a Toray TGP-H-120 carbon paper (4.5 S cm^{-1}). However, the porosity, average pore diameter, and water contact angle were comparable. The maximum PEMFC power density achieved was 168 mW cm^{-2}, compared with 208 mW cm^{-2} for the Toray carbon paper. They attributed this to the much lower surface area (~15 vs 214 m^{2} g^{-1}), but due to theclear difference in the ohmic region on the polarisation curve, it likely to be due to the lower electrical conductivity.

Ghobadi et al. [49] mixed carbon fibre with cellulose as a binder in a wet-laying process to produce an MPS, the cellulose was then removed by phase inversion using an ionic liquid, and the substrate was then sprayed with graphene nanoplates to increase conductivity and hydrophobicity. The carbon fibre content was varied (20, 40, 60 and 80% wt.) as was the volume of ionic liquid used for cellulose removal (20, 50 and 70% v.) SEM micrographs of the composite papers with different volumes of ionic liquid and carbon fibre (Fig. 6) show the cellulose content of the surface structure. Fig. 6 (b) shows clumps of cellulose covering the carbon fibre network and pore space, whereas it is not visible in Fig. 6 (c). The electrical conductivity of the papers increased with carbon fibre weight, where the 80% wt, carbon fibre MPS was comparable to the measured AvCarb MGL190 at (4.5 S m^{-1} and 4.95 S m^{-1} respectively). This carbon fibre/cellulose-based substrate was able to achieve an

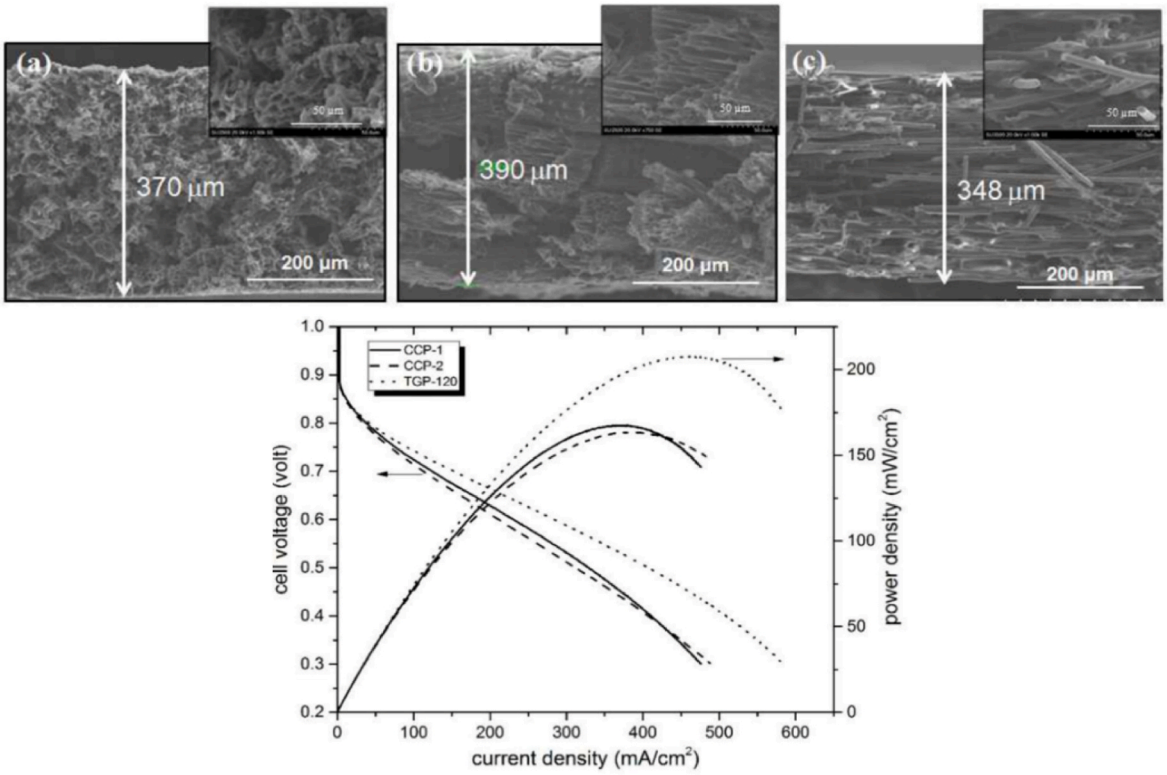

Fig. 5. SEM cross sectional images of the GDL (a) CCCP1-80% carbon powder (b) CCCP2- 70% wt. coconut fibre and 10% wt. carbon powder and (c) Toray TGP-120. The polarisation curve showing power density, voltage and current density. Reproduced with permission from The Journal of Engineering and Technological Sciences [53].

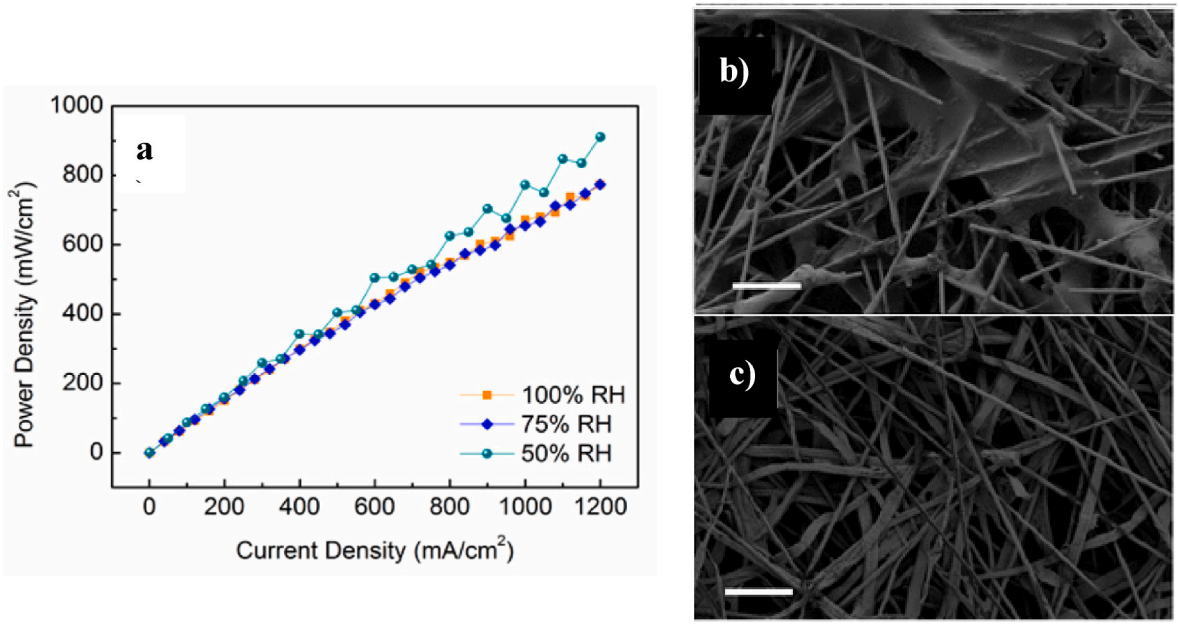

Fig. 6. (b)Power density vs. current density for the 80:20 carbon fibre: cellulose MPS. SEM images of the composite papers with different volumes of ionic liquid (d) 50% v. ionic liquid and 80% carbon fibre (f)70% ionic liquid and 60% carbon fibre. Reprinted with permission from ACS Sustainable Chemistry & Engineering. Copyright (2017) American Chemical Society [49].

impressive 911 mW cm^{-2} at 1200 mA cm^{-2} and 50% relative humidity. However, at 75 and 100% relative humidity, the performance dropped significantly. This was attributed to the hydrophilic nature of the cellulose binder. Wet proofing the cellulose based MPS with a "green" alternative to PTFE was proposed to improve the performance at high relative humidity.

Similarly, Kaplan et al. [50] also experimented with a cellulose-based MPS, with varying amounts of carbon fibre. These were hot pressed, and no MPL was used. An optimal ratio of 70:30 carbon fibre to cellulose had the lowest resistivity and high strength, as well as

pore size distribution similar the conventional AvCarb®MG GDL. In PEMFC polarisation tests conducted at 50 °C the carbon fibre/cellulose based macroporous substrate had a similar performance to the commercially-used AvCarb®MG GDL, featuring relatively low ohmic and mass transport losses in low-voltage region. However, at 60 °C, the performance with fibre/cellulose based MPS was notably worse than that with AvCarb®MG GDL. The authors did not provide an explanation on why the results were different at different temperatures; however, this could be attributed to the superior thermal conductivity of AvCarb®MG GDL that allows for larger heat dissipation at elevated temperatures and subsequently larger level of membrane hydration compared to fibre/cellulose based macroporous substrate.

2.3.4. Pitch-based carbon fibres

Recently Heo et al. [55] fabricated a GDL substrate from a composite of carbon black, pitch-based carbon fibre, and phenolic resin binder. Pitch was used because it is a low-cost waste product. The GDL substrates were carbonised at <800 °C in order to reduce the energy intensity of the production process, and the effect of the carbonisation temperature on the conductivity and porosity was compared. As expected, carbonisation at a higher temperature increased the conductivity significantly. A porosity of 82.6% and a water contact angle of 117.57° were achieved. However, PEMFC measurements were not conducted.

2.3.5. Aerogels

Sodium-carbon aerogels have been investigated as gas diffusion media [56,57]. Glora et al. [56] produced a carbon aerogel with a large surface area and meso-porous pore volumes for gas transport; they reported an electronic conductivity of 28 S cm^{-1} in an 80% porous GDL of <500 μm thick. Wang et al. [57] also researched aerogels; their fabrication method of pyrolysis led to large variation in GDL porosity potentially resulting in large discrepancies in mass transport properties and fuel cell operation. Trefilov et al. [58] fabricated a hybrid graphene-carbon xerogel dual-layer GDL with a gradually decreasing porosity through its profile. Their methodology allowed for a controllable structure, where the centrifugal speed during xerogel formation determined the microstructure, pore size and porosity. As can be seen from the polarisation curves (Fig. 7), increasing the centrifugal speed in aerogel fabrication increased the power density of the GDLs (0 G force:0.07 W cm^{-2}, 125 G force: 0.11 W cm^{-2} and 250 G force: 0.14 W cm^{-2}), which was attributed to the lower porosity and increased bulk density of the aerogel which meant it accumulated liquid water less readily. The addition of graphene layers improved the conductivity and mass transfer of the xerogel.

Although aerogels offer an exciting means of producing the macroporous substrates, the method of fabrication is are, compared to the current materials and methods, less attractive for large scale production on fuel cell manufacturing; the current materials and fabrication methods are more cost-effective and/or simpler.

2.3.6. Metal foams

Conventional carbon-based GDLs suffer severe corrosion in PEMFC cathodes due to start-stop potential cycling at high voltage (~1.5 V),

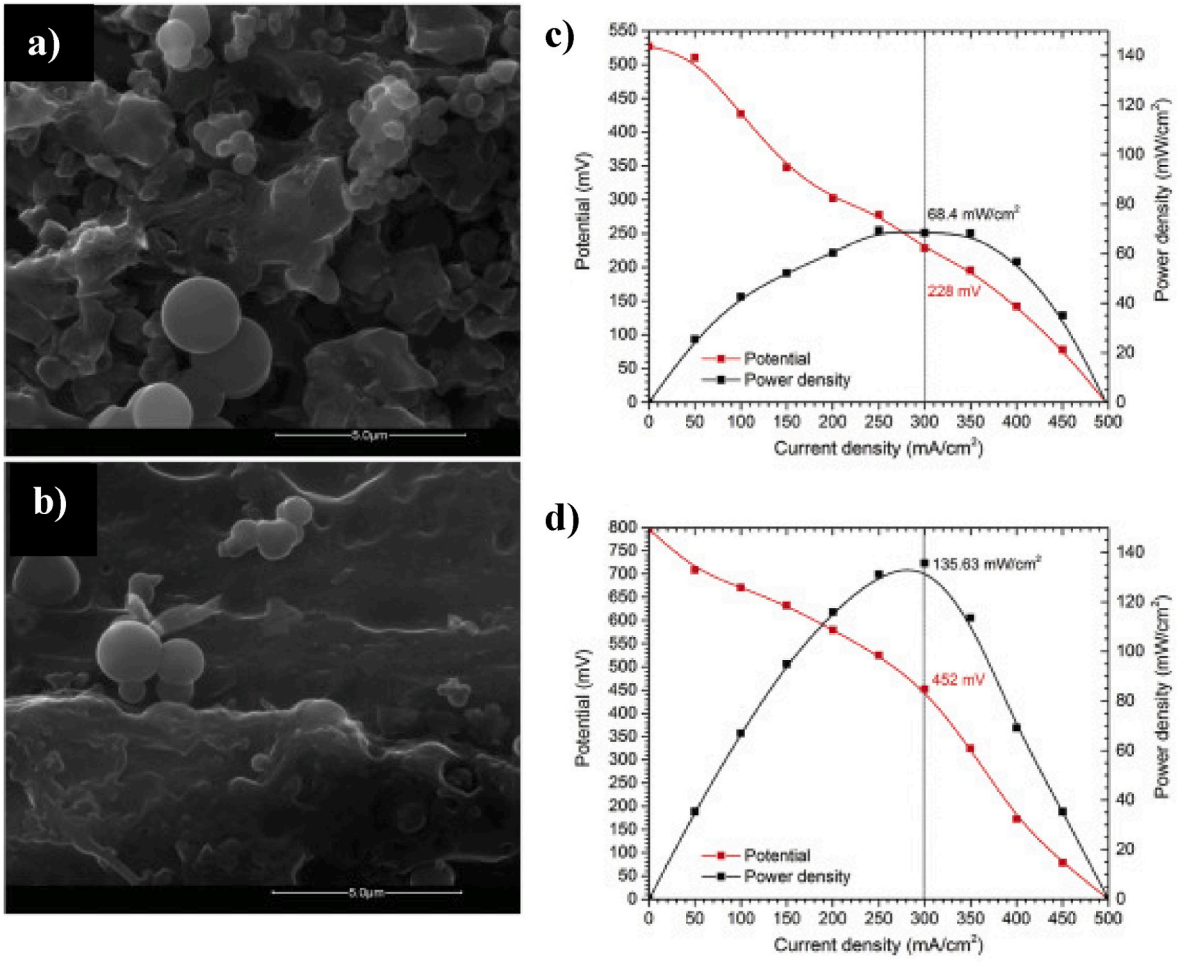

Fig. 7. (Left) SEM images of composite xerogel (a) 0 G centrifuged (b) 250 G centrifuged. (Right) Polarisation and power density curves for xerogels (c) 0 G centrifuged (d)250 G centrifuged. Reproduced with perimission from Elsevier [58].

limiting the durability. In addition, mechanical degradation of the GDL occurs due to compression within the membrane electrode assembly (MEA). The development of a carbon-free GDL could therefore improve the durability, simplify the manufacturing process, and reduce the cost. One tactic is to produce GDLs from metal-based materials which are mechanically stable, have relatively high thermal and electrical conductivity, and can be machined into a desired structure. Titanium metal has been explored as a gas diffusion electrode by various groups [59–63]. Various attempts to fabricate metal-based carbon-free GDLs are discussed in the following sections.

Foams are defined as a gaseous phase uniformly dispersed inside a solid or liquid phase; where metallic foams have been produced from a wide variety of metals including titanium, aluminium, magnesium, copper, zinc and nickel [64]. Their use encompasses biomedical applications, such as tissue engineering [65]; construction materials, for thermal and sonic insulation; and as an impact absorber in vehicular transportation [66]. Lightweight metallic foams made from titanium and aluminium are the most applicable for use in the PEMFC, being strong, highly porous materials with high corrosion resistance and minimal ion leaching. The most desirable aspect of this material is the tunability of the physical structure produced by alteration of the manufacturing parameters and foaming material used, as such the pore size, structure and distribution can be modified, as seen in Fig. 8 (a) and (b) where metallic foams produced from aluminium with a varying number of pores per square inch (6.5 cm^2) were produced. The open pore structure of the foam can be seen in the SEM image (Fig. 8 (c)) [67].

Previous works have demonstrated the validity of metal foams in fuel cell engineering as a flow-field plate [68,69], however the physical properties of metal foams make them highly applicable as the gas diffusion substrate. They possess not only good material characteristics of metals (high electrical and thermal conductivity, weldability and plasticity) but have architectural advantages such as tuneable pore structure and permeability, and high specific surface area [70]. Moreover, some metallic foams (e.g. nickel foams) have adequate corrosion resistance that allows them to be directly used in PEMFCs without the need for applying protective corrosion-resistance coatings to them.

Choi et al. produced a flexible titanium foam GDL with a controlled pore structure from freeze casting [60] which was used as the anodic GDL in a polymer electrolyte fuel cell. The single cell measurements not only exhibited a higher current density than those using the commercial carbon GDLs for the anode, (462 mA cm−2) and (278 mA cm−2) respectively at 0.7 V, but also incurred minimal loss in weight and thickness in accelerated corrosion tests, unlike the commercial GDLs. Their work signifies the potential application of metal foams for the anodic GDL in PEMFC; further research should undertake using their freeze-casting and alternative methodology to produce similar metallic foams from different metals. Fig. 9 shows a comparison of the pore size distribution in the titanium foam anode GDL and SGL 35BC GDL determined by MIP. As their methodology enabled the manipulation of pore size and structure, further research could be undertaken to optimise these two characteristics. However, to gain a fuller understanding of the potential of a material it is important that they are tested as the cathodic GDL where the conditions are more corrosive and the reaction kinetics are less favourable.

2.3.7. *Metal-based machined substrates*

The machining of materials is a proficient method to manufacture substrates into a predetermined form and physical structure. Research groups have used machining to produce GDL substrates of varying architectures, including adjustment of pore diameters, pore location and substrate thickness, to optimise GDL design. The majority of this work has been centred on machined metal GDL substrates, silicon has been used for micro-PEMFC applications [71]. Fushinobu et al. [61] micro-machined thin film titanium GDLs, of 5 μm and 20 μm thick, to produce highly durable components for high performance PEMFC applications and concentration overpotential modelling (Fig. 10, (right)). The design parameters of the titanium film were varied on the cathodic GDL, whilst the porosity was kept constant, to see the effect of film thickness, hole diameter and hole patterning on the i-V performance of the MEA. The performance was shown to be extremely varied depending

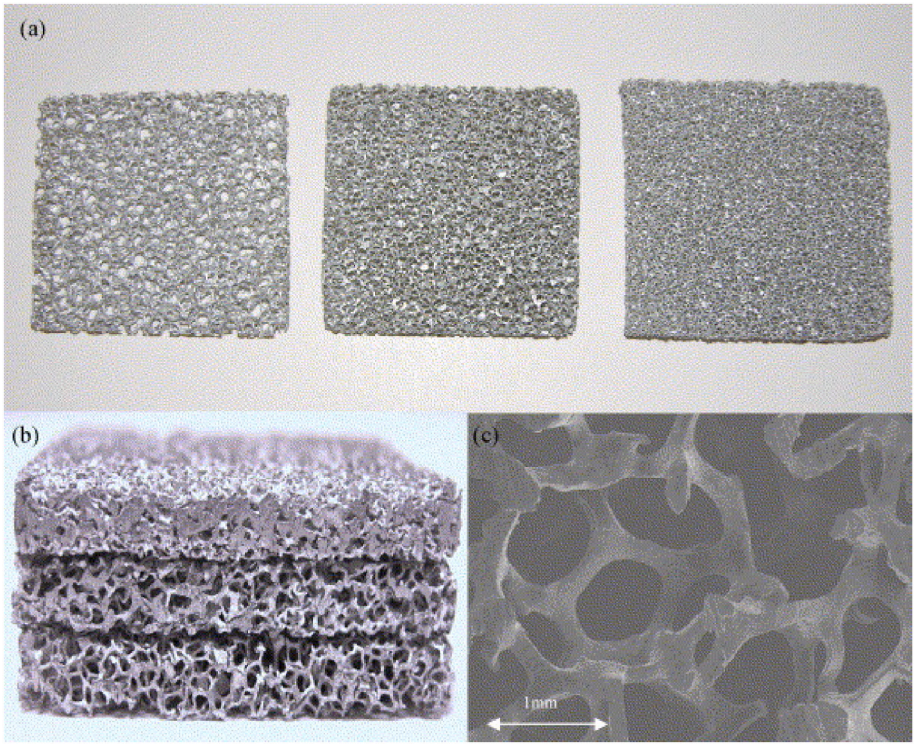

Fig. 8. Metal foams produced. (a) Foams with 10, 20 and 40 pores per 6.5 cm^2 (per square inch, ppi) (b) a cross sectional view (c) SEM image of 20 ppi metal foam with an open pore structure Reproduced with permission from Elsevier [67].

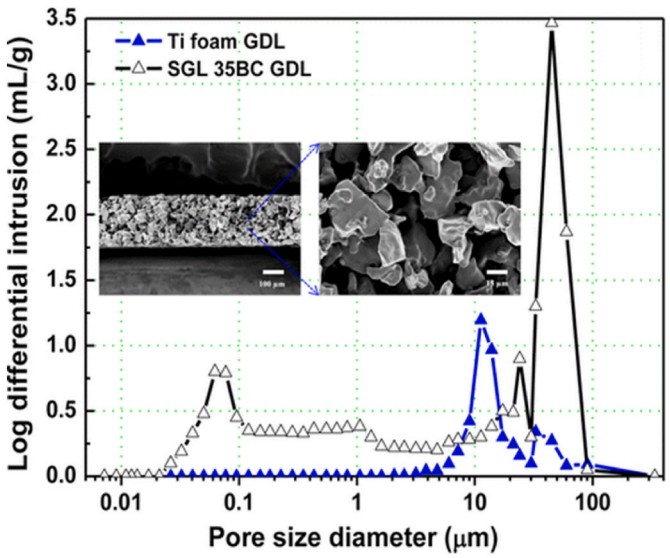

Fig. 9. Pore size distribution in the Ti foam anode GDL (blue line) and SGL 35BC GDL (black line) determined by MIP. SEM images of a cross-section of the Ti foam anode GDL. Reprinted with permission from ACS Appl. Mater. Interfaces. Copyright (2014) American Chemical Society [60].

on the film thickness and the hole diameter, where the thinner film and smaller hole-diameter thickness produced greater power density. The placement of the perforations above the rib as well as the channel further improved cell performance, comparable to the carbon paper GDL in the low current density regions (<350 mA cm^{-2}).

Their work indicates that thin titanium films can be suited for PEMFC gas diffusion media, potentially improving on current carbonaceous materials, however it signifies the importance of well-developed design. Ideally further work would further optimise the design by examination: various hole diameters machined into the same film; smaller hole diameters; thinner films and even more randomised hole distribution models.

Zhang et al. [72] developed a similar porous GDL with improved electrical and thermal conductivity and controlled the porosity using a 12.5 μm thick copper foil with an applied MPL of Vulcan XC-72 (Fig. 10, (left)). Their copper foil substrate had various pore sizes and straight pore profile and when coated measured a contact angle of 152°. Although the Cu GDL exhibited a lower maximum power density (0.45 W cm^{-2}) compared to MPL-coated Toray TGP-H-060 (0.59 W cm^{-2}), the achievable controlled permeability, pore shape, porosity, and surface properties of this method allows for tailored design which will lead to improved reactant and product transport. Other research groups have focused on the use of titanium sinters; Liu et al. [73] used titanium sinters as the GDL in a free-breathing PEM fuel cell, nickel meshes, though for the DMFC.

2.3.8. 3D printed substrates

3D printing is an interesting and novel method to produce microstructured metal sheets for GDL applications. Jayakumar et al. [74] produced a carbon-free nylon-aluminium substrate using 3D printing technology which was infused with graphene to increase electrical and thermal conductivity; it was then compared to the commercial SGL 39 BC. The fabricated GDL exhibited comparable porosity (42%), good tensile strength (≥4 N cm^{-1}), and an excellent thermal conductivity (0.588–0.512 W mK^{-1}). However, it was characterised by a high through-plane resistance resulting in a lower conductivity than the Sigracet GDL. This is attributed to the graphene particles being poorly embedded into the substrate which limited the conductivity of the substrate. 3D printing of substrates offers significant potential as a means of producing GDL substrates with tailored microstructure. However, 3D printing as a technology is currently in its early development. As the technique becomes more widespread, a greater number of materials and thread size would become more available and the technique can be then more easily optimised for MPS designs.

2.4. Summary

The addition of enhancing materials to the GDL such as natural graphite can significantly improve MEA efficiency with very little alteration to the GDL substrate production process. Moreover, the ease of a simplified production process is key to the reduction of manufacturing costs of the GDL and the fuel cell as a whole, thus will make PEMFC more commercially competitive. The idea of cellulose based GDLs and GDLs produced from abundant sustainable biomass material may reduce cost and provide a truly "green" fuel cell. Despite these aspirations, the power density is uncompetitive with the commercial alternatives; therefore, if they are to see any commercialisation as materials, significant research needs to be undertaken to improve the performance before any work can be done to elevate them from the lab-scale.

Non-carbonaceous gas diffusion materials are highly promising, though in their current state they lack the thorough research to elevate them from the research level. Of the materials that have been explored the largest potential seems to lie in metallic foams and aerogels. The desirable characteristics of metals, notably: high electrical conductivity, mechanical strength, wettability and corrosion resistance, make them applicable as a substrate material. However, it is the control over pore size and structure that will lead to significant jumps in the improvement of the fuel cell efficiency and durability. However, metal foams have yet to be tested as the cathodic GDL which is the true test of GDL potential,

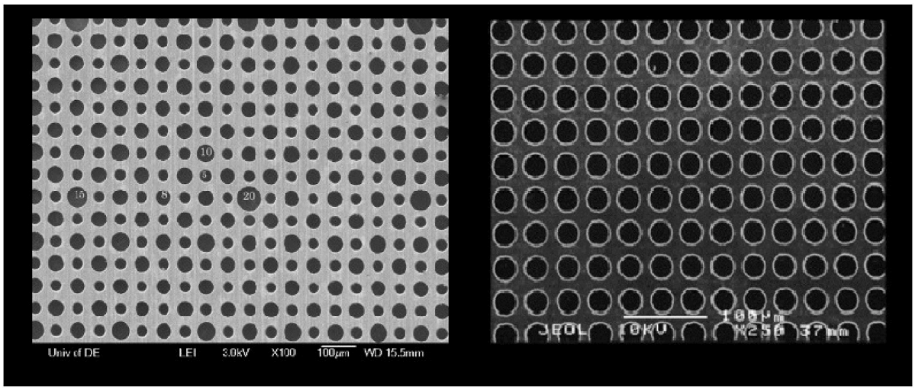

Fig. 10. SEM images of the machined metal GDLs. (Left)Copper foil GDL with varying machined pore sizes produced by Zhang et al. (Right) Ti GDL top view with 25-μm diameter micro through-holes by Fushinobu et al.. Reproduced with permission from Elsevier [72].

due to the potential of water flooding from the ORR.

One area that should not be neglected in the pursuit of novel materials for the macroporous substrate is the effect that compression and fuel cell fabrication via hot pressing of the components on has on these materials and their microstructure. Innovative works have indicated that the temperature of hot pressing [75] and uniformity of the compression [76] is influential in the electrochemical performance of the membrane electrode assembly (MEA) of the fuel cell, and the capability of the GDL for mass and electron transfer.

Table 1 summaries previous investigations into alternative substrate designs and materials (see Table 2).

3. Hydrophobic agents in the macroporous support

As previously discussed in Section 2.1, the hydrophobic treatment of the carbon substrate with PTFE generally has negative effects on the GDL transport properties, including decreased electrical and thermal conductivity, permeability and diffusivity. This has been the motivation for recent research directed at alternative methods of rendering the GDL hydrophobic of which alternative fluorinated polymers have attracted significant attention.

3.1. Conventional binders (PTFE)

The macroporous substrate of the GDL is usually wet-proofed, where it is treated with a coating of polyfluroethylene (PTFE or Teflon™) or fluorinated ethylene propylene (FEP) in order to render it more hydrophobic. This helps prevent flooding of the electrodes due to liquid water generated during the oxygen reduction reaction. Optimisation of the PTFE coating is critical: whilst it reduces flooding, numerous papers have reported negative effects on the GDL characteristics [12,82–86]. For example, PTFE has been shown to affect the microstructure of the GDL by reducing the porosity and altering the pore size distribution [12,87,88], the gas diffusivity [89], and permeability [90,91], as well decreasing the electrical conductivity by increasing the contact resistance [92,93].

The effect of PTFE on the morphology and transport properties of the GDL was investigated at length by Zamel et al. [94] who reported that the overall porosity pore volume decreases as the proportion of PTFE increases. Moreover, they hypothesized that the effect of PTFE depends on the initial pore size: the microporous volume did not change for micropores $\leq$3 μm after PTFE impregnation, whereas significant reduction in the macropore volume was observed for a pore radius $\geq$5 μm. Whilst some studies have indicated that permeability decreases with increasing PTFE loading, Ismail et al. [90] found that an optimum amount of PTFE (i.e. 5 wt%) had a positive effect on the through-plane permeability (more than 5 wt% decreased the permeability). El-Kharouf et al. [12] reported from ex-situ characterisation studies that PTFE increased the permeability of some GDLs and decreased it in others. Increased permeability was attributed to a reduction in tortuosity, whereas reduced permeability was attributed to loss of pore volume.

The influence of PTFE on the thermal conductivity of carbon substrates, either in the in-plane [92,94–96] or through-plane orientation [97–99], has also received much attention. Burheim et al. [97] found that an increased amount of PTFE in the GDL results in a slight reduction in the through-plane thermal conductivity. This is in agreement with a model created by Yablecki and Bazylak [100] and Fishman and Bazylak, and attributed to the insulating effect of PTFE (which has much lower thermal conductivity than carbon) preventing fibre-to-fibre contact in the through-plane direction. Meanwhile, in the in-plane orientation, heat transfer occurs directly along the carbon fibres and the in-plane thermal conductivity is largely unaffected by PTFE impregnation (as reported by Sadeghifar et al. [96]), Whereas in the in-plane direction heat is transferred along the fibres, and the addition of PTFE reduces the contact resistance between the fibres and increases conductivity. This was observed by Sadeghifar et al. [96] who used modelling and

Table 1
Summary of the investigations into alternative architectures and materials for the gas diffusion layer substrates.

Author.	Description	Peak Power Density (W cm^{-2})[a]	Main Findings
Chevalier et al. [24,25]	Electro spun carbon fibre substrate	0.50 (oxidant: air)	• Carbon fibre diameter and pore size shown to reduce flooding. • Smallest fibre diameter and small fibre reduce flooding. • Membrane dry-out reduced when fibre alignment perpendicular to channels.
Hung et al. [77]	Melt spun carbon fibre and with phenolic resin (10% wt.)	0.48	• Melt-spun and electro-spun carbon fibres compared as GDL. • 400 nm fibre diameter-too microporous for two-phase flow through substrate. • 10 % wt. optimal phenolic resin; improves conductivity but reduces permeability.
Kaushal et al. [37]	Non-woven PAN carbon fibre paper doped with natural graphite (1% wt.).	0.56	• Optimum power density produced at 1% wt. natural graphite (NG) inclusion, up to 1% power density increased. 1.5 % wt. NG power density decreased. • 1 % wt. NG increased power density (361 mW cm^{-2} to 563 mW $cm^{-2)}$. • 1 % wt. NG: best PSD for reactant diffusion and liquid water transport.
Maheshwari et al. [46]	MWCNT bucky paper formed by vacuum filtration of MWCNT dispersion.	0.11	• Substrates prepared from MWCNT of different diameters and lengths. Bi-layered GDLs were formed from one layer of MWCNT on top of the other. • High purity MWCNTs improved electrical conductivity and power density. • Small MWCNT GDL; too microporous for two-phase flow (45% $>$ 25 nm). • Bi-layered GDL: more uniform PSD. Highest power density from small MWCNT on larger (0.11 W cm^{-2}), small MWCNT (0.03 W cm^{-2}) and large (0.06 W cm^{-2}).
Kaushal et al. [78]	Non-woven carbon fibre paper with MWCNT grown by CVD (1% wt.)	0.59	• Comparison of addition of MWCNT to carbon paper: slurry and grown by CVD. • CVD method: higher power density: surface area, electrical conductivity (from 66 S cm^{-1} to 175 S cm^{-1})

(continued on next page)

Table 1 (*continued*)

Author.	Description	Peak Power Density (W cm^{-2})[a]	Main Findings
			and flexural modulus (from 5 GPa to 20 GPa).
Hung et al. [79]	Carbon felt composite paper produced from felt and phenolic resin (15% wt. resin). 1400 °C carbonisation.	1.01	• Substrate from oxidised fibre felt and phenolic resin (5,10,15,20 and 25% wt.) • Carbonisation temperature from 700 °C to 1000 °C reduced the resistivity (from ~13,000 Ω cm to ~130 Ω cm) from increased resin crystallinity. • Permeability and through-plane resistivity reduced with increased phenolic resin. • Mass power density at 15% wt. phenolic resin and 1400 °C (1.01 W cm^{-2}).
Ghobadi et al. [49]	Flexible carbon fibre and cellulose substrate with graphene MPL	0.911 (50% RH)	• Cellulose/carbon fibre papers. Graphene coated (conductivity hydrophobicity). • Carbon fibre (20, 40, 60 and 80% wt.) and ionic liquid (20, 50 and 70% v.) varied. • 10% wt. graphene surface coating increased contact angle from 90° to 127°. • Highest electrical conductivity and power density (0.911 W $cm^{2)}$ from 80% wt. carbon fibre and 70% ionic liquid used for the removal of cellulose.
Kaplan et al. [50]	Hot pressed, wet laid composite paper from carbon fibre (70%) and cellulose (30%).	N/A	• Carbon and cellulose fibre substrate from wet laying and 150 °C hot pressing. • Electrical resistivity increased with cellulose. Lowest resistivity observed with 78% carbon: (0.0095 Ω cm comparable to AvCarb: 0.0062 Ω. cm). • 70% carbon GDL: best mechanical strength, electrical resistivity and PSD. Comparable power density at 50 °C, especially mid-current densities.
Destyorini et al. [53]	Carbon composite sheet derived from pyrolyzed coconut coir.	0.17 (55% RH)	• Carbon fibre and powder composite from pyrolyzed coconut coir and ethylene vinyl acetate (binder- 20% wt.). CCP1: 80% carbon powder. CCP2: 70% wt. coconut fibre and 10% wt. carbon powder • Electrical conductivity of composite GDLs was much lower than the commercial (CCP1: 0.50 S cm^{-1}, CCP2:1.53 S cm^{-1}, Toray TGP 120: 4.50 S cm^{-1}).
Kinumoto et al. [51]	Bamboo fibre sheet carbonised at 3000 °C.	0.15 (64% RH)	• Bamboo-derived cellulose sheets with PVA binder, carbonised at 3000 °C. • Electrical conductivity increased with carbonisation temperature (1000 °C: 134 S m^{-1}, 3000 °C 534 S m^{-1}) and PVA addition (854 S m^{-1}). • Degradation test in sulphuric acid at 150 °C for 300-h. PVA increased stability. • PVA increased power density from 0.14 W cm^{-2} to 0.15 W cm^{-2}.
Glora et al. [56]	Carbon aerogel from reinforced carbon (<500 μm thick)	0.09 (50% RH) (oxidant: air)	• Carbon fibre-reinforced carbon aerogel from pyrolysis with argon at 1000 °C. • No aerogel shrinkage with carbon fibre fleece support. PAN samples shrank 20%.
Trefilov et al. [58]	Tri-layered graphene-carbon xerogel GDL	0.14 W (80% RH) (oxidant: air)	• Tri-layered GDL: Toray TGP-H-120, carbon xerogel and carbon black MPL. • Increasing the centrifugal speed in aerogel fabrication increased the power density (0 G force:0.07 W cm^{-2}, 250 G force: 0.14 W cm^{-2}). • Lower porosity and density of 250 G GDL led to less liquid water saturation.
Fushinobu et al. [61]	Micro-machined thin film titanium (5 μm and 20 μm thick)	0.91 (50% RH)	• The design parameters of micro-machined titanium film were altered in terms of hole patterning, hole diameter and film thickness. • Decreasing the through-hole diameter increased the cell performance.
Zhang et al. [72]	Perforated copper foil (12.5 μm thick) with MPL made up from Vulcan XC-72 carbon black.	0.45 (oxidant: air)	• Straight pore profile of the copper foil restricts the in-plane reactant transport, limiting reaction area. Perforations over rib improve reactant access to the CL • Alteration of perforation shape improves mass transport and two-phase flow.
Jayakumar et al. [74]	3D printed substrate from nylon filled with aluminium dust. Coated with graphene.	0.20	• Highly anisotropic porous GDL with non-uniform surface conductivity.

(*continued on next page*)

Table 1 (*continued*)

Author.	Description	Peak Power Density (W cm^{-2})[a]	Main Findings
			• High through-plane ohmic resistance (130 Ω m) (12 Ω m: SGL 39BC). • Comparable thickness (290 μm) to SGL 39BC (325 μm).
Jayakumar et al. [80]	3D-printed substrate from nylon filled with titanium dust.	0.10	• 80% polyamide and 20% titanium had best conductivity and mechanical strength. • Thermal conductivity (0.59 W m^{-1} K^{-1}) twice that of SGL 39BC (0.25 W m^{-1} K^{-1}). • In-plane electrical conductivity (≤10 S cm^{-1}) lower than SGL 39BC (170 S cm^{-1}). • Maximum power density (<0.1 W cm^{-2}) much lower SGL 39BC (0.5 W cm^{-2}).
Hottinen et al. [62]	0.5 mm thick titanium sinter coated with 5 nm platinum sinter	0.13 (0% RH)	• Titanium sinter substrate, comparable porosity to SGL10-BB (55% porosity). • Ti sinter GDL leads to much lower performance than the SGL10-BB due to much higher contact resistance between the Ti sinter and the MEA. • Platinum coating of sinter reduced contact resistance between the Ti sinter and the MEA by over 50%. Coating Ti sinters with carbon black mitigates water flooding.
Choi et al. [60]	Titanium Foam GDL produced from freeze casting	0.32 (oxidant: air)	• Pore size distribution of the Ti foam is between 10 and 50 μm. • Higher current density at 0.7 V with Ti anode GDL (426 mA cm^{-2}) than with SGL 35 BC (375 mA cm^{-2}) and Toray TGP H-60 (278 mA cm^{-2}). • Under accelerated corrosion testing, Ti foam GDL showed a negligible mass loss of 0.4% compared to SGL 35BC (−3%) and minimal change in thickness.
Jo et al. [81]	Nickle foam used as anodic GDL.	0.40	• Nickle foam anodic GDL produced a higher power density (0.42 W cm^{-2}) than Toray TGP H-60 (0.36 W cm^{-2}). • Nickle foam had low durability; it completely dissolved in a weak sulphuric acid solution in 48 h. Could be improved by alloying with copper.

[a] Unless otherwise states, the maximum power density was reported with 100% RH and oxygen as an oxidant.

experimental observations to show that the in-plane thermal conductivity does not decrease with PTFE loading. Electrical conductivity is another important parameter that can be affected by PTFE coating. Zamel et al. [94] modelled the effective electrical conductivity in carbon paper GDLs, but disregarded the effect of PTFE loading. Mathias et al. [2] reported the effect of PTFE loading on the through-plane contact resistance. They found that when the GDL was treated with 3.5% PTFE, the electrical conductivity increased. Meanwhile, Ismail et al. [83] analysed the effect of PTFE loading on the through-plane and in-plane electrical conductivities of the GDL. They found that the in-plane conductivity increases almost directly proportional with the PTFE loading. In addition, they reported an anisotropy of a factor of 2 with the in-plane conductivity.

3.2. *Perfluoropolyether (PFPE)*

Perfluoropolyethers (PFPEs) offer an appealing alternative to PTFE as a hydrophobic coating, as they are thermally and chemically stable and have high hydrophobicity. Moreover, they are liquid in physical form, resulting in easy deposition and high gas permeability when applied to the GDL [101]. In-situ tests show that cell performance is improved when PFPE is used over PTFE, particularly at higher current densities where liquid water saturation and mass transport losses dominate [102,103]. The high surface area and high porosity of carbonaceous materials allows the PFPE to successfully bind the carbon fibres/particles whilst maintaining a degree of contact between them. As shown in Fig. 11, the Perfluoropolyether coating is highly homogenous compared to PTFE, in which webbing is clearly observed between the fibres, detrimentally affecting the porosity.

There are two main types of perfluoropolyethers that have been used as alternatives for PTFE: neutral PFPEs, and functionalised PFPEs. Neutral PFPEs are often used as coating agents and have the benefit of ease of application, where they can be easily adsorbed onto the substrate and cover the surface. Functionalised PFPE form bonds with the substrates via oxygen-containing moieties on the carbonaceous surface. Whilst neutral PFPE can be applied to the GDL relatively easily, carbon fibre functionalised with PFPE offers greater stability due to the covalent bonding rather than physical adsorption. A greater contact angle can also be achieved by the use of functionalised PFPEs [104]. Functionalised PFPEs are obtained from the thermal decomposition of peroxide PFPEs.

The typical structure of a peroxide PFPE is as follows:

$$T\text{-}(CF_2CF_2O)_m(CF_2O)_n(O)_v\text{-}T'O$$

where T and T′ are trifluoromethyl ($–CF_3$), and acyl fluoride (e.g. –C(O)F or $–CF_2C(O)F$) terminal groups [102]. The thermal decomposition of peroxide PFPEs breaks the peroxide moieties, generating oxygen-centred radicals. These oxygen radicals then decompose into carbon-centred radicals which can link to unsaturated structures without a hydrogenated spacer, such as the carbon fibre surface in the GDL, thus creating a stable binder. This is the reason for the larger contact angle that can be achieved with linked PFPEs. The chemical linkage of PFPE with the carbon fibre can be up to 1% wt.; corresponding to near complete surface coverage (>95%). The main drawback of this method is that it requires exclusively fluorinated solvents and the process of application requires heat treatment. As such the process is more complicated than when functionalised PFPEs are used.

When heated, a portion of the functionalised perfluoropolyethers bonds to the carbon substrate, and the remainder flows across the surface [104]. Two commonly used functionalised PFPEs, namely Fluorolink P56 and Fluorolink TLS, have been explored in GDLs. Stampino et al. [103] investigated commercial carbon cloth GDLs in different PFPE dispersions. They found that at high relative humidity (80–100%) and current density, PFPE with lower molecular weight (i.e. P56) outperformed the higher molecular weight PFPE (i.e. TLS), due to improved

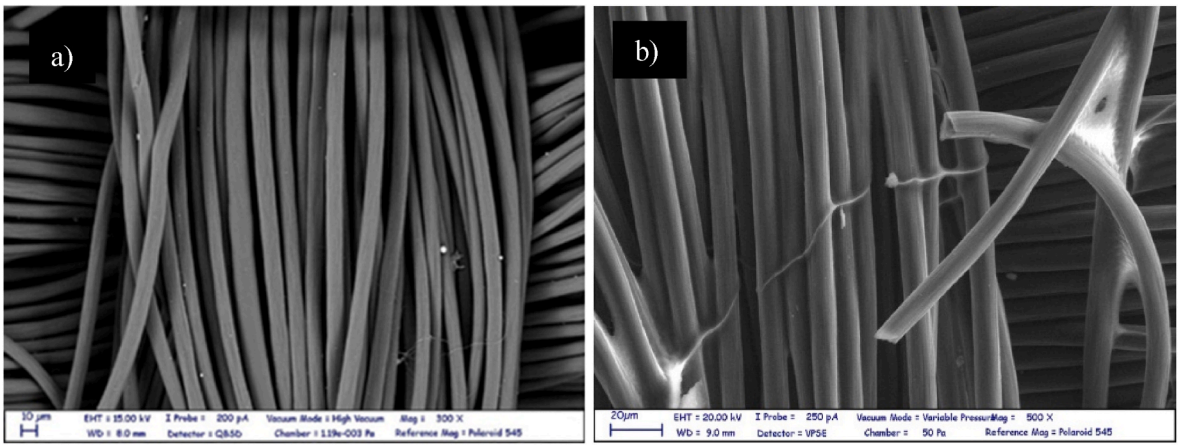

Fig. 11. SEM images of PFPE-functionalised sample (a), and GDL treated with 10%wt PTFE (b). Webbing between carbon fibres is clearly visible in the case of PTFE. Reproduced with permission from Elsevier [104].

water management (and thus enhanced mass diffusion), as confirmed by impedance spectroscopy. Both materials have similar contact angle (147° and 141°), so this was not a major factor in the difference in performance. SEM imaging revealed that P56 was able to bind individual fibres without significantly modifying the GDL microstructure [103].

Gola et al. [105] treated GDLs with the PFPE peroxide Fomblin®, followed by thermal treatment. The contact angle was much higher (171°) compared to the case of PTFE (148°). SEM images revealed webbing between fibres in the case of PTFE, but in the case of PFPE the coating was uniform, leading to improved porosity and the mass transport. Moreover, they reported that replacing a 10 wt% PTFE-based GDL with a 1 wt% PFPE-based GDL improved the fuel cell current density by ~20% as can be seen in Fig. 12.

3.3. Polyvinylidene fluoride (PVDF)

PVDF (polyvinylidene fluoride) has also been considered as a viable alternative to PTFE due to its high chemical stability, thermal resistance, and hydrophobic properties. For example, Cabasso et al. [106] fabricated a GDL with controlled pore size and porosity by using phase inversion of PVDF and carbon blends. PVDF was shown to be a much better binder for carbon black particles than PTFE, providing a suitable support for the electrode. The improvement was attributed to the insolubility of PTFE, resulting in inhomogeneous dispersions and thus non-uniform binding of the carbon particles. The majority of research involving PVDF has been limited to the MPL and the catalyst layer, rather than the GDL.

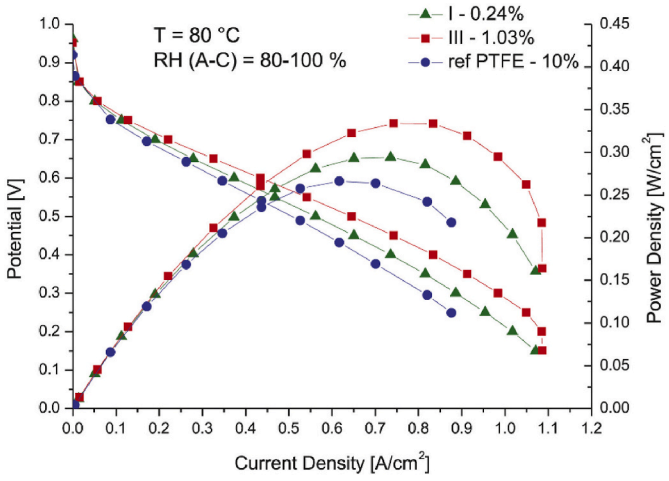

Fig. 12. Polarisation curves of samples I – 0.24% PFPE, III – 1.03% PFPE and (PTFE – 10%) 80 °C and 80–100% RH. Reproduced with permission from Elsevier [105].

3.4. Plasma and alternative hydrophobic materials

Various research groups have investigated how to promote hydrophobicity with materials which are dissimilar to PTFE. Salahuddin et al. [107] attempted a new design by applying commercially available "Ultra Ever-Dry Solution" (Ultra-Tech International Inc.) to carbonised polyacrylonitrile fibres. Their experiment indicates that commercial, cheap and readily available alternatives to fluorinated polymers can be found. Alternatively, Pai et al. [108] used a CF_4 plasma to fluorinate the surface of a carbon cloth substrate, to produce a GDL with a contact angle of 132.8° (Fig. 13 (right)). The measured power density was much greater than for the 10% PTFE treated GDL (0.03 W cm^{-2} and 0.0175 W cm^{-2}, respectively), although the contact angle and through-plane resistance was similar. This was attributed to improved water management and enhanced mass diffusion, since plasma treatment does not hinder the gas transfer pathways in the way that adding a polymer bonder (i.e. PTFE) does.

Silicone materials have also been used successfully to render the carbon substrate superhydrophobic. Wang et al. [109] used a mixture of silica particles and polydimethylsiloxane as a hydrophobic agent for the carbon substrate, resulting in a contact angle of 162° and an increase in peak power density from 0.36 W cm^{-2} to 0.45 W cm^{-2}. Joo et al. [110] produced a superhydrophobic cathode GDL via chemical vapour deposition of polydimethylsiloxane on a carbon paper substrate, increasing the water contact angle from 134 to 150° on the macroporous side (Fig. 13 (left)). However, on the MPL-coated surface the water contact angle was not significantly improved. Despite this, the Si–C coating did lead to improved power output of the received SGL 10BC from 0.30 W cm^{-2} to 0.40 W cm^{-2}. From this we can deduce that improving the non-catalyst facing side of the cathode will improve PEMFC efficiency by maintaining the flow gradient of liquid water.

Ko et al. [111,112] used plasma deposition of hexamethyldisiloxane (hydrophobic silicone) onto polyacrylonitrile carbon fibres to produce a coated carbon mat with a contact angle of 163° [111]. Later, they applied this same method to an uncoated SGL 10AA, to use as a GDL [112]. The contact angle increased from 135° to 145°, and the membrane electrode assembly current density was improved. The contact angle was not significantly changed compared to PTFE, and the electrical resistivity was lower, however, the results were not compared with the SGL 10AA substrates treated with 5% PTFE, so a fair comparison could not be made.

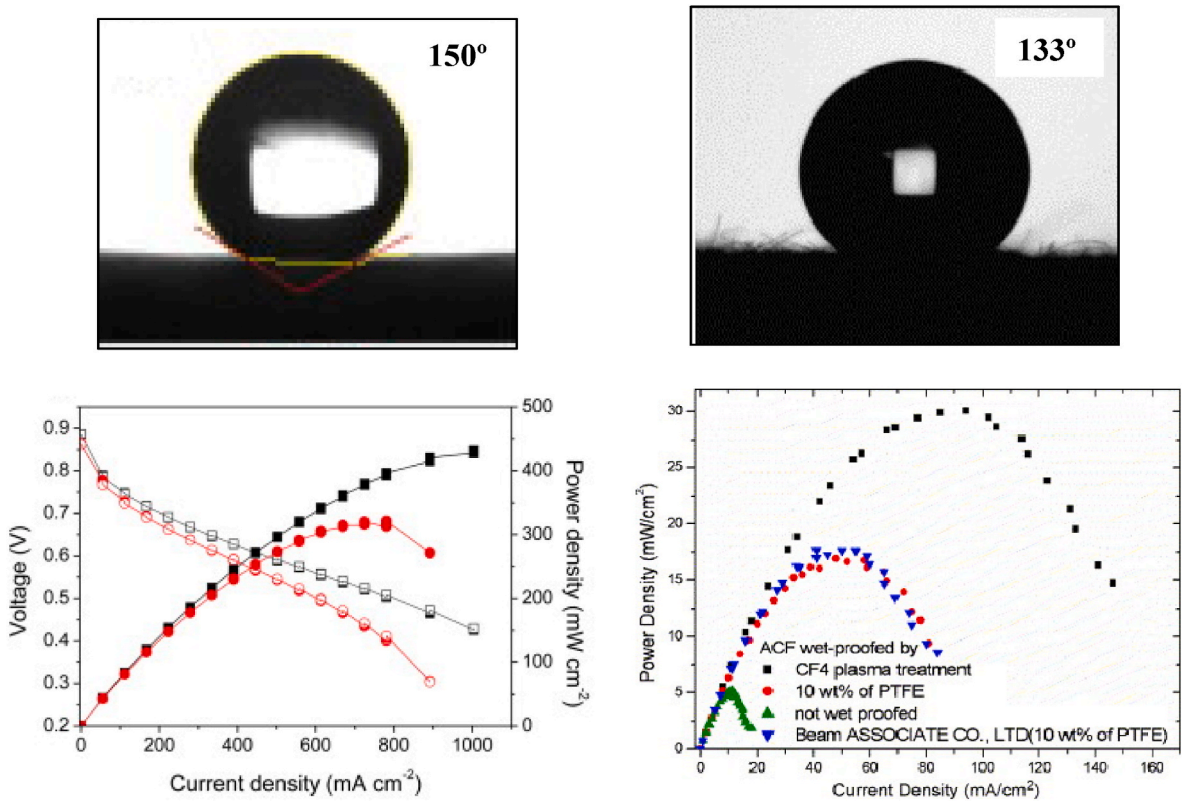

Fig. 13. The contact angle and polarisation curves showing the power density and current density of (left) SiOx- on SGL 10BC (non-MPL side), (right) CF_4 plasma coated active carbon fibres. Reproduced with permission from Elsevier [110].

Chemical reduction of salts with hydrophobic groups has also been investigated. Thomas et al. [113]fabricated a superhydrophobic GDL from the electrochemical reduction of diazonium salt onto SGL 24 GDLs. At 60 °C and 100% RH, the treated GDL exhibited a greater power density (i.e. 790 mW cm^{-2}) than the untreated SGL 24BC (590 mW cm^{-2}). Meanwhile, at 80 °C and 50% RH there was no difference in performance. This indicates that the surface treatment used above may be suitable for PEMFCs in low temperature, high humidity conditions.

4. Summary

Hydrophobic treatment of the GDL substrate has shown to be highly influential at increasing power density by the reduction of flooding. Alternative fluorinated polymers present a viable competitor to PTFE by achieving the hydrophobic threshold from a much smaller weight of polymer, thus substrate structure and transport capabilities are less affected. The functionalisation of carbon fibre with PFPE is a particularly promising candidate offering a simple application method as well as an insignificant effect on the conductive carbon network and pore space. Plasma coated substrates offer significant potential to fuel cell efficiency, though the energy intensity of the process in unfavourable.

Table 2 summarises the recent investigations into alternatives to PFTE for hydrophobic treatment of the GDL.

5. Microporous layers (MPLs)

5.1. Conventional MPLs

The microporous layer is applied to the gas diffusion layer where it is located between the carbon substrate and the electrocatalyst layer [114]. Carbon black is conventionally used as the main component of the MPL, providing excellent contact between the electrocatalyst layer and the macroporous substrate. Carbon black has a wide application in electrochemistry due to its good physical properties such as: a high electrically conductive, porous material with a large surface area, as well as its low cost and relative abundance [115]. It is derived from the incomplete combustion of heavy hydrocarbon products from the petroleum industry, such as coal tar and ethylene cracking tar. Carbon black is subcategorised depending of its production process which determines its physical properties of particle size and crystallinity [116]. Acetylene black is a type of carbon black formed from the thermal degradation of acetylene and is characterised by high degree of crystalline orientation compared to other sources of carbon black, and thus is extremely electrically conductive though comparatively expensive. Due to their lower cost and high availability, high grade oil-furnace blacks, such as Vulcan XC-72, has attracted attention in electrochemical applications as a good compromise between high surface area of about 250 m^2/g and a good electrical conductivity of about 3 S cm^{-1} [115].

Conventionally, the carbon black particles are dispersed in a polymeric hydrophobic binding agent, typically PTFE. The hydrophobicity of the microporous layer provides a high capillary pressure to promote membrane hydration and prevent water flooding. Its presence has been shown to significantly improve fuel cell performance and durability. For example, Owejan et al. [117] found a 20–30% increase in performance when an MPL was applied to Toray TGP-H- 060 and MRC105 under fully humidified conditions. Although initially added to the GDL in order to improve the electrical contact between the GDL and the electrocatalyst layer [118,119], Chen et al. [120] were also able to show that the MPL can improve liquid water management in the MEA. The main improvements are due to the MPL's ability to modify water accumulation and transport through the GDL [119–122]. This reduces flooding of the pores of the microporous layers and increases catalyst availability for the ORR. The effect of MPL composition on its transport properties has been the focus of numerous research papers. In particular the effect of PTFE content [82,83,123], optimisation of carbon loading on the

Table 2
Summary of the investigations into alternatives to PTFE in the GDL.

Authors	Description	Peak Power Density (W cm^{-2})[a]	Contact Angle (°)	Main Findings
Gallo Stampino et al. [102]	*Substrate:* SCCG 5 N carbon cloth *Coating:* Low molecular weight PFPE (TLS) High molecular weight PFPE (P56)	TLS: 0.36 P56: 0.34 (oxidant: air)	TLS:144° P56:147°	• SCCG 5 N carbon cloth: 1% wt. low weight PFPE (TLS- 2000 molecular weight) and a high weight PFPE (P56-20000 molecular weight). • Mass transport resistance prevailed at high current densities when using P56-PFPE.
Gola et al. [105]	*Substrate:* S5 carbon cloth *Coating:* 1.88% wt. Fomblin® Z peroxide PFPE	0.28 (oxidant: air)	172°	• S5 carbon cloth treated with PFPE by thermal decomposition of FOMBLIN® Z peroxide PFPE (1.88 wt %). The maximum PFPE loading achieved was 1.03% wt. • 1.03% wt. PFPE GDL: 172° contact angle and 95% surface coverage. • SEM imaging: preservation of porous matrix and uniform PFPE. • PFPE GDL power density (0.28 W cm^{-2}),10% wt. PTFE (0.17 W cm^{-2}).
Salahuddin et al. [107]	*Substrate:* Electro-spun and icroporo PAN fibres *Coating:* Ultra Ever-Dry Solution	-	162°	• Super hydrophobicity: PTFE, Krytox oil and Ultra Ever Dry coating. • Hydrophilic areas produced from potassium permanganate ($KmnO_4$) and sulphuric acid (H_2SO_4). • CF_2 and CF_3 bonds impart hydrophobicity. Covalent bonds between and PAN fibres, more stable binding than physical adsorption of PTFE. • Low resistivity of the proposed coated carbonised papers (18.77 Ω m).
Pai et al. [108]	*Substrate:* Active carbon fibres *Coating:* CF_4 plasma	0.03	133°	• Carbon cloth treated with CF_4 by plasma deposition. • 10 % wt. PTFE GDL: uneven surface coating. Pores between the carbon fibres filled with PTFE polymer, were not filled by CF_4 plasma. • MEAs were produced using low Pt loading (0.04–0.05 mg cm^{-2}). • CF_4 MEAs had the widest ohmic polarisation range (15–130 mA cm^{-2}), non-wet-proofed (15–18 mA cm^{-2}),10% wt. PTFE (15–80 mA cm^{-2}). • CF_4 MEA power density (0.03 W cm^{-2}), 10% PTFE (0.0175 W cm^{-2}).
Wang et al. [109]	*Coating:* Silica particles and polydimethylsiloxane	0.45	162°	• Silica particle/PDMS coating and heat treated at 180 °C. • Super hydrophobicity from silica/PDMS composite. Contact angle: 162° • Silica particles impart hydrophilic property. Silica particles drew the water droplet into the GDL pores. Silica pores – hydrophilic (27°). • Silica/PDMS composite reduced pore dimeter to 7.1 μm from 11.3 μm. • Silica/PDMS: power density (0.45 W cm^{-2}), MPL (0.36 W cm^{-2}).
Joo et al. [110]	*Substrate:* SGL 10BC *Coating:* Chemical vapour deposition of polydimethylsiloxane to produce SiOx	0.40 (oxidant: air)	150°	• SiO_x coating of SGL 10BC by CVD, heated treated at 200 °C. • Pore size distribution after hydrophobic treatment was unchanged. • Contact angle increased from 135° to 150° on MPL side. • Peak power SiO_x (0.40 W cm^{-2}), SGL 10BC (0.30 W cm^{-2}). • In the high current density region, at 900 mA cm^{-2}, the voltage difference between the SiO_x. treated 10BC and as received 10BC is particularly large, 0.8 V and 0.6 V respectively.
Ko et al. [111, 112]	*Substrate:* PAN fibres *Coating:* Plasma deposition of hexamethyldisiloxane to produce SiOx–C:H	(oxidant: air)	162°	• Oxygen plasma etching followed by plasma-enhanced chemical vapour deposition of hexamethyldisiloxane (HMDSO) produced a SiO_x-C:H nano-structured coating on carbon fibre substrate. • Duration of oxygen plasma etching increased the nano-structure formation on the substrate, becoming longer with a reduced diameter. • 1-h oxygen plasma etching and 30-s hydrophobic SiOx–C:H coating produced super hydrophobic coating of 162°. • Nucleation rate of water droplets was reduced, and droplet formation time was increased by 244% from super hydrophobicity.
Thomas et al. [113]	*Substrate:* SGL 24AA *Coating:* CF_3	0.79 (oxidant: air)	146°	• Grafted CF_3 onto SGL 24AA by chemical reduction of diazonium salts. Formation of covalent bonds of CF_3 onto the carbon fibre surface. • Contact angle:CF_3 (146°), PTFE (142°) and MPL-coated (145°). • CF_3 power (0.79 W cm^{-2}), PTFE (0.59 W cm^{-2}), MPL (0.66 W cm^{-2}).

[a] Unless otherwise states, the maximum power density was reported with 100% RH and oxygen as an oxidant.

substrate [124–126], and the type of carbon [127–129] have been the focal point of research.

Optimisation of the carbon black content in the MPL has been a point of contention for various research groups. Jordan et al. [124] reported that between about 1.25 and 1.9 mg cm^{-2} acetylene black in the MPL was the optimal for cell performance, whereas Park et al. [126] suggested that a carbon loading of 0.5 mg cm^{-2} of acetylene black was optimal for fuel cell operation, this was attributed to better air permeation (and therefore mass diffusion) through the thin MPL layer. More recently, Orogbemi et al. [125] found that a carbon loading of 2.0 mg cm^2 for Ketjenblack EC-300 J and Vulcan XC-72 is the most favourable for gas permeability. Typically, carbon weighting in the MPL ranges from 1.0 to 2.0 mg cm^2, and this has a noticeable effect on MPL thickness and subsequently its mass and water transport capabilities [130]. Fig. 14 shows SEM images of an MPL-coated GDL manufactured by SGL Carbon: (a) the uncoated side of an SGL 39BC carbon fibre GDL, and (b) the MPL-coated surface of an SGL 39BC GDL. The homogeneous MPL coating is strikingly different from that of the uncoated carbon substrate, as a more homogenous layer with several surface cracks.

The application of the MPL to the carbon substrate can carried out by various techniques. These include brush coating, the doctor blade technique, spray coating, rod coating, or screen printing [131]. Other novel methods of application are also under investigation [132]. The viscosity of the MPL slurry dictates the application method by which the MPL is applied to the carbon substrate. More viscous slurries can be applied to the substrate by brush or the doctor blade coating technique, whereas thinner slurries tend to be applied by spray coating. The MPL-coated GDL is then heat treated and sintered at e.g. 350 °C in order to melt the PTFE and thus bind the carbon black particles in the MPL together, as well as laminating the MPL to the carbon substrate [127, 133]. The MPL has been reported to penetrate some way into the GDL under compression, creating a hybrid interlayer of substrate and MPL [11].

Conventional MPLs have been confirmed to increase the power density when used in PEMFCs. However, there are several drawbacks to their design. Thus, material and design improvements have been

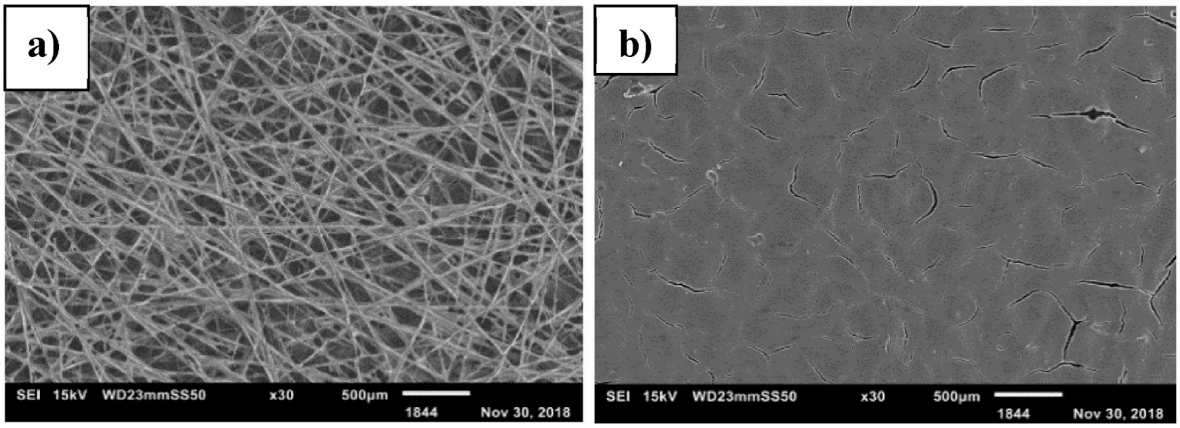

Fig. 14. Shows SEM images of an MPL-coated GDL manufactured by SGL Carbon: (a) the uncoated side of an SGL 39BC carbon fibre GDL, and (b) the MPL-coated surface of an SGL 39BC GDL. Reproduced with permission from Elsevier [210].

explored with in-situ and ex-situ tests to increase PEMFC efficiency. As previously mentioned, although PTFE provides hydrophobicity to the GDL, its presence in the MPL has been shown to compromise reactant transport and the electron conductivity [12,82,83,134]. Moreover, the insolubility of PTFE means that the production of a homogenous carbon black/PTFE MPL slurry is reported to be difficult [135]. Other issues exist with PTFE-based MPL slurries, notably high viscosity, low phase stability (due to viscosity changes over time), cracking on the GDL surface during drying, and difficulty in the coating process [3]. As such, new materials and architectures are required.

Another branch of research is focused on the improvement of the carbon element of the MPL, essentially the substitution of carbon black with alternative carbonaceous materials. The motivation behind this research is largely to improve the physical properties of the MPL and thus PEMFC efficiency, whilst other groups have cited the secondary motivation of sustainability. Carbon black is produced from the partial thermal degradation of oil or natural gas as such its production is based on the fossil fuel industry. The following section details attempted design and material improvements that have been made to the MPL by first addressing the carbonaceous element and then the hydrophobic coating.

5.2. Alternative MPL architectures

There has been a significant volume of work undertaken into the optimisation of carbon black in the microporous layer. These studies largely focus on the microstructural properties of the material, such as pore size distribution [128,136–138], improvements in microporous layer design such as carbon weighting [124–126], and the type of carbon black [139].

As the MPL is a critical component for the transport of reactant gases and liquid water to and away from the electrocatalyst layer, the porosity and the pore size distribution of the MPL are determining factors in its ability to carry out this task successfully. Attempts have been made to control the pore structure of the MPL by using carbon black with different porosity profiles. Wang et al. [139] produced a composite MPL from carbon blacks with dissimilar pore size distribution (Black Pearls 2000 Acetylene Black), in order to create a bi-purpose pore structure for the optimal transport of liquid water and reactant gases. This resulted in higher power density (0.66 W cm^{-2}) in the polarisation curves compared to when a single type of carbon black was used (0.55 W cm^{-2}). More importantly, this technique allowed for the fabrication of an MPL with a graduated porosity, thus providing a gradient for enhanced fluid flow.

Similarly, Tang et al. [138] fabricated a triple-layer MPL with graduated pore sizes. They were able to achieve this by the use of a pore forming agent (NH_4Cl) in their screen-printing production process. They created a porosity gradient where the pore diameter decreased from the substrate to the electrocatalyst layer interface, with the aim of increasing the capillary pressure and forcing liquid water away from the catalyst. This microstructural design was effective at high current densities (>700 mA cm^2), where flooding becomes a limiting factor, in agreement with Wang et al. [139].

In a novel study by Yoshimune et al. [140] used an electrostatic screen printer and a dry MPL coating method to produce MPLs with a controlled pore structure and morphology. Acetylene black and graphene nanoplates were deposited in a layer by layer manner with the aim of controlling the particle arrangement, and thus the pore size through the layer. Polarisation curves performed in condensation state, at 120% relative humidity, showed that the MPLs with acetylene black at the surface i. e smaller particles and smaller pores improved oxygen diffusion rates at the high current density region (>1.5 A cm^{-2}) due to their ability to divert liquid water. These MPLs also displayed a higher flooding tolerance than the commercial MPLs which experienced voltage drops at around 1.0 A cm^{-2}. Their innovative the dry-coating method has several advantages over the conventional solvent deposition method whilst maintaining a comparative hydrophobicity (≈150°), such as the prevention of crack formation on the MPL surface, which are associated with the evaporation of solvents in the drying process. Moreover, this is comprehensive study which investigates the potential upscale of this deposition technique, where MPLs produced meet the dimensional requirements for use in the Toyota Mirai. A progressive academic attitude should allow the collaboration with industry to stress the relevance of lab-scale design improvements to the real world applications of PEMFC.

5.2.1. Perforated and patterned MPLs

Perforation of the microporous layer has been explored as design enhancement for PEMFC, similar to perforation of the macroporous substrate which was discussed in section 2.2.2. Perforation of both the MPS and the MPL was found to be provide the greatest improvement to the MEA performance [30]. A significant body of work has been undertaken on the effect of perforation of the MPL on PEMFC performance [141–145].

Cho et al. used laser-perforation to produce furrows in the MPL which replicate the serpentine land and channel patterns of the flow field plate, aiming at diverting liquid water away from the cathode catalyst layer to the outlet of the flow channel [146]. The furrows produced were ~20 µm wide with 2 mm spacing in the same serpentine pattern as the flow field plate, these were compared to a commercial unmodified MPL and an MPS without an MPL. They reported that the furrowed MPL excelled in high relative humidity condition (100% RH

and 200% RH) with a higher power density than both the uncoated MPS and the pristine MPL coated GDL. The greatest performance enhancements were recorded at 200% relative humidity where it was argued that the furrows acted as liquid water pathways increasing the availability of pore space for reactant diffusion and active sites for the oxygen reduction reaction. Further work could be undertaken on the optimisation of the furrow dimensions to enhance membrane hydration in low relative humidity conditions and to reduce liquid water saturation in high relative humidity conditions.

Patterned microporous layers are an innovative design modification similar to MPL perforation with the purpose of creating areas on the MPL dedicated to the removal of liquid water [144,147]. Lee et al. [144] used laser ablation to produce a ditch-like pattern on the MPL surface which were intended to act as channels for liquid water. MPLs were produced with perforations, and with ditches parallel and perpendicular to the channel; these were compared to a commercial MPL coated GDL. Marked improvements reactant transport were seen when the ditches were positioned perpendicular to the channel, whereas the ditches formed in parallel to the channel decreased mass transport due to liquid water stagnation in the ditches as water is not able to move from the rib to the channel. Polarisation curves performed at 100% relative humidity indicate that the ditch-like etchings on the MPL were more effective at relieving liquid water saturation than dthe perforated MPL. The perforated MPL suffered severe voltage drops at 0.5 A cm $^{-2}$ due to flooding, which was confirmed by the Nyquist plots produced. Various methods and designs have been used to produce patterned MPLs to accelerate liquid water removal. One method used the recrystallization and pyrolysis of ammonium chloride to form flower-like patterns on the MPL [147]. Chen et al. [147] varied the percentage mass of the pore former, ammonium chloride to produce different pore structures. The inclusion of 40 wt % pore former resulted in the formation of perforations through the MPL where not present at 20 wt%. Impedance spectra and polarisation curves show that the 20 wt % MPL suffered mass transport losses and performed significantly worse than the commercial GDL. However, the MPL containing 40 wt % pore former resulted in the formation of perforations through the MPL that were not present at 20 wt%. Impedance spectra and polarisation curves showed that the MPL with 20 wt % pore former suffered from mass transport losses and performed significantly worse than the commercial GDL. However, the MPL containing 40 wt % pore former in the inner layer (close to MPS) and 20 wt % pore former in the outer layer (close to the catalyst layer) produced the highest power density and reduced mass transport limitations particular in humidified conditions (100% relative humidity). The porosity gradient in this MPL provided a higher capillary pressure for water removal which when coupled with the flower-like pattern enhanced the distribution of reactant gases and mitigated the accumulation of liquid water in the pore space.

These novel microporous layer designs open a wealth of possibilities in terms of MPL architectures. Seemingly the best performance improvements are when the MPL is not treated as a homogenous layer but pore graded structure that acts as a corridor between the microporous catalyst layer and the macroporous substrate. The optimisation of the MPL design can be greatly expedited by modelling simulation, thus reducing the time and expenditure associated with experimental work.

5.2.2. *Free-standing MPLs*

Additionally, some groups have investigated carbon black as a free-standing MPL with varying successes [45,148–150]. For example, Shim et al. [45] fabricated a carbon composite GDL from a mixture of Vulcan XC-72 and PTFE (20–50 wt %) which was rolled to form a sheet, then heat treated to 340 °C to melt the PTFE, which acted both as a binder and a hydrophobic agent. Fuel cell MEA tests indicated that the performance of all carbon black based substrate was inferior to the conventional LT 1200 MPS (Fig. 17 (right)).

Similarly, Chen-Yang et al. [148] fabricated composites from Vulcan XC-72 and PTFE (0, 10 and 20 wt%). Again, all of the carbon black based substrate exhibited just half the power density of the commercial MPL coated ELAT® GDL (E-TEK). Since the electrical conductivity of carbon black is comparable to the carbon paper GDLs, the poor performance can be attributed to lower gas permeability. Conventional carbon paper has an abundance of macropores which facilitate high gas flux. However, carbon black composites are largely meso- and microporous, meaning that gaseous reactants must compete with the liquid water when diffusing through the pores, leading to mass transport losses. This limitation of the Vulcan XC-72 GDL is supported by the measured the air flux and the permeability of the carbon black GDL being significantly lower than the LT 1200 MPL coated carbon paper (9.77×10^{-12} and 218.6×10^{-12} respectively). Moreover, the PTFE content of these carbon black GDLs is quite high (up to 50%), this is likely to have reduced the porosity and blocked the pathways for reactant gases. Although Shim found that the power density increases up to 40% wt. PTFE, this is likely due to the reduction in flooding phenomena.

Bauder et al. produced in-house non-woven synthetic supports for a carbon black/PTFE MPL, with 20 and 40% wt. PTFE content [151]. These exhibited lower contact angle and through-plane resistance compared to MPL-coated SGL 25BC, with the 40% wt. PTFE blend having the best properties. By increasing the thickness of the 20% wt. blend MPL, they achieved comparable power density to SGL 25BC. However, at high relative humidity, flooding caused mass transport losses. The electrochemical impedance spectroscopy (EIS) was used to

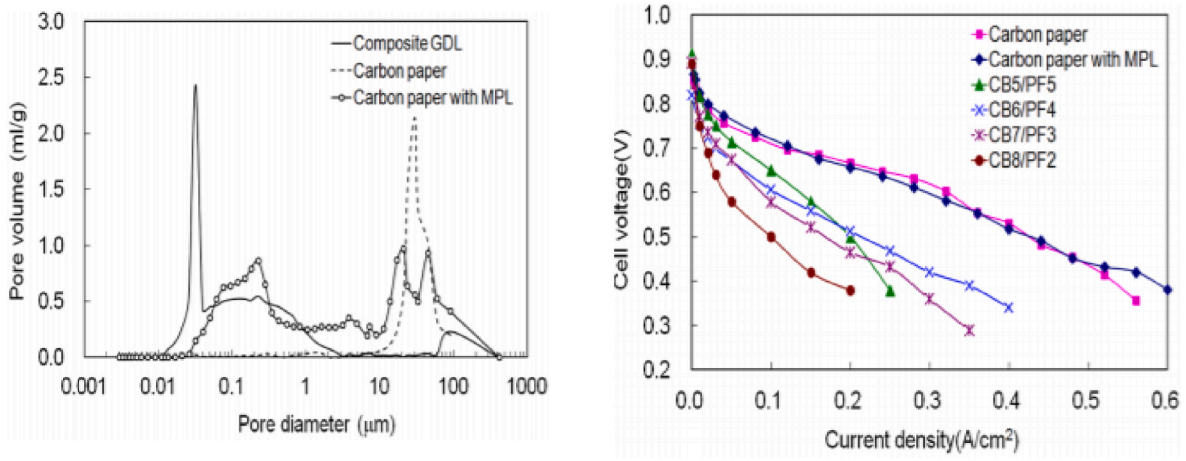

Fig. 15. SEM images of (a) pristine carbon paper, (b) CNTs grown on carbon tubes under C_2H_4 and (d) the polarisation curve of carbon nanotubes grown on SGL 34BA as an MPL/catalyst support. Reproduced with permission from Elsevier [169].

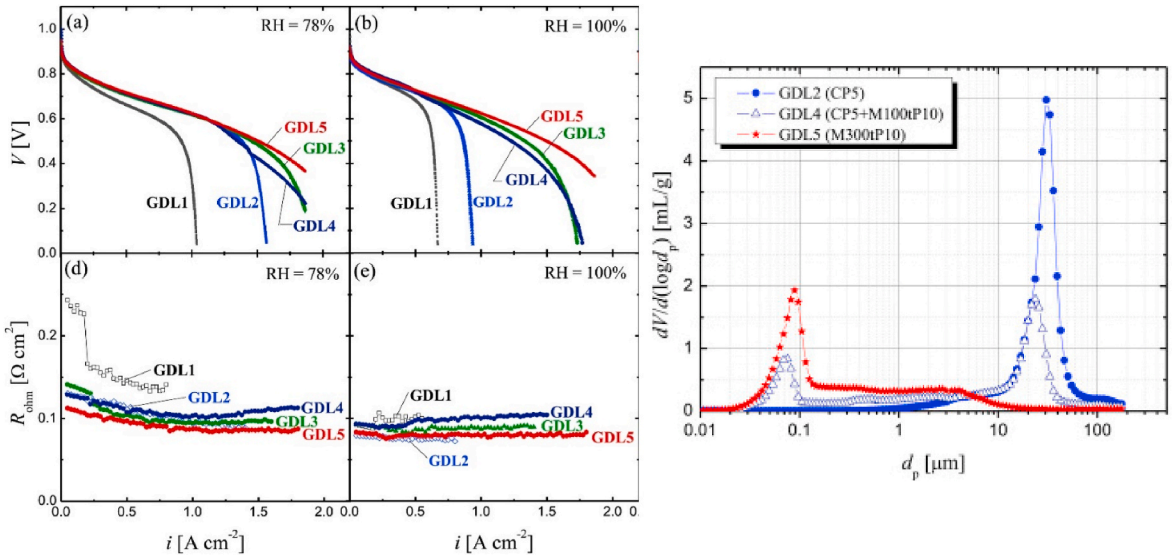

Fig. 16. GDL with graphene based MPL, inset showing the flake-like structure of a graphene particle and (right) cross-sectional image of the GDL with the graphene based MPL. Reproduced with permission from Elsevier [172].

evaluate the resistance losses, and synchrotron radiography was used to assess liquid water distribution, in operando.

Ito et al. [152] produced a free-standing MPL sheet from acetylene black and PTFE (10% wt.). This was tested as it was, as well as being applied to Toray TGP-H090 and H060 carbon substrates. The total thickness was ~300 μm for all samples [152]. Fig. 18 shows the polarisation curves, and the free-standing MPL (i.e. GDL 5) produced the highest voltage, particularly at high current densities, at all values of relative humidity. Interestingly the free-standing MPL was highly micro- and mesoporous (Fig. 18), with very few macropores, like the free-standing MPL produced by Shim et al. [45]. As macropores are believed to be the primary pathway for gas diffusion, the higher power density produced by the free-standing MPL does not corroborate the results of other research groups, although the type of carbon black and PTFE loading may have been influential. Ito et al. [152] attributed the good results of their free-standing MPL to its low thermal conductivity that raises the temperature of the GDL, increasing the saturation pressure and consequently mitigating water liquid.

However, the free-standing MPL, in its present state, was regarded as largely unsuitable for application in PEMFC as it lacked the necessary mechanical strength and flexibility which would limit the durability in the MEA [2]. Despite this, these problems could potentially be overcome by mixing the MPL materials with, for example, some reinforcing carbon fibres or carbon nanotubes to improve the mechanical stability and strength of these free-standing GDL. For example, some research groups have created composite buckypapers from carbon black, carbon nanotubes and carbon fibres [79,153–156].

For example, recent work by Kim et al. [156] produced a free-standing MPLs from multiwall carbon nanotubes using chemical vapour deposition. The thickness of the MWCNT sheet was reported to have the largest effect on the effectivity of the MPL on fuel cell performance, where the thinner the sheet the greater the electrochemical performance. The thinnest sheet fabricated (15 μm) produced the highest power density of all of the sheets (1297 mW cm^{-2}) even compared to the commercial MPL coated 39BC GDL (1023 mW cm^{-2}), as well as the highest OCV and limiting current density. The thicker sheets, 30 μm and 100 μm, had an electrochemical performance far lower than the commercial at 660 mW cm^{-2} and 305 mW cm^{-2} respectively. The favourable reaction kinetics of the 15 μm compared to the thicker sheets was attributed to an inability of the thicker sheets to drain the water produced leading to pore saturation, and reduced reactant diffusion. The greatest improvements of the 15 μm were when the cathode side is supplied with air which implies that, it successfully reduced mass transport losses rather than enhancing electrical conductivity between the MPL and catalyst layer. As the thinnest sheet produced the best performance rather work is needed on producing even thinner MWCNT sheets to see the optimal sheet thickness in regards to performance enhancement.

Finally, Duan et al. [157] electrospun a freestanding carbon nanofibre sheet which possessed good electrical conductivity and hydrophobicity, and applied this as an MPL. This exhibited a higher permeability than a Vulcan XC-72 carbon powder and 40 wt% FEP coated GDL. When used at the cathode, a high peak power density (321 mW cm^{-2}) was achieved, corresponding to 23% improvement compared to the conventional MPL. However, the durability was not assessed.

5.3. Alternative MPL materials

In order to improve MEA efficiency, several research groups have explored other carbonaceous materials, notably carbon nanotubes, graphene, and carbon fibres [99,157]. The aim of using these materials has largely been to enhance two-phase flow in the MPL through improved pore size distribution, and to increase MPL conductivity, enhancing the bulk conductivity and reducing contact resistance.

5.3.1. Carbon nanotubes (CNT)/multi wall carbon nanotubes (MWCNT)

Carbon nanotubes have shown potential as an exciting new MPL material, due to their high electrical conductivity and their resistance to corrosion in oxidative environments [158–163]. A large breadth of investigations has shown their potential as carbonaceous MPL materials. The majority of these studies have focused on multiwall carbon nanotube (MWCNT)/carbon black composites, although early work by Kannan et al. [160,161] completely replaced Vulcan XC-72 carbon black with graphitized MWCNTs grown in-situ by chemical vapour deposition. They reported that the graphitized MWCNTs exhibit more desirable characteristics for use in the MPL; with a contact angle of 150°, and a more homogenous surface morphology. Fuel cell MEA tests revealed greater power density especially in the high current density region. The addition of carbon fibres added to the mechanical stability of the layer.

In general, investigations into carbon nanotube based MPLs show that they are characterised by superior electronic conductivity and permeability. Gharibi et al. [159] showed that the addition of MWCNTs to carbon black increased the gas permeability, pore volume and conductivity (from 233.71 s cm^{-1} to 291.18 s cm^{-1}) of MPLs, consistent

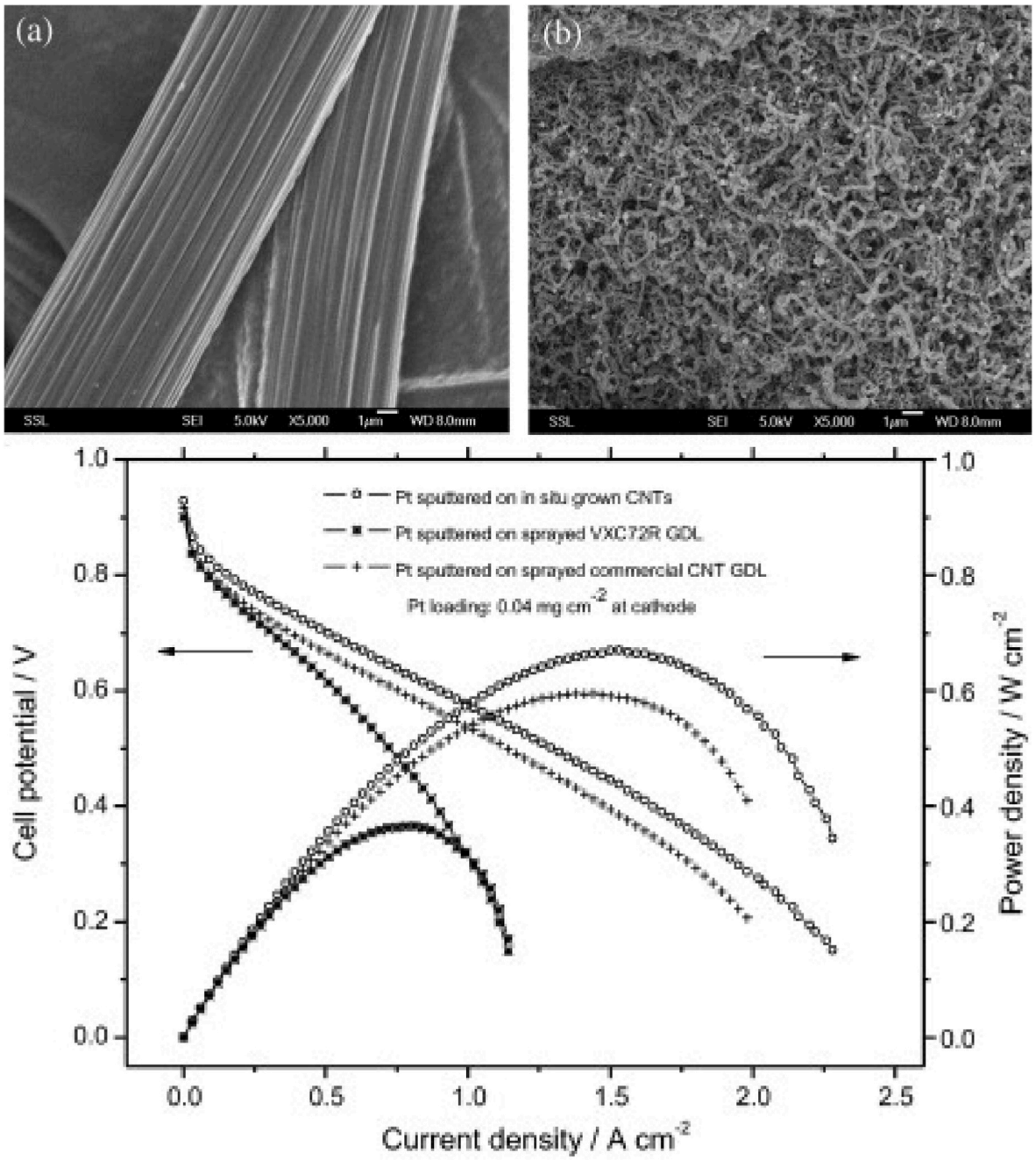

Fig. 17. (Left) The pore size distributions and (right) the polarisation curves of the carbon paper and MPL coated carbon paper and the Vulcan black composite GDL (CB5/PF5,CB6/PF4, CB7/PF3 and CB8/PF2 are wt.% carbon black:PTFE 50:50, 60:40,70:30 and 80:20, respectively). Reproduced with permission from The Korean Hydrogen and New Energy Society [45].

with results and observations by Stampino et al. [158] and Lin et al. [162]. Lin et al. [162]created an MPL using MWCNTs in addition to acetylene black, resulting in greater permeability and electrical conductivity, from 28 S m^{-1} 34 S m^{-1} for 0% MWCNT and 80% MWCNT respectively. They found that a carbon loading of 1.5 mg cm^2 and a 1:4 ratio of acetylene black to MWCNT by mass resulted in optimum fuel cell performance (0.915 W cm^{-2}). Schweiss et al. [163,164] applied an in-house MWCNT MPL to a Sigracet SGL 25BN GDL, which was compared to MPL-coated Sigracet SGL 25 BC. They reported an 8-fold increase in the gas permeability for the MWCNT-based MPL, and the ohmic resistance was reduced by 9%. Interestingly the resulting MPL also had hydrophilic properties and was able to successfully remove liquid water from the electrocatalyst layer.

Lee et al. [16] produced an MPL by blending 21% wt. MWCNT into a carbon black and PTFE dispersion. This was compared with uncoated SGL 25BA and MPL-coated SGL 25BC. The pore size distribution was wider for the MWCNT-based MPL, and the mass transport resistance was lower. This was attributed to the prevention of carbon black agglomeration due to the high aspect ratio of MWCNT and resulted in an increase in fuel cell power density. At 2.5 A cm^{-2} and 3.0 A $cm^{-2}$the in-house 25BN MWCNT MPL were 6.7% and 94.1% higher than the commercial SGL 25BC; the much higher cell voltage difference at 3.0 A cm^{-2} was due to the massive mass transport losses demonstrated by the fuel cell running with SGL 25BC. In a highly informative innovation, they visualised the in-operando liquid water distribution in the MEA. Interestingly, although the liquid water saturation was shown to be

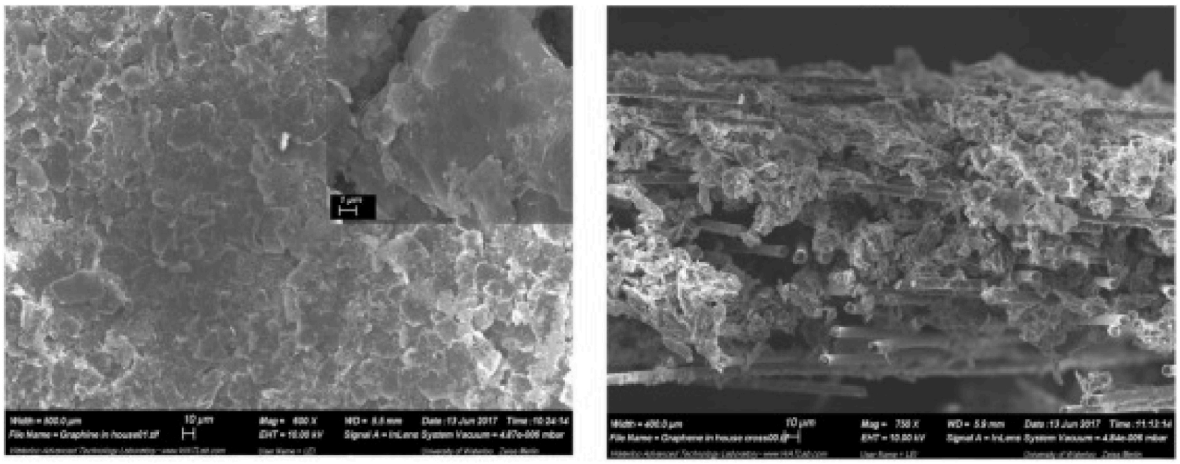

Fig. 18. Polarisation curve and ohmic resistance (left) and the pore size distribution (right) of different GDLs. Where GDL 1, 2, 3, 4 and 5 are the blank Toray 090, 5% wt. PTFE treated Toray 090, Toray 90 coated with MPL (50 μm and 10% wt. PTFE), Toray 60 coated with MPL (100 μm and 10% wt. PTFE), and the free standing MPL, respectively. GDL Reproduced with permission from Elsevier [152].

greater in the case of the CNT-MPL, the fuel cell performance was better even at high relative humidity. At high current densities (i.e. > 250 mA cm^{-2}), the MWCNT-based MPL improved the power density by 94.1%, attributed to the MPL being thinner, the higher porosity, and the larger pores. This research highlighted the importance of pore size in the MPL, in support of the theory proposed by Kong et al. [165] that a higher proportion of small macropores (5–10 μm) in the MPL can enhance PEMFC performance. This structure is thought to allow liquid water permeation, whilst not restricting the reactant gas pathways. Similar findings were reported by Tanuma et al. [166], who conducted a thorough comparison of composite MPLs. They prepared hydrophilic MPLs from carbons with different physical and micro-structural properties, namely carbon black, MWCNTs, vapour grown carbon fibres (VGCFs), and melt-spun carbon fibre. They investigated the pore size distribution and mean pore diameter, finding that the VGCFs had the largest median pore diameter, whilst carbon black and melt-spun carbon fibres had the lowest. VGCF-based MPLS also yielded the highest fuel cell power density, with carbon black and melt-spun carbon fibres having the lowest. Thus, larger pore volume was linked to performance via enhanced mass transport, by providing gas diffusion pathways and preventing flooding.

Innovative work has been also undertaken by growing carbon nanotube directly on carbon paper substrates, via chemical vapour deposition [160,167–170]. The aim of this is to increase the contact between the GDL and the electrocatalyst layer, and the formation of a hybrid catalyst/microporous, thus improving the diffusion characteristics, reducing charge transfer losses, and increase catalyst utilisation. For example, Sandström et al. [167] grew carbon nanotubes on an SGL 34 AA carbon paper using different temperatures and flow rates of C_2H_4 These were then doped with Pt particles and acted as a multifunctional layer. They reported a reduction in charge transfer resistance of 38% using this technique compared with Vulcan XC-72 as Pt support. Tang et al. [169] used the same methodology grow CNT on Toray TGPH 090, as a hybrid microporous/catalyst layer. Fig. 15 shows the (a) pristine carbon fibre and (b) the grown CNT. The maximum power density of 670 mW cm^{-2} was reached from the MEA with the in-situ grown CNT MPL compared to carbon black and commercial CNT, with a peak power density of 590 mW cm^{-2} and 365 mW cm^{-2} respectively.. However, the durability of such fragile fibres in fuel cell conditions remains to be evaluated.

5.3.2. Graphene

A recent trend has seen graphene being explored as an alternative to carbon black in the MPL. Graphene is a two-dimensional monolayer of graphitic carbon atoms, with good mechanical stiffness and elasticity [171], as well as extremely high electrical conductivity (~108 S m^{-2}) and thermal conductivity (1500–2500 W m K^{-1}) [172].

For example. Leeuwner et al. [173] fabricated a free-standing MPL for the cathode GDL from commercially available compressed 3D free-standing graphene foam (ACS Materials). The initial 3D honeycomb structure is reduced to a layered flake-like structure on compression. The in-plane electrical conductivity was relatively high in comparison to SGL 25 BC (333 S m^{-1} and 29 S m^{-1}) respectively) due to the conductive pathways within the graphene foam, and the compressibility of the foam enabled good contact between the GDL and the electrocatalyst layer, reducing charge transfer losses. However, the lack of treatment with hydrophobic agent was a limiting factor, resulting in a large variation in the contact angle (87° ± 16.5), and attributed inhomogeneity of the surface when compressed. From the polarisation curves, the graphene MPL performs well at mid-range current density (e.g. 362 mW cm^{-2}, compared to 334 mW cm^{-2} for SGL 25BC commercial MPL coated at 500 mA cm^2). However, at higher current densities (>1500 $mAcm^{-2}$) the commercial MPL was better, due to flooding in the less hydrophobic graphene MPL.

Najafabad et al. [172]produced electrochemically exfoliated graphene for use as an MPL material. Fig. 16 shows the SEM micrographs of the flake-like graphene structure and the cross-section of the graphene MPL. However, the graphene sheet-like structure prevented water removal from the three-phase boundary, and hence led to a performance drop under high-humidity operation, due to flooding. This was addressed by mixing the graphene platelets with more spheroidal carbon black particles. Meanwhile, Leeuwner et al. [174] used the same methodology to make electrochemically exfoliated graphene, and compared the physical and transport properties with reduced graphene oxide (HP-RGO-05G) and natural graphite (14,736, Alfa Aesar). These were sprayed onto Toray TGP H-060 carbon paper with a loading of 5% wt. PTFE and 20% wt. PTFE in the MPL. The graphene-based MPLs were shown to have a lower contact and in-plane resistances compared to a conventional Vulcan XC-72 carbon black MPL. However, their lower hydrophobicity led to mass transport losses at high relative humidity due to flooding at the interface between the MPL and catalyst layer. Again, a composite MPL formed from graphene and carbon black exhibited higher power density at high relative humidity, as well as enhanced galvanostatic durability.

Similarly, Ozden et al. [175] fabricated an MPL from Grade DU25 graphene (NanoXplore) which was compared to a Vulcan XC-72 based MPL. The graphene-based MPL exhibited a higher in-plane conductivity than the Vulcan carbon black MPL, and the peak fuel cell power density

was higher than the Vulcan-based MPLs in the range of 40–100% relative humidity. This was attributed to improved water management and reactant transport in the graphene MPL. Specifically, the graphene flakes used in this study have slightly different structure compared to the platelet-type graphene used in the previous studies, which could account for this difference.

Overall, research into graphene based MPLs remains extremely limited, although it can potentially increase cell efficiency. Further research is required to understand the limitations of the material and how it can reduce membrane dry-out without losing efficiency at high relative humidities and current densities. Greater knowledge is needed to understand the performance loss from restacking of graphene platelets and the optimal microstructure for reactant transport and water management. Mixing graphene with carbon black, or a mixture of graphene with different morphologies has the potential for a synergetic effect on MPL morphology and microstructure optimal for two-phase flow.

5.4. Carbon-free MPLs

Carbon-free, metallic MPL materials have also been explored due to the high electronic conductivity and corrosion resistance of some metals. The work in this field is as yet extremely limited, though research has been conducted into metal powders [134,176–179] and steel plates [173]. Leeuwner et al. [173] investigated a series of free-standing MPLs fabricated from different materials, one of which was a perforated stainless steel sheet, of the same thickness as SGL 25 BC (50 μm) with a 21% porosity and 500 μm pore size. Although the in-plane resistance was extremely low, the interfacial contact resistance with the catalyst layer was three times larger than the SGL 25BC. This is attributed to the steel plate having low surface roughness, corresponding to a contact area between the steel surface and the electrocatalyst interface. The fuel cell polarisation curve showed that the perforated steel sheet produced a lower power density than even the uncoated GDL substrate. Again, this is attributed to the high contact resistance, but also the much lower porosity compared to typical MPLs, which is essential for reactant transport.

Titanium has also attracted research interest as an MPL material. Fang et al. [179] deposited titanium on to SGL10 BA carbon paper as a thin film by magnetron spluttering (Fig. 19 (right)). Titanium-based powders also seem to offer potential as MPL materials: iridium-titanium nitride (Ir–TiN) [178], iridium oxide and titanium particles IrO_2/T [177], and titanium (Ti) [176,179] have all been explored. Hwang et al. found that a titanium powder MPL applied to a titanium felt substrate (Fig. 19 (left)) increased the mesopore size and the MPL hydrophobicity, improving liquid water management and reactant transport at high relative humidity (100%). However, at lower relative humidity (<66%), where water is more present in the vapour phase, it proved less effective. Metal powders are promising in terms of their desirable transport characteristics and pore structure. Moreover, advances in 3D metal powder printing, as demonstrated by Jayakumar [74] for the substrate, will allow control over pore size and structure. However, limitations exist in the cost of materials, production costs and arguably dimensions of the MEA on upscale.

6. Summary

Novel MPL materials present an exciting future in fuel cell

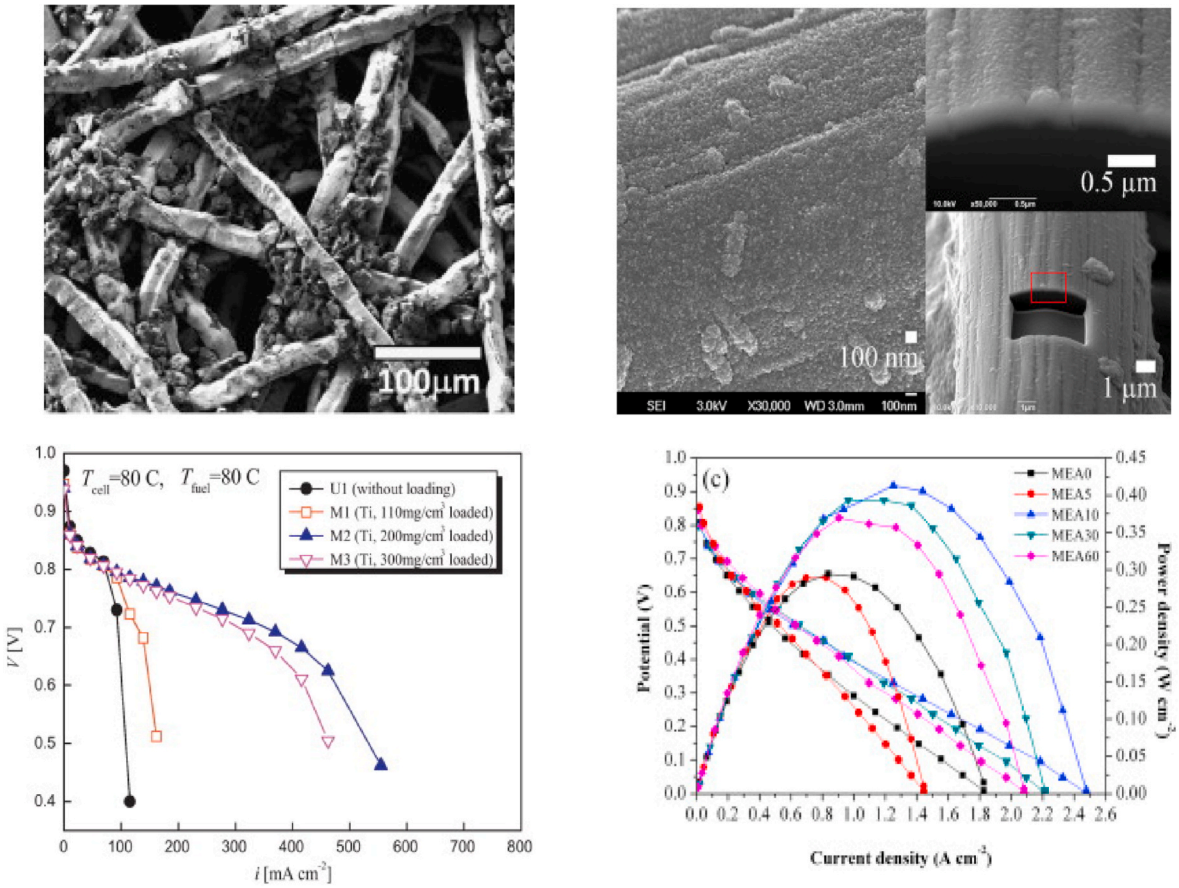

Fig. 19. Titanium coated GDL. (Left) SEM micrograph of the Ti felt substrate surface with Ti powder (300 mg cm^{-3}) (top) and polarisation curve of Ti substrate with different Ti loading, 80 °C (bottom) (Right) SGL 10BA after 10 min Ti spluttering (top), and the polarisation curve and power density of GDL with varying Ti spluttering time, 65 °C (bottom) Reproduced with permission from Elsevier [176].

engineering, especially the application of carbons with differing aspects to conventional carbon black, e.g. graphene platelets and carbon nanotubes. The material basis of the MPL determines the morphology and microstructure of the porous media, and thus influences the reactant pathways and water management in the MPL and the MEA as a whole. Due to its unique MPL micro-structure, graphene based MPLs are becoming an extremely popular research area. Moreover, composite MPLs formed of carbons with different aspects have a synergetic effect on the MPL morphology, where reactant transport and liquid water is better managed than the single material based MPL. This opens up a multitude of possibilities for MPL material compositions, the optimisation of which can be greatly accelerated by the use of micro-scale modelling. Current MPL research is limited by a lack of consistency, which makes comparison of the effect of the materials themselves highly difficult. For example, characterisation methods vary between papers making it hard to establish the cause for high/low power density or good/bad water transport phenomena. Furthermore, these findings are drawn from in-house MPLs where the method of application of the MPL to the substrate is variable. It has been remarked that the application method can affect the microstructural properties of the whole GDL, particularly the substrate MPL/interface [180]. This is largely disregarded, and conclusions are drawn on the basis of the material composition of the applied layer.

Table 3 summarises investigations into new architectures and alternative materials to carbon black in the MPL.

7. Alternative binders in the MPL

Conventionally the carbon black in the microporous layer is mixed with PTFE as a hydrophobic binder, in order to prevent flooding of the porous media during fuel cell operation, especially at high current densities. However, the use of PTFE as a hydrophobic agent has an adverse effect on the physical, microstructural and transport characteristics of the MPL. To this end, a large volume of research has been conducted into alternative means of preventing flooding.

7.1. Fluorinated polymers

Super hydrophobicity is achieved when the contact angle of a material exceeds 150°. One branch of research is focused on improving the hydrophobicity of the microporous layer using similar materials to PTFE, aiming to increase the contact angle whilst also reducing ohmic and mass transfer losses. For example, a significant amount of research has also been conducted into the viability of polyvinylidene fluoride (PVDF) as a replacement binder for use in the porous media of PEMFC. For example, Su et al. [182] fabricated gas diffusion electrodes using 15% wt. PVDF as the catalyst layer binder. They concluded that polyvinylidene fluoride improved surface morphology, and improved distribution of catalyst particles on the surface, increasing the availability of active sites. A peak power density to 0.56 W cm^{-2} was measured compared to 0.20 W cm^{-2} using Nafion as a binder. Zhang et al. [183] investigated PVDF for the anion exchange membrane fuel cells; similarly they found that using PVDF as a binder in the MPL increases the catalytic activity.

Meanwhile, Park et al. [135] fabricated a polyvinylidene fluoride-based MPL from a slurry with carbon black, which was applied to a carbon cloth GDL using the doctor blade method. MPLs with various ratios of PVDF and carbon black were compared with a PTFE-based MPL, and uncoated GDLs. SEM images revealed that the surface morphology of the PVDF-based MPL had greater uniformity than the PTFE-based MPL. The large cracks that are characteristic of PTFE-based MPLs were not present for PVDF; which was instead characterised by small pores. The use of PVDF as a binder resulted in significantly higher fuel cell power density, which they attributed to the appropriate in-plane and through-plane microstructure observed in the SEM images. However, hydrophobicity of the MPL could also have been highly influential, as the untreated GDL only reached a maximum current density 0.3 Acm^2 compared to the 1.2 Acm^2 for the PVDF-based MPL. Since no contact angle measurements were performed and the relative humidity of the fuel cell tests was not recorded, it is difficult to draw conclusions from this study.

Bottino et al. [184] produced MPLs using phase inversion technique by immersion in a water bath of a mixture of either polyvinylidene fluoride or sulfonated polyvinylidene fluoride and using Vulcan XC-72 carbon black and Timrex HSAG 300 graphite as the electroconductive filler. The exposure time of the cast MPL prior to immersion in the coagulation bath was varied, from 0.5 min to 8 min as was the solvent used, *N*-methyl-2-pyrrolidone (NMP) and Dimethyl sulfoxide (DMSO). The MPL from DMSO solvent, PVDF, and an 8-min expose time measured the highest contact angle at 130°. The PVDFS MPL produced the highest cell performance, at 0.60 A cm^{-2} a voltage of 0.60 V was recorded compared to 0.43 V for the PVDF.

Ong et al. [185] also prepared a PVDF-based MPL via phase-inversion of PVDF and Vulcan XC-72 carbon black, which was then applied to a commercial wet-proofed cloth E-TEK GDL which was exposed for 30s and then immersed in a water bath. Increasing the PVDF content of the MPL from 5 to 10% wt. decreased the permeability significantly from 23.99 to 0.57 $\times$ 10^{-4} mol s^{-1} Pa^{-1} m^{-2} and whereas the increase in resistivity of MPL is insignificant (0.50–0.52 Ω). Two PVDF solutions were prepared for the carbon black dispersion, using different solvents: *N*,N-dimethylformamide (DMF) and *N*-methyl-2--pyrrolidone (NMP). The DMF cast MPL measured a higher resistance (0.062 Ω) than the NMP cast MPL (0.053 Ω), though the permeability values did not vary. The PVDF MPL GDL produced a higher limiting current density and greater peak power density (0.33 W cm^{-2}) than the blank and the 40% wt. PTFE MPL (0.25 W cm^{-2}). The difference in potential was particularly higher in current densities >0.3 A cm^{-2} thus having superior mass transport properties at higher current densities. This was attributed to the microstructure of the PVDF MPL being an asymmetric porous structure with cavities, in which the in-plane and through-plane mass transport is enhanced. As this GDL was not subject to heat treatment or sintering, a comparison of the surface morphology of the PVDF MPL heat treated and immersed would prove interesting, especially when combined with in-situ imaging of water distribution. Phase immersion may produce a smoother, more homogeneous PVDF coating, yielding different results to when the MPL is heat treated.

In addition, perfluoropolyether-based microporous layers have been studied [186,187]. PFPE binds strongly with carbon black due to its high surface area and porosity, allowing for the ease of adsorption of PFPE. Moreover, perfluoropolyethers can be chemically linked to the carbon black producing PFPE-functionalised carbons which are highly stable and can reach the super-hydrophobic threshold (157° at 8% wt.) [104]. PFPE-functionalised carbon blacks offer a promising alternative to carbon black-PTFE composites as unlike PTFE, the conductivity is preserved in the PFPE-modified carbon black because the electrical continuity of the conductive carbon network is maintained [188]. Where Vulcan XC-72 has been chemically functionalised with 10% wt. peroxide PFPE the resistivity remains very close to the value of the pristine carbon black [186,188].

Experiments conducted by Navarrini et al. [186] into functionalised-PFPE carbon blacks in the MPL indicated that 1% wt functionalised-PFPE has better performance in the mass transport zone than 10% wt. PTFE, where the voltage drop occurs at 1.30 A cm^{-2} rather than 1.0 A cm^{-2}. Thus a 30% increase in current density was achieved by the substitution of PTFE with functionalised-PFPE. The peak density was increased from around 0.42 W cm^{-2} to 0.45 W cm^{-2}, which was attributed to better reactant diffusion due to improved water management and higher gas permeability. Likewise, a recent study by Latorrata et al. [189] concluded that a 10% higher power density can be obtained using PFPE-functionalised Vulcan XC-72 in the MPL in the place of conventional PTFE at 80 °C and RH 60%.A peak power density of 460 mW cm^{-2} was achieved at 80 °C and 100% (Fig. 20 (right)). Fig. 20 (left) shows the

Table 3
Summary of the investigations into new architectures and alterative materials to carbon black for the microporous layer.

Author	Description	Method	Peak Power Density (W m^{-2})[a]	Main Findings
Duan et al. [157]	*Substrate:* P50T *MPL:* electro-spun carbon nanofibre sheet.	Spray Coated	0.32 (oxidant: air)	• Carbonised nanofibre sheet, hot pressed onto carbon fibre paper at 150 °C. • Uniform thickness of 25 μm was achieved with the CNFS MPL. • The 3D interconnected structure led to improved permeability and power density compared to the conventional GDL.
Gharibi et al. [159]	*Substrate:* TGP H-060 *MPL:* Vulcan XC-72 and MWCNT.	Roll Coated	0.07: (80:20 MWCNT: Vulcan, 0.5 mg cm^{-2} Pt)	• Pure carbon black and MWCNT based MPLs produced small pores volumes. Composite MPL produced greater pore volumes from different aspects of the two carbons. • Highest permeability was achieved with 80% MWCNT in the MPL. • MWCNT MPL highest electrical conductivity (423 s cm^{-1}), Vulcan (234 s cm^{-1}) and composite (291 s cm^{-1}). • Optimum ratio of MWCNT: carbon black depended on Pt catalyst loading.
Gallo Stampino et al. [158]	*Substrate:* S5 carbon cloth *MPL:* Vulcan XC-72 and MWCNT.	Doctor Blade	0.83: (10% wt. CNT) (oxidant: air)	• Ohmic resistance of the MWCNT-MPL lower than the Vulcan MPL at all air RH. • Addition of MWCNT to the MPL improved cell power density at all RH and temperatures. At 100% RH, the peak power density was ~0.83 W cm^{-2} with the MWCNT-MPL and ~0.60 W cm^{-2} with Vulcan XC-72 CB-MPL. • Charge transfer resistance is higher for MWCNT: CB MPL at low current densities.
Lin et al. [162]	*Substrate:* SGL 25BA *MPL:* Acetylene black and MWCNT	Blade Coated	0.92: (1:4, acetylene black: MWCNT) (oxidant: air)	• The internal pore structure of the MPL was changed from mixing the carbons with different aspect ratios, resulting in better transport for water and reactant gases. • Ohmic resistance varies with the mixing ratio of acetylene black to MWCNT. Charge transfer resistance was smaller with the composite MPLs. • Optimum carbon loading of the MPL was 1.5 mg cm^{-2}.
Lee et al. [16]	*Substrate:* SGL 25 BA *MPL:* 21% wt. MWCNT 64% wt. carbon black.		1.50 (I-R compensated voltage (the voltage compensated for the ohmic loss).	• 64% wt. carbon black, 21% wt. MWCNT and 15% wt. PTFE MPL. • Less mass transport resistance with MWCNT-MPL than SGL 25BC (at 2.5 A cm^2, 0.4 Ω cm and 1.0 Ω cm respectively). Due to thinner MPL and less intrusion into the substrate. • SGL 25 BC experienced significant potential drops at increasing current densities (above 2.0 A cm^{-2}). At 2.0 A cm^{-2} and 2.5 A cm^{-2} power densities of in-house 25BN MWCNT MPL were 6.7% and 94.1% higher respectively, compared to the commercial 25BC.
Leeuwner et al. [173,174]	*Substrate:* TGP H-060 *MPL:* Natural graphite, reduced graphene oxide and exfoliated graphene	Spray Coated	1.27: (NG) 1.70: (RGO) 0.98 (Ex. G) (oxidant: air)	• Produced exfoliated graphene using Najafabad et al. [172] methodology. • Natural graphite MP: high limiting current density: 3800 mA cm^{-2} at 0.2 V. • Natural graphite MPL highest power density: high air and water permeabilities. • High water permeability of carbon black MPL enhanced water transport away from the CL reducing ionic conductivity of the catalyst layer at the cathode side of the membrane. • At 20% RH, natural graphite MPL has lower peak power density: 1.17 W cm^{-2}.
Najafabad et al. [172]	*Substrate:* TGP H-060 *MPL:* Electrochemically exfoliated graphene.	Spray Coated	1.19: (Composite Graphene and Vulcan) (oxidant: air)	• Electrochemically exfoliated graphene, Vulcan XC-72 MPL and a composite. • The composite MPL had lowest through-plane resistance suggesting the addition of carbon particles between the graphene plates increases electron transfer. • Limiting current density increased from 1500 mA cm^{-2}, with pure exfoliated graphene MPL, to 3200 mA cm^{-2}, with composite MPL.
Ozden et al. [175]	*Substrate:* AvCarb EP40 *MPL:* Graphene	Spray Coated	0.88 (oxidant: air)	• Contact angle 2.0 mg cm^{-2} 20% PTFE: graphene: 140°; KJ carbon black 116°. • In-plane resistivity of the graphene MPL is generally smaller than KJ black MPL. • At 40% and 70% RH, graphene MPL highest peak power density (0.62 vs. 0.40 W cm^{-2} and 0.70 W vs. 0.67 W cm^{-2}). Graphene flake morphology created resistance to discharge water from the catalyst, thus maintaining membrane hydration. • At 100% RH, carbon black MPL had a higher peak power density (0.88 vs. 0.89 W cm^{-2}).
Mariani et al. [181]	*Substrate:* SCCCG5N *MPL:* Vulcan XC-72, graphene nanoplates and exfoliated graphite.	Doctor Blade	0.42: (Medium GNP/CB) 0.36: (Small GNP/CB) 0.34: (EG/CB) (60% RH and 60 °C) (oxidant: air)	• Graphene nanoplates (small and medium nanoplatelets); exfoliated graphite and MWCNT. Composite MPLs mixed with Vulcan XC-72 (1:1 ratio). • Graphene nanoplates: increased meso and macropores, increasing water retention. Reduced membrane dry-out but increased tortuosity which exacerbated flooding. • Carbon black: produced micropores in the MPL, reducing liquid water accumulation but the carbon black agglomerates reduce gas permeability.

(*continued on next page*)

Table 3 (*continued*)

Author	Description	Method	Peak Power Density (W m^{-2})[a]	Main Findings
				• Small graphene nanoplatelets and large exfoliated graphite suffered mass transfer resistance. Small graphene nanoplates form small pore limiting oxygen diffusivity. Exfoliated graphite forms large macro pores easily permeated at low-mid current densities. Liquid water expulsion is reduced, and flooding occurs.
Leeuwner et al. [174]	*Substrate:* TGP H-060 *MPLs:* Graphene foam, stainless-steel sheet, perforated graphitic sheet.	Free-standing	0.62: (GF) 0.15: (SSS) 0.58: (PGS) (oxidant: air)	• Compressed graphene foam: lowest contact resistance between MPL and CL. • Novel MPLs: higher mass transport losses, due to lack of hydrophobic treatment. • Compressed graphene MPL highest potential at 500 mA cm^{-2} (0.724 V, graphitic sheet: 0.668 V and steel: 0.200 V). At 2000 mA, graphene has high potential drop with lower power density than SGL 25BC (360 mW cm^{-2} and 600 mW cm^{-2}). • Compressed graphene MPL favoured cathode side water retention, maintaining a good ionic conductivity at low RH conditions. Best durability: 80 polarisation cycles over 150 h.
Fang et al. [179]	*Substrate:* SGL 10BA *MPL:* Titanium powder	Spluttered	0.41: (10 min) 0.39 (30 min) 0.37: (60 min) 65 °C	• Titanium sputtering time for MPL coating was varied from 10, 30 and 60 min. • Spluttering time decreased contact angle. Highest measured: 131° after 10 min. • 10 min: titanium sputtering had highest peak power at 0.413 W cm^{-2}. MPL film thickness maybe influential (220 nm- 10 min, 1125 nm thickness- 60 min).
Hwang et al. [176]	*Substrate:* Titanium felt *MPL:* Titanium powder and PTFE	Screen Printing	0.22:(300 mg) 0.28: (200 mg) 0.079: (100 mg) (oxidant: air)	• Ti MPL modified pore structure of the Ti GDL: the main pore size shifted from 50 to 60 μm to <50 μm. Meso-pores volume increased with Ti loading, no micro-pores were generated. • Fully humidified, the addition of Ti-MPL (200 and 300 mg cm^{-2}) improved power density. At 66% RH, mass transport resistance increased due to increased capillary barrier effect. • Increased mesopores: effective removal of liquid water from CL/MPL interface.
Ito et al. [152]	*Substrate:* Toray TGP H-060 Toray TGP H-090 Standalone MPL *MPL:* Acetylene black	Free-standing Slip Rolled	0.75: (no substrate) 0.65: (Acetylene black and TGP H-090) (oxidant: air)	• Self-supporting MPL and coated substrates were 300 μm thick. • Self-supporting MPL was microporous with very few pores larger than 10 μm. • Self-supporting MPL was found to be extremely fragile being fractured by liquid water injection even at low injection pressure, < 10 kPa. • Power density produced from the self-supporting MPL was the highest. The cause was identified as the high temperature profile and the contact resistance between the MPL and the flow field plates and catalyst layer.
Shim et al. [45]	Vulcan XC-72 and PTFE (20–50% wt. PTFE)	Free-standing rolled sheet	0.11 (oxidant: air)	• Carbon black and PTFE paper was mainly microporous (0.01–3.0 μ m). • Lack of macropores (>3.0 μ m) limited bulk diffusion. • Highest power density, 0.11 Wcm^{-2}, from 60% carbon and 40% PTFE. • Increasing PTFE: increased electrical conductivity, decreased pore diameter and air flux. Pore diameter and air flux were more critical in improving power density.

[a] Unless otherwise states, the peak power density was reported with 100% RH and oxygen as an oxidant.

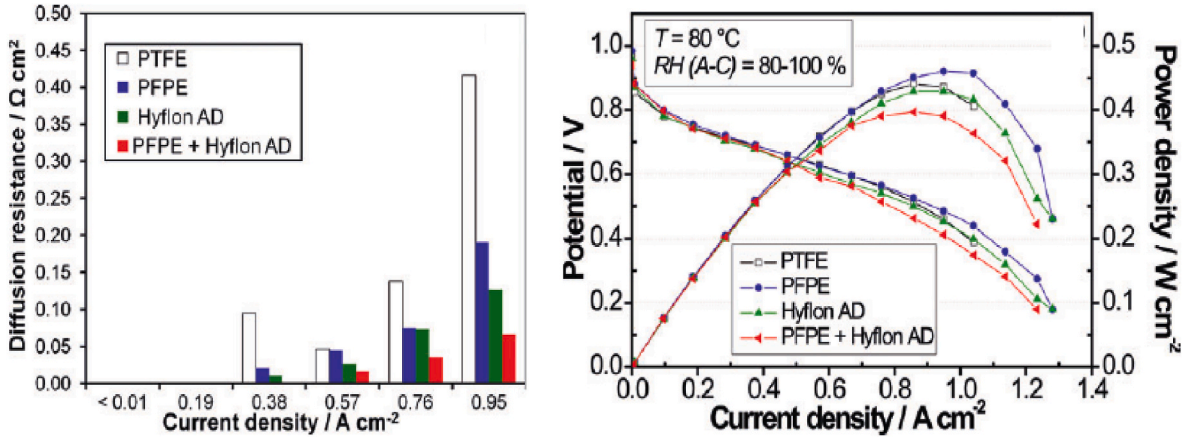

Fig. 20. The diffusion resistance of the GDLs with MPL different compositions (60 °C, 80–100% RH). (Right) Polarisation curve of MEAs with the differing MPL compositions (80 °C and 80–100% RH). Reproduced from Fuel Cells with the permission of John Wiley and Sons [189].

mass transfer or diffusion resistance of the different MPL coated GDLs, where at 60 °C and 100% RH the PTFE MPL experiences mass transport losses at high current density. This indicates the inferior water management of the conventional PTFE MPL.

Balzarotti et al. [187] used a high molecular weight PFPE-based MPL (i.e. Fluorolink® P56) with different wt. %, which was applied to B1-A, E-TEK carbon cloth GDL. A contact angle of 149° was achieved with 12% wt. PFPE, whilst the value was 154° for 6% wt% PFPE. A higher power density was also achieved for 6% wt. ' PFPE compared to the 12% wt, 0.59 W cm^{-2} and 0.53 W cm^{-2} respectively. The authors' explanation was that the larger cracks in the MPL surface improved permeability and diffusive properties of the MPL, however this is not conducive with other findings as larger cracks increase the resistance at the MPL and catalyst layer interface. It is more likely that the increase in PFPE concentration reduced the available pore space and thus limited reactant diffusion.

The characterisation of fluorinated polymers in the MPL by Latorrata et al. [190] is highly informative. The work compared PTFE with alternative fluorinated polymer binders, namely fluorinated ethylene polymer (FEP), perfluoropolyether (PFPE), and perfluoroalcoxy (PFA). The FEP-based MPL was reported to have the highest contact angle of 160°, whilst the PTFE-based MPL had the lowest contact angle, making it the least hydrophobic. Correspondingly, the fluorinated ethylene polymer -based MPL had the highest maximum power density, and the lowest mass transport losses in fuel cell tests. For example, at 1.0 A cm^{-2}, the FEP-based MPL was measured to have a potential of 1.0 V, compared to 0.8 V for the PTFE-based MPL (Fig. 21). The same group [191] then conducted further experiments into the stability and durability of FEP-based MPLs, with minimal difference in fuel cell performance after 1000 h of mechanical and chemical accelerated stress testing.

Park et al. [192] also conducted research into 10% wt. FEP-based MPLs deposited on Toray carbon cloth, and reached similar conclusions. The use of FEP resulted in higher water contact angle (145°) compared with PTFE-based microporous layers (141 °C), which may have increased the water repelling capability of the MPL. The FEP-based MPL produced a more precise and uniform pore size distribution than PTFE-based MPL due to the smaller particle size, moreover an absence of large pores and crude cracks on the MPL surface was observed. These two factors are believed to reduce contact resistance between the MPL and catalyst layer, however contact resistance measurements were not conducted. In fuel cell performance tests, the fluorinated ethylene polymer -based MPL produced a higher power density of ~0.3 W cm^{-2}, compared to ~0.25 W cm^{-2} for the PTFE-based MPL.

Meanwhile, Yan et al. [180] found that 30 wt % of FEP in the MPL was optimal for minimising flooding and improving the fuel cell performance, and obtained a maximum power density of 1.4 W cm^{-2}. Moreover, they compared different MPL coating methods (i.e. spray coating and screen printing), concluding that screen printing resulted in better cell performance. This was attributed to the formation of cracks in the spray coated MPL coating, reducing the contact area between the electrocatalyst layer and the MPL, thus increasing the contact resistance.

7.2. Hydrophilic and mixed-wettability MPLs

Another branch of research is directed towards the study of hydrophilic MPLs. Instead of conventional hydrophobic MPLs, where the aim is to push water through and out of the fuel cell, the aim of hydrophilic MPLs is to pull water out of the electrocatalyst layer. The potential of hydrophilic MPLs to mitigate water flooding at high current densities has been reported in several studies [164,166,193,194]. For example, Aoyama et al. [166] compared hydrophobic and hydrophilic MPLs of various thicknesses, conducting polarisation measurements in fully humidified conditions. They reported that hydrophobic MPLs had the highest cell resistance, and that the hydrophilic carbon fibre MPL produced a higher voltage than the hydrophobic carbon black MPL at high current densities (0.4 V and 0.3 V respectively at 1.6 A cm^{-2}). It was deduced that the hydrophilic MPL surface allows water to spread across the MPL surface and promotes evaporation within the large pores and thus the thick hydrophilic MPLs may be more effective when there is more liquid water produced. Similarly, Tanuma et al. [195] also developed a novel hydrophilic MPL composed of vapour grown carbon fibres with hydrophilic ionomer, resulting in MEAs with higher power density compared to those with hydrophobic MPLs, across a range of different relative humidities. Different MPL architectures were more

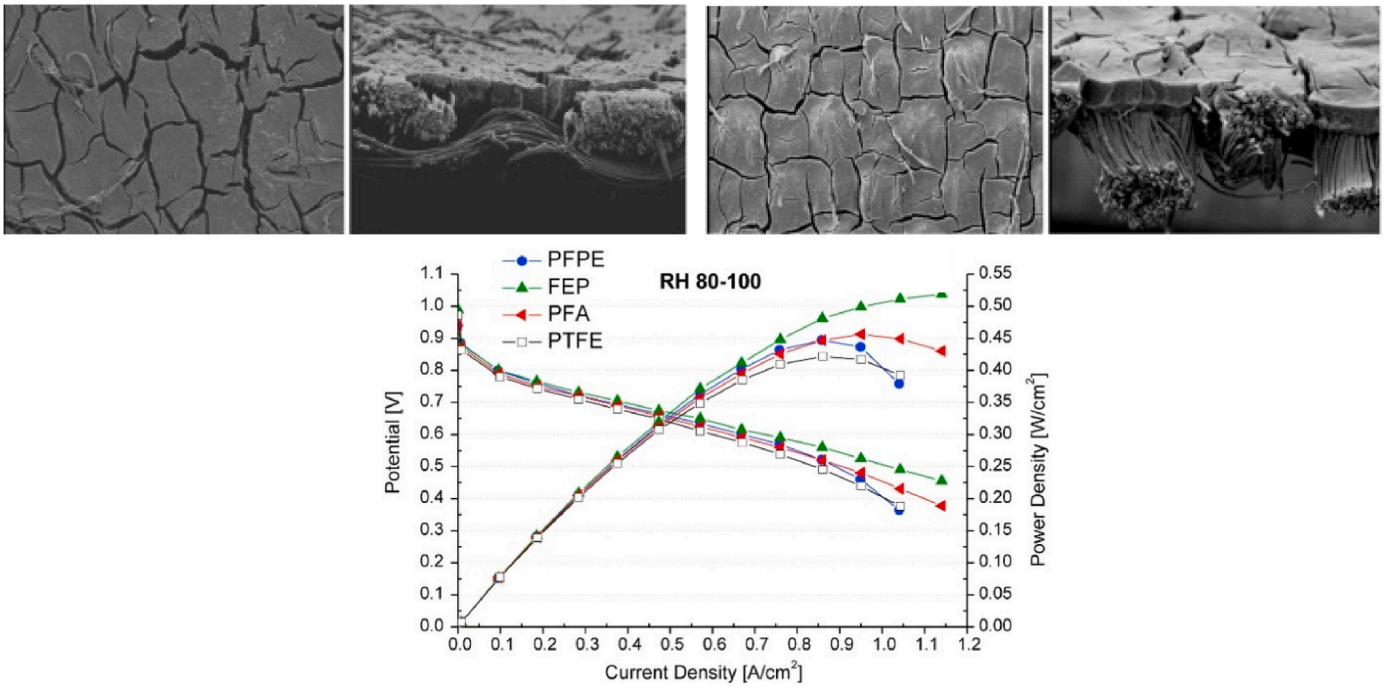

Fig. 21. (Top) SEM images of the surface and cross section of the MPL (left) FEP, (right) PTFE. (Bottom) MPLs fabricated with different hydrophobic agents at RH 80–100. Reproduced with permission from Elsevier [190].

influential at different relative humidities; where at low RH (30%) the mean pore diameter was the largest factor, conversely at high RH (100%) pore volume was the greatest contributor to power density. The greatest power density (0.75 W cm^{-2}) was achieved at 30% RH.

The majority of research into PEMFC is targeted at improving MEA performance in high humidity conditions; however it is also necessary to optimise PEMFC design for low humidity condition > this is because PEMFCs are to be applied to a broad spectrum of applications (aerospace, stationary and portable applications) and these have different operating requirements and reactant feeds. In low relative humidity conditions, maintaining membrane hydration for optimal ionic conductivity is the largest challenge. To this end, investigations on how to create hydrophilic MPLs allowing for PEMFC self-humidification have been conducted [196,197]. A hydrophilic anodic was produced Guo et al. [196] by ultraviolet treatment of TiO_2 particles, to reduce the membrane resistance in low humidity conditions. The hydrophilic MPL reportedly decreased both the charge transfer resistance at low current densities, and the ohmic and mass transport resistance at high current densities, improving performance at both low (100 mA cm^{-2} and high (1200 mA cm^{-2}) current densities. Other works have used UV treatment of the MPL to create hydrophilic regions with the aim of producing a GDL with graded hydrophobicity for the diversion of liquid water away from the catalyst layer [198]. The UV treatment leads to the formation of OH radicals on the of the gas flow channel side of the GDL, thus reducing the hydrophobicity and creating a GDL with graded wettability from the catalyst layer to the gas flow channel [198].

In order to provide deeper understanding of how hydrophilic regions in the MPLs facilitate liquid water transport in MEAs, Mukundan et al. [199] used neutron radiography to visualise the liquid water distribution, in-situ. An MPL was produced by incorporating 10% hydrophilic alumosilicate fibres into a conventional hydrophobic carbon black MPL slurry and applied to an SGL 24AA GDL, and comparison made with a commercial SGL 25BC. The addition of the hydrophilic fibres increased voltage by 150 mV at 2 A cm^{-2}, increasing power density by 30% Liquid water distribution was analysed to understand the different in power density. The water profile across a cross-section of the cell operating at 1.0 A cm^{-2} was obtained by neutron imaging (Fig. 22). In the hydrophobic MPL, indicated by the red line, the peak indicates that liquid water saturation is concentrated close to the cathode catalyst layer, moreover the MPL has a low water content as can be seen by the drop when moving away from the MEA. In contrast the MPL with hydrophilic fibres, shown by the blue line, has a more liquid water in the MPL region evidenced by the steadier water content profile. Additionally, there is no peak at the cathode catalyst area, indicating that liquid water saturation is lower at the cathode catalyst layer, thus, indicating that the loss in power of the hydrophobic 25BC were mass transport losses due to liquid water saturation.

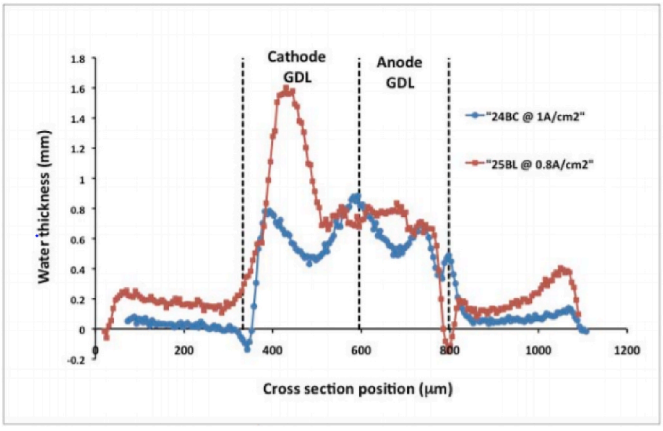

Fig. 22. Water profiles at 2.5 cm^2at 80 °C and 100% RH using the 2 GDLs. 25BL (10% hydrophilic fibres in MPL) and 25BC (hydrophobic MPL). © The Electrochemical Society. Reproduced by permission of IOP Publishing. All rights reserved [199].

Furthermore, the addition of alumosilicate, hydrophilic fibres into the hydrophobic MPL improved mean pore diameter. The increased pore diameter facilitated the movement of liquid water away from the MPL/catalyst interface, where the hydrophilic pores provided pathways in the MPL, wicking the water away from the cathode.

Additionally, Aoyama et al. [166,200] and Nozaki et al. [194] used cryogenic scanning electron microscopy of cross-sections of the cathode side microporous layer to visualise the liquid water distribution inside hydrophilic and hydrophobic MPLs. They found that much less liquid water was present in a thick hydrophilic MPL compared to a thin hydrophilic MPL or a conventional hydrophobic MPL. They postulated that thick hydrophilic MPLs facilitate the passage of liquid water, which is then able to more rapidly evaporate into the gaseous phase to be transported effectively through the porous media.

7.2.1. *Multi-layer MPLs*

An innovative dual-layer MPL was developed by Kitahara et al. [149,201], with a thin hydrophilic MPL deposited directly onto a conventional hydrophobic MPL, for low relative humidity operation. The hydrophilic MPLs were composed of 95% carbon black mixed with 5% polyvinyl alcohol (PVA) or TiO_2 (titanium dioxide). They reported that the hydrophilic MPL preserves the membrane humidity, whilst the hydrophobic layer prevents removal of water from the hydrophilic MPL by evaporation. The dual-layer hydrophilic/hydrophobic (5%. wt PVA) MPL produced greater power than the hydrophobic PTFE MPL, particularly in the mass transport region, where at 1.2 A cm^{-2} the voltage was 0.5 V and 0.3 V respectively. Further performance enhancements was done by optimising the PTFE content, and thus the hydrophobicity of the hydrophobic layer [149]. A further innovation was the development of a triple-layer MPL by the Kitahara et al. [202] where, the substrate was coated in a hydrophobic MPL (10 wt% PTFE), followed by another hydrophobic MPL (30 wt% PTFE), and finally a hydrophilic PVA-based MPL (Fig. 23). This resulted in further improvements in the fuel cell performance, which was attributed to the hydrophobic gradient which successfully expelled liquid water from the electrocatalyst layer at high relative humidity. The most influential aspect of this group's work is the introduction of the concept of gradated MPLs, rather than limiting the design to one single layer with a homogeneous microstructure.

8. Summary

The optimisation of liquid water displacement in the microporous layer and the membrane electrode assembly as a whole will lead to significant increases in fuel cell efficiency. The superhydrophobic threshold of the MPL is easily achieved with alternative fluorinated polymers and by plasma deposition of smaller wt.% than conventional PTFE. The lower polymer content equates to small reductions in pore size and conductivity, thus increasing the capability of the MPL for two-

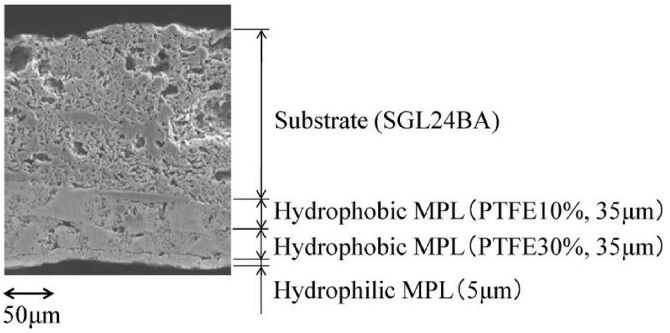

Fig. 23. Cross-sectional SEM micrograph of a triple-layer MPL-coated GDL. Reproduced with permission from Elsevier [202.

phase and electron transport. Moreover, in particular, the PFPE-functionalised carbon black, or even other carbon materials, can rectify many of the problems encountered with the conventional PTFE adsorption on carbon black, such as increased durability and minimal impact on MPL pore size distribution.

Innovative MPL architectures with mixed wettabilities have been shown to improve power density, where hydrophilic regions act as pathways to push liquid water away from cathode electrocatalyst area. Further research is needed to improve these hydrophilic/hydrophobic MPLs by optimising the ratio of hydrophilic: hydrophobic areas, as well as their correct profile, shape and distribution.

Table 4 summarises recent investigations into alternative materials and architectures to enhance the wettability of the MPL.

9. Modelling GDLs

Whilst many experimental studies have been used to optimise the structure and performance of GDLs, modelling can be an effective tool to visualise transport phenomena in PEMFCs. Pore-scale modelling using the Lattice-Boltzmann method (LBM) has recently proved an effective technique for the visualisation of liquid water and transport mechanisms. Satjaritanun et al. [206] predicted the water breakthrough pressure of the MPL and substrate at different levels of hydrophobicity, and their model agreed with reported experimental data. Similarly, Jinuntuya et al. modelled GDLs with three different structures, different water contact angles, over a range of different pressures [207]. Their model showed that the water contact angle has the largest effect on water transport, and that there is a sharp transition between stable water displacement for hydrophilic contact angles ($60^\circ < \theta < 90^\circ$) and capillary fingering for hydrophobic contact angles ($100^\circ < \theta < 140^\circ$).

Recently, the effect of a non-uniform pore distribution on liquid water transport in the GDL has been numerically modelled [208,209]. Shangguan et al. produced 5 GDL geometries with different pore distributions: uniform porosity; graduated pore size from large (macro) to small (micro) with different intensity; and graduated from small (micro) to large (macro) with different intensity [209]. Their model predicted that the GDL with a non-uniform porosity distribution from macro to micro pores, with a low porosity gradient liquid promotes rapid water removal and relieves water saturation. Their model also predicted that the hydrophilic (70°) GDL experienced liquid water saturation regardless of the pore structure.

In a related work Kanchan et al. [209] produced 5 different geometries for the cathodic GDL to investigate their influence on oxygen concentration and power density. The porosity distribution was varied by increasing and decreasing porosity from the inlet to the outlet (in the streamwise direction), and increasing and decreasing porosity from the gas flow channels to the catalyst layer (stepwise direction). The model indicates that when the porosity is decreased from the inlet to the outlet, the molar oxygen concentration is the highest, and power density and current density are the highest. This is attributed to the high porosity (0.6) of the cathode inlet allowing for less resistance to the flow of oxygen. The model also indicates that when porosity is increased from the catalyst layer to the flow channels the resulting power density and current density are relatively higher, in agreement with experimental and modelling data [209].

Although significant improvements have been made to computational models of porous media in PEMFCs, there are still a number of challenges that need to be overcome to simulate an accurate reflection of the porous media, and the transport phenomena therein. One such area that requires a deeper understanding is the thermal conductivity in the gas diffusion media. Ex-situ characterisation of the thermal transport is highly simplified for what is extremely complicated due the differences in the thermal conductivity of the solid and pore spaces, and the anisotropic microstructure. Yet the thermal conductivity of the porous media is essential for a complete understanding of liquid water behaviour in the MEA, both by causing membrane dry-out and reducing pore saturation by enabling entrance into the vapour phase and subsequent transport. The inaccurate modelling of thermal conductivity of the gas diffusion is thus a current limitation to the accurate modelling of reactant and water transport in the GDL.

10. Conclusions

GDLs are widely acknowledged as critically important components for optimal performance of PEMFCs. To this end, they have been subject to a great deal of research. The use of alternative materials for the macroporous substrate and the MPL has seen various successes, where the importance of pore size distribution is an integral factor. Developments in more sustainable source materials, such as bamboo fibre for the carbon substrate, divergence from PTFE, and simplification of the manufacturing process will further improve the sustainability and reduce the cost of production of PEMFCs.

The potential of the GDL in the management of liquid water in the MEA is the largest driver of this research. Various methods have been explored to reduce flooding, whilst maintaining membrane hydration. One branch of research aims to reduce catalyst flooding by creating superhydrophobic GDLs. On the other hand, gradation of the MPL microstructure and water contact angle can effectively manage the water distribution in the PEMFC. In-operando imaging has allowed for the visualisation of liquid water in the MEA, making it possible to further optimise the pore structure of the porous media. The duality of two-phase flow of reactants and liquid is still not fully understood particularly at higher current densities; the potential for simulations based on in-operando data will greatly assist in this as a prior step to experimental work.

11. Recommendations for future work

11.1. Recommendations for the macroporous substrate

The alternative macroporous substrate architectures and materials hold potential in improving the gas diffusion media. Many alternative materials and designs have matched or exceeded the PEMFC performance using conventional carbon substrates as gas diffusion layers. It is important to consider the feasibility of the production of these substrates on a large scale which would allow for their use in the energy sector, automotive industry and in portable electronics. Many of the materials are innovative and exciting, yet the fabrication of these designs requires simplification, and in their present state they are unsuitable for deployment on a large scale.

Electro spun and metal foams gas diffusion substrates are considered highly promising components for the fuel cell industry. Their method of fabrication allows for control over the structure and physical properties to produce an optimised GDL for cell performance. More importantly though, these methods have been shown to have a reliable reproducibility and ease of fabrication on a larger scale; both of these characteristics are essential for fuel cell manufacturers. Of course these fabrication technologies for GDL design are still in their early stages of development, and there is optimisation that needs to be done to reduce mechanical and chemical degradation.

The third consideration for the enhancement of the gas diffusion substrate is sustainability. This is of particular importance when considering a low-carbon technology like PEMFC component design. This can only be assessed through thorough cradle to grave, life-cycle analysis of the component from the sourcing of the materials, the energy intensity of the production, and the recovery of the materials post use. This has been touched upon by researchers by, for example, reducing the heat treatment temperature, and substrate manufacturing from coconut and bamboo fibres; however this area is important when considering life cycle analysis of the final commercial product. This is particularly apparent when imparting hydrophobicity to the GDL, which is almost universally done by fluorinated polymers. The environmental

Table 4
Summary of the investigations into alternative materials and architectures to enhance the wettability of the microporous layer.

Authors	Description	Coating Method	Peak Power Density (W cm^{-2})[a]	Contact Angle (°)	Main Findings
Latorrata et al. [190,191]	*Substrate:* S5 carbon cloth *MPL:* Vulcan XC-72 with PFPE, FEP, PFA and PTFE.	Doctor Blade	FEP: 0.52 PFPE:0.38 PFA:0.43 PTFE:0.36 (oxidant: air)	FEP:160° PFPE: >150 PFA: > 150 PTFE: 145	• FEP based MPL had the highest power density attributed to low mass transfer resistance. • PFPE based MPL exhibited the lowest ohmic resistance but highest mass transfer resistance. • PFPE based MPL exhibited better performance at low humidity conditions. • PFPE based MPL may have lost adhesion with the substrate at higher humidities.
Park et al. [192]	*Substrate:* FEP coated E-TEK carbon cloth *MPL:* Vulcan XC-72 and 10% wt. FEP	Doctor Blade	FEP: 0.3	FEP:145° PTFE:141°	• The contact resistance resulting from the integration of the FEP-MPL was much less than the PTFE MPL due to less surface cracks. • Pore size distribution is more uniform with the FEP-MPL as the particle size is smaller. • Better compressive strength of the FEP compared to PTFE gave the FEP-MPL better substance mobility and current density distribution.
Yan et al. [203]	*Substrate:* TGP-H-090 *MPL:* 30% wt. FEP and Vulcan XC-72.	Spray Screen printing	FEP: 1.4 (30% wt.)	–	• Screen printed MPL produced higher power densities than the spraying of MPL ink. • Spraying process produced larger surface fractures; improving gas permeability, though reducing contact at the MPL/CL interface leading to high ohmic losses. • 30% wt. FEP produced highest current densities compared to 10% and 20% wt.
Öztürk et al. [204]	*Substrate:* X0090 IX92 Freudenberg *MPL:* Polydimethylsiloxane (PDMS) 3% wt. and Vulcan XC-72	Spray Coating	PDMS:0.19 (3% low weight PDMS 1 mg/cm^{-2} CB 64% RH)	PDMS (3% wt):142° FEP (20% wt) :1478° PTFE (20% wt):143°	• Low Pt catalyst loading used (0.1 mg cm^{-2}). • For the lower weight PDMS, at 5% wt. a higher maximum power was achieved as relative humidity increased, whereas for 3% wt. the highest power density was achieved at 64% RH. 5% wt. PDMS in the MPL is the most suitable for working at high current density region when water flooding is considered. • The high molecular weight PDMS polymer was unsuitable for the MPL due to its high viscosity that creates excess resistance to water flow.
Park et al. [135]	*Substrate:* E-TEK *MPL:* Vulcan XC-72 and PVDF	Doctor Blade	PVDF:0.35	-	• Less surface cracks with PVDF; resulting in less contact resistance and ohmic losses. • PVDF 40% wt. in MPL: comparable pore size distribution of PTFE MPL. • Mass transport losses were reduced with the PVDF in the MPL due to improved in-plane and through-plane microstructure.
Bottino et al. [184]	*Substrate:* B1-A, E-TEK *MPL:* Sulfonated PVDF and Vulcan XC-72	Blade Coating	PVDFS: 0.36 PVDF:0.26 (oxidant: air)	PVDFS: 119° PVDF: 130°	• Sulfonated PVDF MPL produced higher power density than the non-sulfonated one. • Increased exposure time to 8 min from slurry casing to immersion increased the surface porosity and pore depth of the MPL. • Permeability of the MPL was higher using dimethyl sulfoxide (DMSO) compared to *N*-methyl-2-pyrrolidone (NMP).
Ong et al. [185]	*Substrate:* E-TEK *MPL:* PVDF and Vulcan XC-72	Blade Coating	0.30 (oxidant: air)	–	• PVDF produced an MPL with asymmetrical hydrophobic porous structure which enhanced the mass transport at high current densities. • Increased amount of Vulcan XC-72 carbon black increased the electrical conductivity of the MPL but reduced the permeability.
Balzarotti et al. [187]	*Substrate:* SCCG5 *MPL:* Vulcan XC-72 and P56-PFPE	Blade Coating	PFPE: 0.59 (6 % wt.). PFPE: 0.53 (12 % wt). (oxidant: air)	PFPE:154° (6 % wt.). PFPE: 149° (12 % wt).	• P56 PFPE increased the viscosity of the slurry compared to PTFE based MPL slurry. • Compared to PTFE, PFPE (6% wt.): higher power density at all RHs and temperatures. • Drying temperature of the MPL affects surface morphology with larger cracks appearing in quickly dried cast slurries.
Latorrata et al. [189]	*Substrate:* S5 *MPL:* Vulcan XC-72 functionalised Fomblin Z PFPE	Spray Coating	PFPE: 0.46 PFPE/Hyflon AD: 0.43 Hyflon AD:0.40 (oxidant: air)	PFPE: 165 PFPE/Hyflon AD: 168 Hyflon AD:168	• Conventional PTFE experiences high mass transport resistance at high current densities in high humidity, low temperature conditions (100% RH and 60 °C). • High temperature and cathode inlet RH (80-100 °C/100% RH) had greatest power density. • Durability tests of PFPE MPL, stressed MPL had slight increase in mass transport resistance at high current density. Though minimal change in cell performance.
Aoyama et al. [200]	*Substrate:* H2315, Freudenberg *MPL:* Hydrophilic carbon fibre and ionomer.	–	0.90	–	• At high current densities, hydrophilic MPL produced a higher voltage, this situation was reversed at the low current densities. • Large pore diameters and hydrophilicity contribute to increased cell performance.

(*continued on next page*)

Table 4 (*continued*)

Authors	Description	Coating Method	Peak Power Density (W cm^{-2})[a]	Contact Angle (°)	Main Findings
					• Freezing and cryo-SEM observations: water remains in the CL side pores of the MPL and in the GDL side. Thus, reactant diffusion is not affected. • Hydrophilic surface water spreads across MPL surface and evaporates in the large pores.
Tanuma et al. [195]	*Substrate:* H2315 *MPL:* Hydrophilic MPL from vapour grown carbon fibre	Wire rod coating	VGCF-H: 0.75 (30% RH) (oxidant: air)	–	• Vapour grown carbon fibre (VGCF-H) -highest cell voltages in wet and dry conditions. • Mean pore volume of carbon black and MWCNT fibre was the smallest (0.068 μm and 0.055 μm), whereas the VGCF-H has the largest mean pore diameter (0.77 μm). • At low RH (30%), the mean pore diameter was the largest contributor to power density. • At high RH (100%), pore volume was the greatest contributor to power density.
Mukundan et al.	*Substrate:* 24AA *MPL:* Alumosilicate carbon fibres (10 % wt.), carbon black and PTFE.	–	1.16 (oxidant: air)	–	• Mixing of hydrophilic fibres into hydrophobic MPL improved mass transfer of oxygen. • Addition of alumosilicate carbon fibres to the MPL increased the mean pore diameter. • The increased pore diameter was believed to have improved the movement of water away from the CL/MPL interface. • The inclusion of hydrophilic fibres produces hydrophilic pathways in the MPL, wicking the water away from the cathode.
Nozaki et al. [194]	*Substrate:* H2315 *MPL:* Carbon black and PTFE and hydrophilic carbon fibres.	–	0.78	-	• Freezing and cryo-SEM to visualise liquid water saturation at the MPL/CL interface. • Residual water at MPL/CL increases oxygen transport resistance from reduced flow. • A narrow land and wide channel configuration prevent water accumulation in the hydrophobic MPL and the GDL, thus reducing oxygen transport resistance. • Oxygen transport resistance was lower in the hydrophilic MPL than the hydrophobic one; the hydrophilic MPL was better at draining liquid water away from the CL.
Chun et al. [205]	*Substrate:* PB6B, Hyupjin *MPL:* Hydrophilic/hydrophobic double layered	Screen Printing	0.5 (oxidant: air)	Hydrophobic :139° Hydrophilic :113°	• Hydrophilic MPL acts as internal humidifier due its water absorption ability. • A middle hydrophilic layer exhibited better cell performance than a single hydrophobic layer or a hydrophobic layer underneath a hydrophilic layer. • At low humidification, the internal hydrophilic MPL prevented the membrane from dehydration.
Kitahara et al. [202]	*Substrate:* SGL 24BA *MPL:* Hydrophilic/hydrophobic triple layered	Bar Coated	~1.0 30 + 40% wt. PTFE 30 + 10% wt. PTFE (oxidant: air)	Hydrophobic:130° Hydrophilic:82°	• Hydrophilic MPL: TiO_2 (25% wt.), silicone (5% wt.), and carbon black. Hydrophobic MPL: PTFE (30% and 40% wt. or 30% and 10% wt.) and carbon black. • Hydrophilic layer works to preserve catalyst and membrane humidification. • Triple layered MPL: higher power density in high humidity conditions. Two hydrophobic layers removed excess water from CL. • Triple layer with 30 + 10% wt. PTFE, created hydrophobic gradient promoting the movement of water towards the substrate from the MPL.

[a] Unless otherwise states, the maximum power density was reported with 100% RH and oxygen as an oxidant.

impact on the widespread use of these fluorinated polymers is becoming more apparent. Thus the minimisation of the use of these polymers to impart hydrophobicity is recommended as research shows many options exist.

11.2. Recommendations for the microporous layer

In terms of the microporous layer, it seems that alternative materials to carbon black, particularly carbon nanotubes, can improve the peak power density of the fuel cell, although there is a definitive lack of durability testing which raises questions for the suitability of these materials in practice. Likewise, preliminary studies undertaken using graphitized carbon black and graphene have exhibited promising results (higher power density and preferential ex-situ characteristics), yet again they are limited by a lack of research into their applicability for commercial use. Further research into graphene as a replacement for carbon black is necessary, owing to its preferential physical characteristics and early studies have shown its potential for use in the microporous layer. Moreover, the cost of materials is an important consideration in the commercial fuel cell sector. Performance enhancements with carbon nanotubes and graphene need to be balanced against increased cost of materials.

The majority of improvements to MPL design have been changes to hydrophobicity and porosity of the structure. When the microporous layer is given a non-uniform structure with a pore gradient decreasing from the substrate to the catalyst layer interface, the PEMFC has an enhanced performance and does not suffer liquid water saturation. The fabrication of graduated microporous layers would be a simple addition to the manufacturing process which can greatly improve the performance of the commercial GDLs. The deposition of larger carbon particles followed by smaller carbon particles in the MPL would be a simple method of creating the graduated pore profile that is reported to significantly improve liquid water management and power density.

11.3. General recommendations for GDL research

The potential of polymer electrolyte membrane fuel cells should not be understated. They have been hailed numerous times as one of the greatest means of meeting global energy demand; reducing global consumption of fossil fuels; and diminishing anthropogenic carbon emissions. However, a recurring issue in the field of fuel cell research, and academic engineering is in general maintaining relevance to commercial industry and real world application. Although this article presents pioneering performance improvements from modifications of one of the key fuel cell components (GDLs), very few of these are elevated from the single cell laboratory scale, or subject to durability testing.

The adage that our time is running out is not one that should easily be dismissed. Thus it would be desirable to see greater emphasis on upscale, and feasibility of designs and application methodology for a commercially viable product. These improvements would not only accelerate the development of fuel cell technology and infrastructure but attract increased financial investment.

Declaration of competing interest

The authors declare that they have no known competing financial interests or personal relationships that could have appeared to influence the work reported in this paper.

Acknowledgments

The first author would also like to thank the ESPRC CDT for Clean Fossil Energy and Carbon Capture Storage (EP/L016362/1) as well as the International Flame Research Foundation for their financial support. The authors would like to acknowledge the support of the Royal Society (RS): The bilateral Royal Society (RS) – Japan Society for the Promotion of Science (JSPS) research grant (IEC\R3\170032).

References

[1] Yuan X, Zhang J. PEM Fuel Cell Fundementals, in PEM Fuel Cell Electrocatalysts and Catalyst Layers: Fundamentals and Applications. In: Zhang J, editor. London: Springer; 2008.
[2] Mathias MF, et al. Handbook of Fuel Cells, Fundamentals, Technology and Applications., vol. 3. Fuel Cell Technology and Applications. , New York: John Wiley & Sons; 2003. p. 517–37.
[3] Park S, Lee J-W, Popov BN. A review of gas diffusion layer in PEM fuel cells: materials and designs. Int J Hydrogen Energy 2012;37(7):5850–65.
[4] Cindrella L, et al. Gas diffusion layer for proton exchange membrane fuel cells—a review. J Power Sources 2009;194(1):146–60.
[5] Arvay A, et al. Characterization techniques for gas diffusion layers for proton exchange membrane fuel cells – a review. J Power Sources 2012;213:317–37.
[6] Omrani R, Shabani B. Gas diffusion layer modifications and treatments for improving the performance of proton exchange membrane fuel cells and electrolysers: a review. Int J Hydrogen Energy 2017;42(47):28515–36.
[7] Ozden A, et al. A review of gas diffusion layers for proton exchange membrane fuel cells—with a focus on characteristics, characterization techniques, materials and designs. Prog Energy Combust Sci 2019;74:50–102.
[8] Yang Y, et al. Recent progress of the gas diffusion layer in proton exchange membrane fuel cells: material and structure designs of microporous layer. Int J Hydrogen Energy 2021;46(5):4259–82.
[9] Zhang J, et al. A review of the microporous layer in proton exchange membrane fuel cells: materials and structural designs based on water transport mechanism. Renew Sustain Energy Rev 2022;156:111998. 111998.
[10] Wang CY, Chen KS. Elucidating differences between carbon paper and carbon cloth in polymer electrolyte fuel cells. Electrochim Acta 2007;52:3965–75.
[11] Pfrang A, Didas S, Tsotridis G. X-ray computed tomography of gas diffusion layers of PEM fuel cells: segmentation of the microporous layer. J Power Sources 2013;235:81–6.
[12] El-kharouf A, et al. Ex-situ characterisation of gas diffusion layers for proton exchange membrane fuel cells. J Power Sources 2012;218:393–404.
[13] Chang WR, et al. Effect of clamping pressure on the performance of a PEM fuel cell. J Power Sources 2007;166(1):149–54.
[14] Naing KSS, Tabe Y, Chikahisa T. Performance and liquid water distribution in PEFCs with different anisotropic fiber directions of the GDL. J Power Sources 2011;196(5):2584–94.
[15] Karvonen S, et al. Modeling of polymer electrolyte membrane fuel stack end plates. J Fuel Cell Sci Technol 2008;5(4).
[16] Lee J, et al. Multiwall carbon nanotube-based microporous layers for polymer electrolyte membrane fuel cells. J Electrochem Soc 2017;164(12):F1149–57.
[17] Eller J, et al. Progress in in situ X-ray tomographic microscopy of liquid water in gas diffusion layers of PEFC. J Electrochem Soc 2011;158(8).
[18] Meyer Q, et al. Effect of gas diffusion layer properties on water distribution across air-cooled, open-cathode polymer electrolyte fuel cells: a combined ex-situ X-ray tomography and in-operando neutron imaging study. Electrochim Acta 2016;211:478–87.
[19] Shrestha P, et al. Pore-scale liquid water visualization for understanding water transport in operating fuel cells. ECS Transactions 2019;92(8):61–9.
[20] Jose Varghese R, et al. Introduction to nanomaterials: synthesis and applications. Nanomaterials for Solar Cell Applications 2019:75–95.
[21] Balakrishnan M, et al. Designing tailored gas diffusion layers with pore size gradients via electrospinning for polymer electrolyte membrane fuel cells. ACS Appl Energy Mater 2020;3(3):2695–707.
[22] Delikaya Ö, et al. Porous electrospun carbon nanofibers network as an integrated electrode@gas diffusion layer for high temperature polymer electrolyte membrane fuel cells. Electrochim Acta 2020;345:136192. 136192.
[23] Ren G, et al. Liquid water transport and mechanical performance of electrospun gas diffusion layers. Int J Green Energy 2022;19(2):210–8.
[24] Chevalier S, et al. Novel electrospun gas diffusion layers for polymer electrolyte membrane fuel cells: Part II. In operando synchrotron imaging for microscale liquid water transport characterization. J Power Sources 2017;352:281–90.
[25] Chevalier S, et al. Novel electrospun gas diffusion layers for polymer electrolyte membrane fuel cells: Part I. Fabrication, morphological characterization, and in situ performance. J Power Sources 2017;352:272–80.
[26] Balakrishnan M, et al. Degradation characteristics of electrospun gas diffusion layers with custom pore structures for polymer electrolyte membrane fuel cells. ACS Appl Mater Interfaces 2021;13(2):2414–27.
[27] Fang WZ, et al. Influences of the perforation on effective transport properties of gas diffusion layers. Int J Heat Mass Tran 2018;126:243–55.
[28] Gerteisen D, Heilmann T, Ziegler C. Enhancing liquid water transport by laser perforation of a GDL in a PEM fuel cell. J Power Sources 2008;177(2):348–54.
[29] Gerteisen D, Sadeler C. Stability and performance improvement of a polymer electrolyte membrane fuel cell stack by laser perforation of gas diffusion layers. J Power Sources 2010;195(16):5252–7.
[30] Haußmann J, et al. Synchrotron radiography and tomography of water transport in perforated gas diffusion media. J Power Sources 2013;239:611–22.
[31] Niu Z, et al. Two-phase flow and oxygen transport in the perforated gas diffusion layer of proton exchange membrane fuel cell. Int J Heat Mass Tran 2019;139:58–68.
[32] Okuhata G, et al. Effect of perforation structure of cathode GDL on liquid water removal in PEFC. ECS Transactions 2013;58(1):1047–57.
[33] Wang X, et al. Laser-perforated gas diffusion layer for promoting liquid water transport in a proton exchange membrane fuel cell. Int J Hydrogen Energy 2017;42(50):29995–30003.
[34] Alink R, et al. The influence of porous transport layer modifications on the water management in polymer electrolyte membrane fuel cells. J Power Sources 2013;233:358–68.
[35] Markötter H, et al. Visualization of the water distribution in perforated gas diffusion layers by means of synchrotron X-ray radiography. Int J Hydrogen Energy 2012;37(9):7757–61.
[36] Manahan MP, Mench MM. Laser perforated fuel cell diffusion media: engineered interfaces for improved ionic and oxygen transport. J Electrochem Soc 2012;159(7):F322–30.
[37] Kaushal S, et al. Upshot of natural graphite inclusion on the performance of porous conducting carbon fiber paper in a polymer electrolyte membrane fuel cell. Mater Res Express 2017;4(9).
[38] Gurau V, Zawodzinski T, Wayne R. In-Situ Characterization of GRAFCELL® Flexible Graphite Film as Gas Diffusion Layers for PEMFCs. The Electrochemical Society; 2008.
[39] Zhang R, et al. Superstrong ultralong carbon nanotubes for mechanical energy storage. Adv Mater 2011;23(30):3387–91.
[40] Peng B, et al. Measurements of near-ultimate strength for multiwalled carbon nanotubes and irradiation-induced crosslinking improvements. Nat Nanotechnol 2008;3(10):626–31.
[41] Zhao Q, Nardelli MB, Bernholc J. Ultimate strength of carbon nanotubes: a theoretical study. Physical Review B. Condensed Matter and Materials Physics 2002;65(14):1–6.
[42] Caradonna A, et al. Electrical and thermal conductivity of epoxy-carbon filler composites processed by calendaring. Materials 2019;12(9).
[43] Kim P, et al. Thermal transport measurements of individual multiwalled nanotubes. Phys Rev Lett 2001;87(21):215502–4.
[44] Tang JM, et al. Carbon nanotube free-standing membrane as gas diffusion layer in hydrogen fuel cells. Micro & Nano Lett 2006;1(1):62. 62.
[45] Shim J-P, et al. Preparation and characterization for carbon composite gas diffusion layer on polymer electrolyte membrane fuel cells. Transactions of the Korean hydrogen and new energy society 2012;23(1):34–42.
[46] Maheshwari PH, et al. CNT membrane as a free standing electrode for PEM fuel cell. J Electrochem Soc 2014;161(12):F1146. F1153.
[47] Gao Y, et al. Carbon nanotubes based gas diffusion layers in direct methanol fuel cells. Energy 2010;35(3):1455–9.
[48] Deng H, et al. A CNT (carbon nanotube) paper as cathode gas diffusion electrode for water management of passive μ-DMFC (micro-direct methanol fuel cell) with highly concentrated methanol. Energy 2015;82:236–41.

[49] Ghobadi S, et al. Green composite papers via use of natural binders and graphene for PEM fuel cell electrodes. ACS Sustainable Chem Eng 2017;5(9):8407–15.
[50] Yarar Kaplan B, Işıkel Şanlı L, Alkan Gürsel S. Flexible carbon–cellulose fiber-based composite gas diffusion layer for polymer electrolyte membrane fuel cells. J Mater Sci 2017;52(9):4968–76.
[51] Kinumoto T, et al. Material processing of bamboo for use as a gas diffusion layer in proton exchange membrane fuel cells. ACS Sustainable Chemical Engineering 2015;3(7):1374–80.
[52] Matsumura T, et al. Preparation of carbonaceous fiber sheets derived from bamboo and application to gas diffusion layer of proton exchange membrane fuel cells. ECS Transactions 2015;64(45).
[53] Destyorini F, et al. Properties and performance of gas diffusion layer PEMFC derived from coconut coir. Journal of Engineering and Technological Sciences 2018;50(3):409–19.
[54] Indayaningsih N, et al. Preparation of carbon composite from coconut fiber for gas diffusion layer. Ionics 2016;22(8):1445–9.
[55] Heo Y-J, et al. Preparation and characterization of carbon black/pitch-based carbon fiber paper composites for gas diffusion layers. Compos B Eng 2019;159:362–8.
[56] Glora M, et al. Integration of carbon aerogels in PEM fuel cells. J Non-Cryst Solids 2001;285(1–3):283–7.
[57] Wang J, et al. Carbon cloth reinforced carbon aerogel films derived from resorcinol formaldehyde. In: Journal of Porous Materials; 2001. p. 159–65.
[58] Trefilov AMI, et al. Carbon xerogel as gas diffusion layer in PEM fuel cells. Int J Hydrogen Energy 2017;42(15):10448–54.
[59] Bystron T, et al. Enhancing PEM water electrolysis efficiency by reducing the extent of Ti gas diffusion layer passivation. J Appl Electrochem 2018;48(6):713–23.
[60] Choi H, et al. Next-generation polymer-electrolyte-membrane fuel cells using titanium foam as gas diffusion layer. ACS Appl Mater Interfaces 2014;6(10):7665–71.
[61] Fushinobu K, Takahashi D, Okazaki K. Micromachined metallic thin films for the gas diffusion layer of PEFCs. J Power Sources 2006;158(2):1240–5.
[62] Hottinen T, et al. Titanium sinter as gas diffusion backing in PEMFC. J Power Sources 2003;118(1–2):183–8.
[63] Wan N, Wang C, Mao Z. Titanium substrate based micro-PEMFC operating under ambient conditions. Electrochem Commun 2007;9(3):511–6.
[64] Patel P, Bhingole PP, Makwana D. Manufacturing, characterization and applications of lightweight metallic foams for structural applications: Review. Mater Today Proc 2018;5(9):20391–402.
[65] Matsushita T, Fujibayashi S, Kokubo T. Titanium foam for bone tissue engineering. Metallic Foam Bone 2017:111–30.
[66] Banhart J. Aluminum foams: on the road to real applications. MRS Bull 2003;28(4):290–5.
[67] Arisetty S, Prasad AK, Advani SG. Metal foams as flow field and gas diffusion layer in direct methanol fuel cells. J Power Sources 2007;165(1):49–57.
[68] Fly A, et al. Characterisation of the diffusion properties of metal foam hybrid flow-fields for fuel cells using optical flow visualisation and X-ray computed tomography. J Power Sources 2018;395:171–8.
[69] Fly A, et al. X-ray tomography and modelling study on the mechanical behaviour and performance of metal foam flow-fields for polymer electrolyte fuel cells. Int J Hydrogen Energy 2019;44(14):7583–95.
[70] Yuan W, et al. Porous metal materials for polymer electrolyte membrane fuel cells – a review. Appl Energy 2012;94:309–29.
[71] Modroukas D, Modi V, Fréchette LG. Micromachined silicon structures for free-convection PEM fuel cells. J Micromech Microeng 2005;15(9):S193–201.
[72] Zhang FY, Advani SG, Prasad AK. Performance of a metallic gas diffusion layer for PEM fuel cells. J Power Sources 2008;176(1):293–8.
[73] Liu P, Yin GP, Lai QZ. Gold-plated Ni mesh as the gas diffusion medium for air-breathing direct methanol fuel cell. Int J Energy Res 2009;33(1):1–7.
[74] Jayakumar A, et al. A novel 3D printing technique to synthesise gas diffusion layer for PEM fuel cell application. 2016.
[75] Meyer Q, et al. Investigation of hot pressed polymer electrolyte fuel cell assemblies via X-ray computed tomography. Electrochim Acta 2017;242:125–36.
[76] Kulkarni N, et al. The effect of non-uniform compression and flow-field arrangements on membrane electrode assemblies - X-ray computed tomography characterisation and effective parameter determination. J Power Sources 2019;426:97–110.
[77] Hung C-J, et al. Effect of diffusion layers fabricated with different fiber diameters on the performance of low temperature proton exchange membrane fuel cells. J Power Sources 2013;221:134–40.
[78] Kaushal S, et al. Multiwall carbon nanotubes tailored porous carbon fiber paper-based gas diffusion layer performance in polymer electrolyte membrane fuel cell. Renew Energy 2019;142:604–11.
[79] Hung C-J, et al. Effect of conductive carbon material content and structure in carbon fiber paper made from carbon felt on the performance of a proton exchange membrane fuel cell. Renew Energy 2015;78:364–73.
[80] Jayakumar A, et al. Manufacturing the gas diffusion layer for PEM fuel cell using a novel 3D printing technique and critical assessment of the challenges encountered. Materials 2017;10(7).
[81] Jo H, et al. Morphological study of directionally freeze-cast nickel foams. Metall Mater Trans 2016;3(1):46–54.
[82] Chang H-M, et al. Optimization of polytetrafluoroethylene content in cathode gas diffusion layer by the evaluation of compression effect on the performance of a proton exchange membrane fuel cell. J Power Sources 2011;196(8):3773–80.
[83] Ismail MS, et al. Effect of polytetrafluoroethylene-treatment and microporous layer-coating on the electrical conductivity of gas diffusion layers used in proton exchange membrane fuel cells. J Power Sources 2010;195(9):2700–8.
[84] Lobato J, et al. Influence of the Teflon loading in the gas diffusion layer of PBI-based PEM fuel cells. J Appl Electrochem 2008;38(6):793–802.
[85] Park G-G, et al. Effect of PTFE contents in the gas diffusion media on the performance of PEMFC. J Power Sources 2004;131(1–2):182–7.
[86] Liu C-H, et al. Effect of hydrophobic gas diffusion layers on the performance of the polymer exchange membrane fuel cell. J Power Sources 2009;191(2):489–94.
[87] Gurau V, et al. Characterization of transport properties in gas diffusion layers for proton exchange membrane fuel cells: 1. Wettability (internal contact angle to water and surface energy of GDL fibers). J Power Sources 2006;160(2):1156–62.
[88] Lim C, Wang CY. Effects of hydrophobic polymer content in GDL on power performance of a PEM fuel cell. Electrochim Acta 2004;49(24):4149–56.
[89] Zamel N, et al. Experimental measurements of effective diffusion coefficient of oxygen–nitrogen mixture in PEM fuel cell diffusion media. Chem Eng Sci 2010;65(2):931–7.
[90] Ismail MS, et al. Through-plane permeability for untreated and PTFE-treated gas diffusion layers in proton exchange membrane fuel cells. J Fuel Cell Sci Technol 2010;7(5):510161–7.
[91] Neehall ND, et al. Effect of composition and structure of gas diffusion layer and microporous layer on the through-plane gas permeability of PEFC porous media. Int J Energy Res 2021;45(15):20988–1005.
[92] Alhazmi N, et al. The in-plane thermal conductivity and the contact resistance of the components of the membrane electrode assembly in proton exchange membrane fuel cells. J Power Sources 2013;241:136–45.
[93] Velayutham G, et al. Effect of PTFE content in gas diffusion media and microlayer on the performance of PEMFC tested under ambient pressure. Fuel Cell 2007;7(4):314–8.
[94] Zamel N, et al. Measurement of in-plane thermal conductivity of carbon paper diffusion media in the temperature range of −20 °C to +120 °C. Appl Energy 2011;88(9):3042–50.
[95] Gostick JT, et al. In-plane and through-plane gas permeability of carbon fiber electrode backing layers. J Power Sources 2006;162(1):228–38.
[96] Sadeghifar H, Djilali N, Bahrami M. A new model for thermal contact resistance between fuel cell gas diffusion layers and bipolar plates. J Power Sources 2014;266:51–9.
[97] Burheim OS, et al. Through-plane thermal conductivity of PEMFC porous transport layers. J Fuel Cell Sci Technol 2011;8(2).
[98] Teertstra P, Karimi G, Li X. Measurement of in-plane effective thermal conductivity in PEM fuel cell diffusion media. Electrochim Acta 2011;56(3):1670–5.
[99] Zamora H, et al. Improving of micro porous layer based on advanced carbon materials for high temperature proton exchange membrane fuel cell electrodes. Fuel Cell 2015;15(2):375–83.
[100] Yablecki J, Bazylak A. Determining the effective thermal conductivity of compressed PEMFC GDLs through thermal resistance modelling. J Power Sources 2012;217:470–8.
[101] Sianesi D, Marchionni G, De Pasquale RJ. Perfluoropolyethers (PFPEs) from perfluoroolefin photooxidation Fomblin ® and galden ® fluids. In: Banks RE, editor. Organofluorine Chemistry. New York: Springer; 1994. p. 431–61.
[102] Gallo Stampino P, et al. Investigation of hydrophobic treatments with perfluoropolyether derivatives of gas diffusion layers by electrochemical impedance spectroscopy in PEM-FC. Solid State Ionics 2012;216:100–4.
[103] Stampino PG, et al. Surface treatments with perfluoropolyether derivatives for the hydrophobization of gas diffusion layers for PEM fuel cells. J Power Sources 2011;196(18):7645–8.
[104] Sansotera M, et al. Peroxidic perfluoropolyether for the covalent binding of perfluoropolyether chains on carbon black surface. J Fluor Chem 2011;132(12):1254–61.
[105] Gola M, et al. Perfluoropolyether-functionalized gas diffusion layers for proton exchange membrane fuel cells. J Power Sources 2014;258:351–5.
[106] United States Patent 19 Cabasso et al. 54.
[107] Salahuddin M, et al. Superhydrophobic PAN nanofibers for gas diffusion layers of proton exchange membrane fuel cells for cathodic water management. Int J Hydrogen Energy 2018;43(25):11530–8.
[108] Pai Y-H, et al. CF4 plasma treatment for preparing gas diffusion layers in membrane electrode assemblies. J Power Sources 2006;161(1):275–81.
[109] Wang Y, et al. Fabrication of Hydrophobic coating on GDL with silicone based materials. Environ Sci Technol 1980:351. 351.
[110] Joo J, et al. Controlled water flooding of polymer electrolyte fuel cells applying superhydrophobic gas diffusion layer. Curr Appl Phys 2014;14(10):1374–9.
[111] Ko T-J, et al. Water condensation behavior on the surface of a network of superhydrophobic carbon fibers with high-aspect-ratio nanostructures. Carbon 2012;50(14):5085–92.
[112] Ko TJ, et al. High performance gas diffusion layer with hydrophobic nanolayer under a supersaturated operation condition for fuel cells. ACS Appl Mater Interfaces 2015;7(9):5506–13.
[113] Thomas YRJ, et al. New method for super hydrophobic treatment of gas diffusion layers for proton exchange membrane fuel cells using electrochemical reduction of diazonium salts. ACS Appl Mater Interfaces 2015;7(27):15068–77.
[114] Litster S, et al. Active water management for PEM fuel cells. J Electrochem Soc 2007;154(10).
[115] Antolini E. Carbon supports for low-temperature fuel cell catalysts. Appl Catal B Environ 2009;88(1–2):1–24.

[116] Bezerra CWB, et al. A review of heat-treatment effects on activity and stability of PEM fuel cell catalysts for oxygen reduction reaction. J Power Sources 2007;173(2):891–908.
[117] Owejan JP, et al. Water transport mechanisms in PEMFC gas diffusion layers. J Electrochem Soc 2010;157(10):B1456. B1456.
[118] Lee J, Hinebaugh J, Bazylak A. Synchrotron X-ray radiographic investigations of liquid water transport behavior in a PEMFC with MPL-coated GDLs. J Power Sources 2013;227:123–30.
[119] Qi Z, Kaufman A. Improvement of water management by a microporous sublayer for PEM fuel cells. J Power Sources 2002;109:38–46.
[120] Chen J, Matsuura T, Hori M. Novel gas diffusion layer with water management function for PEMFC. J Power Sources 2004;131(1):155–61.
[121] Nam JH, et al. Microporous layer for water morphology control in PEMFC. Int J Heat Mass Tran 2009;52:2779–91.
[122] Weber AZ. Improved modeling and understanding of diffusion-media wettability on polymer-electrolyte-fuel-cell performance. J Power Sources 2010;16:5292–304.
[123] Chang HM, Chang MH. Effect of gas diffusion layer with double-side microporous layer coating on polymer electrolyte membrane fuel cell performance. J Fuel Cell Sci Technol 2013;10(2).
[124] Jordan LR, et al. Diffusion layer parameters influencing optimal fuel cell performance. J Power Sources 2000;86:250–4.
[125] Orogbemi OM, et al. Through-plane gas permeability of gas diffusion layers and microporous layer: effects of carbon loading and sintering. J Energy Inst 2018;91(2):270–8.
[126] Park S, Lee J-W, Popov BN. Effect of carbon loading in microporous layer on PEM fuel cell performance. J Power Sources 2006;163(1):357–63.
[127] Antolini E, Passos RR, Ticianelli EA. Effects of the carbon powder characteristics in the cathode gas diffusion layer on the performance of polymer electrolyte fuel cells. J Power Sources 2002;109(2):477–82.
[128] Yu J, et al. Improving the performance of a PEMFC with Ketjenblack EC-600JD carbon black as the material of the microporous layer. Electrochem Solid State Lett 2005;8(6).
[129] Carcadea E, et al. A computational fluid dynamics analysis of a PEM fuel cell system for power generation. Int J Numer Methods Heat Fluid Flow 2007;17(3):302–12.
[130] Antonacci P, et al. Balancing mass transport resistance and membrane resistance when tailoring microporous layer thickness for polymer electrolyte membrane fuel cells operating at high current densities. Electrochim Acta 2016;188:888–97.
[131] Zhang J. PEM Fuel Cell Electrocatalysts and Catalyst Layers. , London: Springer; 2008.
[132] Millington B, Whipple V, Pollet BG. A novel method for preparing proton exchange membrane fuel cell electrodes by the ultrasonic-spray technique. J Power Sources 2011;196(20):8500–8.
[133] Kim Y-S, et al. Effects of the microstructure and powder compositions of a micro-porous layer for the anode on the performance of high concentration methanol fuel cell. Int J Hydrogen Energy 2013;38(17):7159–68.
[134] Ioroi T, et al. Influence of PTFE coating on gas diffusion backing for unitized regenerative polymer electrolyte fuel cells. J Power Sources 2003;124(2):385–9.
[135] Park SB, et al. Fabrication of GDL microporous layer using PVDF for PEMFCs. In: Journal of Physics: Conference Series. Institute of Physics Publishing; 2009.
[136] Chun JH, et al. Determination of the pore size distribution of micro porous layer in PEMFC using pore forming agents under various drying conditions. Int J Hydrogen Energy 2010;35(20):11148–53.
[137] Simon C, et al. Impact of microporous layer pore properties on liquid water transport in PEM fuel cells: carbon black type and perforation. J Electrochem Soc 2017;164(14):F1697–711.
[138] Tang H, et al. Porosity-graded micro-porous layers for polymer electrolyte membrane fuel cells. J Power Sources 2007;166:41–6.
[139] Wang X, et al. A bi-functional micro-porous layer with composite carbon black for PEM fuel cells. J Power Sources 2006;162(1):474–9.
[140] Yoshimune W, et al. Managing the pore morphologies of microporous layers for polymer electrolyte fuel cells with a solvent-free coating technique. ACS Sustainable Chem Eng 2021;9(23):7922–9.
[141] Manahan MP, et al. Laser modified fuel cell diffusion media: engineering enhanced performance via localized water redistribution. J Electrochem Soc 2014;161(10):1061–9.
[142] Manahan MP, et al. Laser perforated fuel cell diffusion media. Part I: related changes in performance and water content. J Power Sources 2011;196(13):5573–82.
[143] Lu Z, et al. Influence of MPL structure modification on fuel cell oxygen transport resistance. ECS Transactions 2015;69(17):1341–53.
[144] Lee D-H, et al. Ditch-structured microporous layers fabricated by nanosecond-pulse laser ablation for enhancing water transport in polymer electrolyte membrane fuel cells †. This journal is Cite this: Mater. Adv 2020;1:254. 254.
[145] Mohseninia A, et al. Influence of structural modification of micro-porous layer and catalyst layer on performance and water management of PEM fuel cells: hydrophobicity and porosity. Fuel Cell 2020;20(4):469–76.
[146] Cho J, et al. Unveiling water drainage through microporous layer with laser-ablated open furrows in proton exchange membrane fuel cells. J Power Sources 2021;491:229563. 229563.
[147] Chen L, et al. Microporous layers with different decorative patterns for polymer electrolyte membrane fuel cells. ACS Appl Mater Interfaces 2020;12(21):24048–58.
[148] Chen-Yang YW, et al. Novel single-layer gas diffusion layer based on PTFE/carbon black composite for proton exchange membrane fuel cell. J Power Sources 2007;173(1):183–8.
[149] Kitahara T, et al. Novel hydrophilic and hydrophobic double microporous layer coated gas diffusion layer to enhance performance of polymer electrolyte fuel cells under both low and high humidity. J Power Sources 2013;234:129–38.
[150] Terayama Y, et al. Carbon black/PTFE composite hydrophobic gas diffusion layers for a water-absorbing porous electrolyte electrolysis cell. Int J Hydrogen Energy 2018;43(4):2018–25.
[151] Bauder A, et al. Self-Supporting microporous layers (MPLs) for PEM fuel cells. ECS Transactions 2013;58(1):1391–9.
[152] Ito H, et al. Application of a self-supporting microporous layer to gas diffusion layers of proton exchange membrane fuel cells. J Power Sources 2017;342:393–404.
[153] Liu CH, Ko TH, Liao YK. Effect of carbon black concentration in carbon fiber paper on the performance of low-temperature proton exchange membrane fuel cells. J Power Sources 2008;178:80–5.
[154] Mathur RB, et al. Processing of carbon composite paper as electrode for fuel cell. J Power Sources 2006;161:790–8.
[155] Xie ZY, et al. Improved properties of carbon fiber paper as electrode for fuel cell by coating pyrocarbon via CVD method. Trans Nonferrous Metals Soc China 2010;20:1412–7.
[156] Kim J, et al. Carbon nanotube sheet as a microporous layer for proton exchange membrane fuel cells. Energy 2021;227:120459. 120459.
[157] Duan Q, et al. Fabrication of a carbon nanofiber sheet as a micro-porous layer for proton exchange membrane fuel cells. J Power Sources 2010;195(24):8189–93.
[158] Gallo Stampino P, et al. Characterisation of nanocarbon-based gas diffusion media by electrochemical impedance spectroscopy. Fuel Cell 2010;10:270–7.
[159] Gharibi H, Javaheri M, Mirzaie RA. The synergy between multi-wall carbon nanotubes and Vulcan XC72R in microporous layers. Int J Hydrogen Energy 2010;35(17):9241–51.
[160] Kannan AM, Kanagala P, Veedu V. Development of carbon nanotubes based gas diffusion layers by in situ chemical vapor deposition process for proton exchange membrane fuel cells. J Power Sources 2009;192:297–303.
[161] Kannan AM, Munukutla L. Carbon nano-chain and carbon nano-fibers based gas diffusion layers for proton exchange membrane fuel cells. J Power Sources 2007;167(2):330–5.
[162] Lin S-Y, Chang M-H. Effect of microporous layer composed of carbon nanotube and acetylene black on polymer electrolyte membrane fuel cell performance. Int J Hydrogen Energy 2015;40(24):7879–85.
[163] Schweiss R, et al. Enhancement of proton exchange membrane fuel cell performance by doping microporous layers of gas diffusion layers with multiwall carbon nanotubes. J Power Sources 2012;220:79–83.
[164] Schweiss R, Steeb M, Wilde PM. Mitigation of water management in PEM fuel cell cathodes by hydrophilic wicking microporous layers. Fuel Cell 2010;10(6):1176–80.
[165] Kong CS, et al. Influence of pore-size distribution of diffusion layer on mass-transport problems of proton exchange membrane fuel cells. J Power Sources 2002;108:185–91.
[166] Aoyama Y, et al. Effect of hydrophilic micro-porous layer structure on microscopic water distribution and cell performance in PEFC. In: ECS Transactions. Electrochemical Society Inc; 2015.
[167] Sandström R, et al. Fabrication of microporous layer-free hierarchical gas diffusion electrode as a low Pt-loading PEMFC cathode by direct growth of helical carbon nanofibers. RSC Adv 2018;8(72):41566–74.
[168] Soehn M, et al. Design of gas diffusion electrodes using nanocarbon. J Power Sources 2008;176:494–8.
[169] Tang Z, et al. In situ grown carbon nanotubes on carbon paper as integrated gas diffusion and catalyst layer for proton exchange membrane fuel cells. Electrochim Acta 2011;56(11):4327–34.
[170] Andersen SM, et al. Durability of carbon nanofiber (CNF) & carbon nanotube (CNT) as catalyst support for Proton Exchange Membrane Fuel Cells. Solid State Ionics 2013;231:94–101.
[171] Park S, et al. Design of graphene sheets-supported Pt catalyst layer in PEM fuel cells. Electrochem Commun 2011;13:258–61.
[172] Najafab AT, et al. Electrochemically produced graphene for MicroporousLayers in fuel cells. ChemSusChem 2016;9:1689–97. 1689 –1697.
[173] Leeuwner MJ, Wilkinson DP, Gyenge EL. Novel graphene foam microporous layers for PEM fuel cells: interfacial characteristics and comparative performance. Fuel Cell 2015;15(6):790–801.
[174] Leeuwner MJ, et al. Graphene and reduced graphene oxide based microporous layers for high-performance proton-exchange membrane fuel cells under varied humidity operation. J Power Sources 2019;423:192–202.
[175] Ozden A, et al. Assessment of graphene as an alternative microporous layer material for proton exchange membrane fuel cells. Fuel 2018;215:726–34.
[176] Hwang CM, et al. Effect of titanium powder loading in gas diffusion layer of a polymer electrolyte unitized reversible fuel cell. J Power Sources 2012;202:108–13.
[177] Song S, et al. Bifunctional oxygen electrode with corrosion-resistive gas diffusion layer for unitized regenerative fuel cell. Electrochem Commun 2006;8(3):399–405.
[178] Huang S-Y, et al. Development of supported bifunctional oxygen electrocatalysts and corrosion-resistant gas diffusion layer for unitized regenerative fuel cell applications. J Power Sources 2012;198:23–9.

[179] Fang S-Y, et al. Enhancement of proton exchange membrane fuel cell performance by titanium-coated anode gas diffusion layer. Int J Hydrogen Energy 2014;39(36):21177–84.
[180] Yan WM, et al. Effects of fabrication processes and material parameters of GDL on cell performance of PEM fuel cell. Int J Hydrogen Energy 2007;32(17):4452–8.
[181] Mariani M, et al. Characterization of novel graphene-based microporous layers for Polymer Electrolyte Membrane Fuel Cells operating under low humidity and high temperature. Int J Hydrogen Energy 2020;45(11):7046–58.
[182] Su H, et al. Optimization of gas diffusion electrode for polybenzimidazole-based high temperature proton exchange membrane fuel cell: evaluation of polymer binders in catalyst layer. Int J Hydrogen Energy 2013;38(26):11370–8.
[183] Zhang F, et al. Poly(vinylidene fluoride) based anion conductive ionomer as a catalyst binder for application in anion exchange membrane fuel cell. J Power Sources 2011;196(6):3099–103.
[184] Bottino A, et al. Microporous layers based on poly(vinylidene fluoride) and sulfonated poly(vinylidene fluoride). Int J Hydrogen Energy 2015;40(42):14690–8.
[185] Ong AL, et al. Effect of preparative parameters on the characteristic of poly (vinylidene fluoride)-based microporous layer for proton exchange membrane fuel cells. J Power Sources 2008;183(1):62–8.
[186] Navarrini, W., et al., Perfluoropolyethers as superhydrophobizing agents for carbon-based surfaces of fuel cell gas diffusion layers.
[187] Balzarotti R, et al. Development and characterization of non-conventional microporous layers for PEM fuel cells. Energies 2015;8(7):7070–83.
[188] Sansotera M, et al. The role of perfluoropolyethers in the development of polymeric proton exchange membrane fuel cells. In: Ameduri B, Sawada H, editors. Fluorinated Polymers: Applications, vol. 2. Cambridge: Royal Society of Chemistry; 2016. p. 158–78.
[189] Latorrata S, et al. Innovative perfluoropolyether-functionalized gas diffusion layers with enhanced performance in polymer electrolyte membrane fuel cells. Fuel Cell 2020;20(2):166–75.
[190] Latorrata S, et al. Novel superhydrophobic microporous layers for enhanced performance and efficient water management in PEM fuel cells. Int J Hydrogen Energy 2014;39(10):5350–7.
[191] Latorrata S, et al. Performance evaluation and durability enhancement of FEP-based gas diffusion media for PEM fuel cells. Energies 2017;10(12).
[192] Park SB, Eon Kim J, Oh M-H. Fabrication of GDL Microporous Layer Using FEP for PEMFCs, in Semiconductors and Superlattices. Gordon and Breach Science Pub; 2000. p. 1969. 1969.
[193] Tanuma T, Kinoshita S. Impact of gas diffusion layers (GDLs) on water transport in PEFCs. J Electrochem Soc 2012;159(2).
[194] Nozaki R, et al. Analysis of oxygen transport resistance components and water transport phenomena with hydrophilic and hydrophobic MPL in PEFC. ECS Transactions 2017;80(8):335–44.
[195] Tanuma T, Kawamoto M, Kinoshita S. Effect of properties of hydrophilic microporous layer (MPL) on PEFC performance. J Electrochem Soc 2017;164(6):F499–503.
[196] Guo X, et al. Improvement of the proton exchange membrane fuel cell (PEMFC) performance at low-humidity conditions by exposing anode in Ultraviolet light. Electrochem Commun 2014;44:16–8.
[197] Hou S, et al. Enhanced low-humidity performance in a proton exchange membrane fuel cell by developing a novel hydrophilic gas diffusion layer. Int J Hydrogen Energy 2020;45(1):937–44.
[198] Wang X, et al. Ultraviolet-Induced Bi-gradient gas diffusion electrode for high-performance fuel cells. Ind Eng Chem Res 2022;61(10):3561–9.
[199] Mukundan R, et al. Effect of hydrophilic treatment of microporous layer on fuel cell performance. In: ECS Transactions; 2010.
[200] Aoyama Y, et al. Analysis of water transport inside hydrophilic carbon fiber micro-porous layers with high-performance operation in PEFC. J Electrochem Soc 2018;165(7):F484–91.
[201] Kitahara T, Nakajima H, Mori K. Hydrophilic and hydrophobic double MPL coated GDL to enhance PEFC performance under low and high humidity conditions. In: ECS Transactions; 2011.
[202] Kitahara T, et al. Triple microporous layer coated gas diffusion layer for performance enhancement of polymer electrolyte fuel cells under both low and high humidity conditions. J Power Sources 2014;248:1256–63.
[203] Yan Q, Toghiani H, Wu J. Investigation of water transport through membrane in a PEM fuel cell by water balance experiments. J Power Sources 2006;158(1):316–25.
[204] Öztürk A, et al. Facilitation of water management in low Pt loaded PEM fuel cell by creating hydrophobic microporous layer with PTFE, FEP and PDMS polymers: effect of polymer and carbon amounts. Int J Hydrogen Energy 2017;42(33):21226–49.
[205] Chun JH, et al. Development of a novel hydrophobic/hydrophilic double micro porous layer for use in a cathode gas diffusion layer in PEMFC. Int J Hydrogen Energy 2011;36(14):8422–8.
[206] Satjaritanun P, et al. Micro-scale analysis of liquid water breakthrough inside gas diffusion layer for PEMFC using X-ray computed tomography and Lattice Boltzmann Method. J Electrochem Soc 2017;164(11):E3359–71.
[207] Jinuntuya F, et al. The effects of gas diffusion layers structure on water transportation using X-ray computed tomography based Lattice Boltzmann method. J Power Sources 2018;378:53–65.
[208] Shangguan X, et al. Effect of the porosity distribution on the liquid water transport in the gas diffusion layer of PEMFC. Electrochim Acta 2021;371:137814. 137814.
[209] Kanchan BK, Randive P, Pati S. Numerical investigation of multi-layered porosity in the gas diffusion layer on the performance of a PEM fuel cell. Int J Hydrogen Energy 2020;45(41):21836–47.